Analysis of Tumor-Immune Dynamics in an Evolving Dendritic Cell Therapy Model

by

Lauren Rachelle Dickman

A Dissertation Presented in Partial Fulfillment
of the Requirements for the Degree
Doctor of Philosophy

Approved April 2020 by the
Graduate Supervisory Committee:

Yang Kuang, Chair
Steven Baer
Carl Gardner
Abba Gumel
Eric Kostelich

ARIZONA STATE UNIVERSITY

May 2020

ABSTRACT

Cancer is a worldwide burden in every aspect: physically, emotionally, and financially. A need for innovation in cancer research has led to a vast interdisciplinary effort to search for the next breakthrough. Mathematical modeling allows for a unique look into the underlying cellular dynamics and allows for testing treatment strategies without the need for clinical trials. This dissertation explores several iterations of a dendritic cell (DC) therapy model and correspondingly investigates what each iteration teaches about response to treatment.

In Chapter 2, motivated by the work of de Pillis *et al.* (2013), a mathematical model employing six ordinary differential (ODEs) and delay differential equations (DDEs) is formulated to understand the effectiveness of DC vaccines, accounting for cell trafficking with a blood and tumor compartment. A preliminary analysis is performed, with numerical simulations used to show the existence of oscillatory behavior. The model is then reduced to a system of four ODEs. Both models are validated using experimental data from melanoma-induced mice. Conditions under which the model admits rich dynamics observed in a clinical setting, such as periodic solutions and bistability, are established. Mathematical analysis proves the existence of a backward bifurcation and establishes thresholds for $\mathcal{R}_0$ that ensure tumor elimination or existence. A sensitivity analysis determines which parameters most significantly impact the reproduction number $\mathcal{R}_0$. Identifiability analysis reveals parameters of interest for estimation. Results are framed in terms of treatment implications, including effective combination and monotherapy strategies.

In Chapter 3, a study of whether the observed complexity can be represented with a simplified model is conducted. The DC model of Chapter 2 is reduced to a non-dimensional system of two DDEs. Mathematical and numerical analysis explore the impact of immune response time on the stability and eradication of the tumor,

including an analytical proof of conditions necessary for the existence of a Hopf bifurcation. In a limiting case, conditions for global stability of the tumor-free equilibrium are outlined.

Lastly, Chapter 4 discusses future directions to explore. There still remain open questions to investigate and much work to be done, particularly involving uncertainty analysis. An outline of these steps is provided for future undertakings.

To my family,

for their continual love and support.

ACKNOWLEDGMENTS

I would first like to express my sincerest gratitude to my advisor, Dr. Yang Kuang, for his incredible mentorship and for his continual support and patience while I have pursued various interests. Dr. Kuang has been a mentor in all aspects of life, not simply research, providing a constant source of wisdom, guidance, and encouragement. His contagious enthusiasm for mathematical biology allowed me to better see all of its beauty, and I am deeply appreciative to have studied under his supervision.

I would additionally like to thank the remainder of my committee, Dr. Steven Baer, Dr. Carl Gardner, Dr. Abba Gumel, and Dr. Eric Kostelich, for their encouragement, expertise, and insights. I would like to thank my collaborator, Dr. Evan Milliken. I am deeply grateful for all I have been able to learn from you.

I am grateful for the faculty members who have taught and mentored me at Arizona State University and for the staff members who have been a source of support and encouragement. I would like to give a special thank you to Katie Kolossa and Rhonda Olson for all they have both done for the graduate students. Your desires to help each of us succeed have been inspiring and have had a profound impact in my life. I am grateful for the excellent Graduate Program Coordinators both past and present, Jennifer May, Melissa Delgado, and Joelle Park. I am also grateful for my fellow graduate students and friends for their support and for always helping me to remember that life exists outside of school. I would especially like to thank Elpiniki Nikolopoulou, my officemate, collaborator, academic "sister," and dear friend, for being a sounding board for all of my ideas and, more importantly, a constant I could turn to for advice, encouragement, and laughter. I will always be grateful to have gone through these years with you.

I would like to thank my family for their immense love and support. I would like to thank my parents who instilled in me a love of learning and a love of challenges at

a young age. You have always helped me believe I was capable enough to accomplish anything, and that belief brought me to where I am today. I would like to thank my siblings for their encouragement and for inspiring me to be better. Your examples have propelled me to push myself in an attempt to reach the bar you all have set. I would also like to thank my in-laws for their love and encouragement. A special recognition goes to my little brother and mom for always being my inspiration to continue to research.

Last, and certainly not least, I would like to thank my husband Austin, for a constant outpouring of love, encouragement, and praise during this journey and throughout all our years together. Thank you for always believing in me in whatever I pursue. I could not have done this without you, and I would not want to imagine doing it without you. I cannot wait to see what our post-graduation life has in store for us.

TABLE OF CONTENTS

CHAPTER Page

LIST OF TABLES

LIST OF FIGURES

Figure Page

Figure Page

Figure Page

Figure Page

Figure Page

Chapter 1

INTRODUCTION

1.1 Immunotherapy

It is a well-established fact that cancer is a worldwide burden. Each year, tens of millions of new cases are diagnosed and nearly ten million cancer-related deaths occur. With the staggering need for improvements in treatment, research is ongoing in the search for the next breakthrough. Recently, much attention has been focused on the potential of immunotherapy, particularly in combination with the standard treatments: surgery, radiation, and chemotherapy. Excitement surrounding immunotherapy lies in its use of the body's innate defenses, as it entices the immune system to attack cancer cells, infections, and other diseases.

Though immunotherapy is currently a rapidly growing area of cancer research, it is not a recent medical advancement. It is possible that cancer immunotherapy can be traced back as early as 2600 BC, as documented in the ancient Egyptian medical text, the *Ebers Papyrus*, attributed to the physician Imhotep (Ebbell, 1937). Treatment for tumors was advised to be "a poultice, followed by incision," which would undoubtedly cause infection at the tumor site (Ebbell, 1937). Historical accounts across thousands of years detailed spontaneous tumor regression, with nearly all accounts involving regression concomitant with infection, as was the case for Saint Peregrine in the late 13th century (Jackson, 1974). Treatment in the 1700s and 1800s AD largely consisted of crude immunotherapies inducing deliberate infections.

In the late 19th century, Busch (1868) and Fehleisen (1882) independently noted a connection between tumor regression and erisypelas infection. Busch (1868) became

the first to deliberately infect a cancer patient with erysipelas, resulting in shrinkage of the tumor. Shortly after, unaware of the past work in the field, Coley (1893) noted a tumor regression in a patient infected with erisypelas and attempted to reproduce the results by infecting other cancer patients with erisypelas. Observing mixed results from this attempt, ranging from difficulty inducing infection to patient fatalities, Coley then developed a vaccine known as "Coley's toxins" using two killed bacteria, *Streptococcus pyogenes* and *Serratia marcescens*, to produce symptoms of bacterial infections without actually producing an infection (McCarthy, 2006). Over 1000 patients were reported to experience tumor regression or elimination as a result (Cann *et al.*, 2002). This foundational work has contributed to Coley being deemed the "Father of immunotherapy." Unfortunately during Coley's lifetime, the subsequent development of chemotherapy and radiation therapy, along with other factors, caused immunotherapy to be pushed to the side (Oiseth and Aziz, 2017). The 1980s brought key discoveries in how the immune system works (Allison *et al.*, 1982), fostering a vast resurgence of interest in immunotherapy that continues to this day.

1.2 Cancer Vaccines

Cancer vaccines are a form of immunotherapy that train the immune system to recognize and attack cancer cells. Vaccines treating diseases caused by viruses or bacteria are regularly preventive, acting to protect the body against contracting the disease. In a similar manner, there exists a class of preventive cancer vaccines that protect against development of certain cancers. The United States Food and Drug Administration (FDA) has approved two preventive cancer vaccines, namely the human papillomavirus (HPV) vaccine and the hepatitis B virus (HBV) vaccine. HPV and HBV are known to be associated with several forms of cancer, including cervical, anal, and liver cancer (Bansal *et al.*, 2016). Thus, by preventing HPV and

HBV infections, the vaccines additionally inhibit the process that could cause the development of HPV- and HBV-related cancers.

While preventive cancer vaccines are effective for virus-induced cancers, most cancers are not believed to be caused by infections. Thus, a large class of cancer vaccines studied are categorized as therapeutic vaccines and are administered following the onset of cancer. Therapeutic vaccines can act to eliminate residual cancer cells, prevent tumor recurrence, or stop metastasis. At this point, the FDA has only approved a single therapeutic cancer vaccine, sipuleucel-T (Provenge®), though there are countless clinical trials currently investigating various others (Kantoff *et al.*, 2010). While cancer vaccines have shown promise in early clinical trials (Gameiro *et al.*, 2013), a greater understanding of the immune response following treatment would serve to increase their efficacy.

1.3 Mathematics in Population Ecology

Mathematics possesses the ability to quantify surrounding phenomena, allowing researchers to simulate behavior and thereby recognize underlying patterns and properties. For centuries, mathematics has been utilized as a tool for better understanding living organisms and how populations change and interact over time. One of the oldest known mathematical models of population growth dates back to the commencement of the 13th century, when Pisano (Fibonacci) famously studied how quickly rabbits could reproduce, with the answer found in the Fibonacci sequence (Pisano, 1202).

Nearly 600 years later, Malthus (1798) thought to model population growth geometrically and created the exponential law, referred to as the "first principle of population dynamics" (Berryman, 1997), to describe when growth goes unchecked. Malthus (1798) additionally theorized that food supply increased arithmetically, and the geometric increase of a population would eventually exceed the arithmetic pro-

gression of resources, thereby leading to death from food shortage. Recognizing the need to account for resource limitations when modeling population growth, as uncontrolled exponential growth is an unreasonable assumption, Verhulst (1838) cited Malthus's work as motivation and formulated the highly influential logistic growth equation, thus developing the first density-dependent model. In his initial findings, Verhulst (1838) demonstrated the logistic equation agreed with population data from Belgium, Essex, France, and Russia that spanned periods from late 18th century up to 1833. Since Pearl and Reed (1920) rediscovered and popularized the equation with a population growth model of the United States, logistic growth has remained a commonly used growth term, with applications in fields such as ecology, oncology, economics, and engineering.

Mathematical modeling further advanced in the 1920s with the introduction of predator-prey models, as first formulated by Lotka (1920) to describe interactions between plants and herbivores. Their interactions were found to produce indefinite, undamped oscillations in both populations. Lotka (1925) developed his analysis in a more general framework of predator-prey interactions with his classic book, *Elements of Physical Biology*. Additionally, Volterra (1926) independently derived a predator-prey model, with application to predator and prey fish in the Adriatic Sea during World War I, similarly concluding the populations would have sustained oscillations from their interactions. The predator-prey interactions, now known as the "Lotka-Volterra model," represented a shift in several ways, one of which being the representation of the species' interactions with the law of mass action, where the response from each species is directly proportional to the product of their population densities.

Not long after, Holling (1959a,b) later expanded upon the Lotka-Volterra model, considering three main types of functional responses, a term coined by Solomon (1949)

to describe the relationship between predation rate and prey density. In the Lotka-Volterra model, the functional response is a linear increase in predation rate as prey density increases. Taking into account a predator's eventual loss of appetite, along with time for prey searching and handling, Holling (1959a,b) described two alternative functional responses in which the predation rate is a nonlinear function of prey density, increasing hyperbolically or sigmoidally until eventually reaching a saturation threshold. Different manners of representing species' interactions has proved invaluable in mathematical modeling, allowing researchers to better tailor models to address their specific questions and gain further insight into underlying patterns.

1.4 Mathematical Oncology

Mathematical models have the ability to make sense of complicated interactions and address key questions, including when and why treatments fail and which components are key players in determining treatment response. Though often not originally developed with the intent of cancer modeling, ecological models have a history of successful applications in the realm of mathematical oncology. Mechanisms of ecology share many similarities with that of cancer biology, such as competition, control, extinction, invasion, movement, mutations, and predator-prey dynamics, thus allowing for the adaptation of ecological models to cancer models.

With the growing attention surrounding immunotherapy as a form of cancer treatment, which relies on the interplay between the tumor cells and immune system, there has been increased interest in tumor-immune models within the realm of mathematical oncology. Many deterministic models have viewed the tumor-immune system through the lens of an ecological predator-prey system (Agarwal and Bhadauria, 2013; Sotolongo-Costa *et al.*, 2003; Kaur and Ahmad, 2014). Though the killing of tumor cells by immune cells would seemingly be applicable to the Lotka-Volterra model, the

assumptions of the model do not line up with reality. In a classical predator-prey model, the predators die in the absence of the prey, and interactions between predator and prey benefit the predator but are harmful to the prey. Assuming a lack of immune cell growth in the absence of the tumor cell population would be clearly inaccurate. Additionally, while tumor cells can trigger production of new immune cells, the immune cells also experience harmful effects as a result of interactions with tumor cells. These effects result from the immunosuppressive tumor microenvironment or a loss of an immune cell's ability to kill in the future following each interaction (de Pillis and Radunskaya, 2014).

In a predator-prey approach accounting for the tumor microenvironment and independent growth of the immune cells, Kuznetsov *et al.* (1994) used Michaelis-Menten kinetics, the equivalent of a Holling type II functional response, to model infiltration of the tumor by the effector cells and mass action to describe the resulting inactivation of effector cells by the tumor. Their model allowed for capturing and explaining previously unexplained behaviors, including tumor dormancy, oscillatory behavior, and "sneaking through," in which a low burden can escape immune control and rapidly grow to a large tumor, but larger tumor burdens can be eliminated. Shortly after, Galach (2003) simplified the Kuznetsov *et al.* (1994) model by replacing Michaelis-Menten kinetics with mass action. It was shown that the the "sneaking through" phenomenon was no longer able to be captured, though the dynamics of dormancy and tumor escape were maintained.

To understand the impact of immunotherapy on the immune system, Kirschner and Panetta (1998) explored the tumor-immune system without treatment, then under adoptive cellular immunotherapy and administration of the cytokine IL-2, both as monotherapies and in conjunction with each other. They were able to establish conditions needed to produce optimal treatment responses. In recent years, many

models exploring immunotherapy have been developed to understand tumor-immune dynamics and aid in improving treatment design (de Pillis *et al.*, 2013; d'Onofrio, 2005; Rutter and Kuang, 2017), with each making conclusions regarding key factors in cancer eradication.

1.5 Motivation and Goals

The de Pillis *et al.* (2013) model examines dendritic cell therapy, a form of therapeutic cancer vaccine, through a system of nine ordinary differential and delay differential equations representing dendritic cells, activated and memory T lymphocytes, and tumor cells. In this work, we seek to build off the work of de Pillis *et al.* (2013) and present the evolution of a dendritic cell model and insights from each model iteration regarding immune response dynamics following treatment. In Chapter 2, we reduce the system to four ordinary differential equations. In Chapter 3, we modify the system to be represented by two delay differential equations.

Chapter 2

ORDINARY DIFFERENTIAL EQUATION MODEL

2.1 Abstract

Melanoma, the deadliest form of skin cancer, is regularly treated by surgery in conjunction with a targeted therapy or immunotherapy. Dendritic cell therapy is an immunotherapy that capitalizes on the critical role dendritic cells play in shaping the immune response. We formulate a mathematical model employing ordinary differential and delay differential equations to understand the effectiveness of dendritic cell vaccines, accounting for cell trafficking with a blood and tumor compartment. We reduce our model to a system of ordinary differential equations. Both models are validated using experimental data from melanoma-induced mice. The simplicity of our reduced model allows for mathematical analysis and admits rich dynamics observed in a clinical setting, such as periodic solutions and bistability. We give thresholds for tumor elimination and existence. Bistability, in which the model outcomes are sensitive to the initial conditions, emphasizes a need for more aggressive treatment strategies, since the reproduction number below unity is no longer sufficient for elimination. A sensitivity analysis exhibits the parameters most significantly impacting the reproduction number, thereby suggesting the most efficacious treatments to use together with a dendritic cell vaccine.

2.2 Introduction

Skin cancer is the most common cancer diagnosis in the United States, with melanoma accounting for approximately 1% of all skin cancer (Siegel *et al.*, 2019).

Though a small percentage of the diagnoses, melanoma is the deadliest form of skin cancer and thus causes the majority of skin cancer-related deaths. Over the past 30 years, rapid increases have been seen in the incidences of melanoma (Siegel *et al.*, 2019). The rise in melanoma has inspired additional research and advancements in its treatment.

Options for treatment consisted of excision, burning the tumor, amputation, and extirpation in the mid-late 19^{th} century (Rebecca *et al.*, 2012). Eventually chemotherapy was introduced, though it did not result in improvements to the overall survival (Wilson and Schuchter, 2016). The introduction of chemotherapy represented a greater shift towards treating the internal cause of melanoma, as opposed to simply alleviating the associated pain. Treatment for melanoma now generally involves surgery followed by adjuvant therapies, often consisting of targeted therapy and immunotherapy. Targeted therapy uses drugs to target proteins, genes, and molecules which promote cancer growth, while immunotherapy works to enhance the immune system response against cancer, either through teaching it to react against something not previously considered foreign, like cancer cells, or releasing it to attack known antigens, as in the case of immune checkpoint inhibitors (Castiglione and Piccoli, 2006). Compared to previous routine therapies, immunotherapy has shown great promise for melanoma patients (Domingues *et al.*, 2018).

Dendritic cells (DCs) originate in the bone marrow and are the most potent antigen-presenting cells (APCs) with a singular ability to initiate naive T cells (Arabameri *et al.*, 2018). As such, dendritic cell therapy has been employed to take advantage of the role DCs play in shaping the immune response. In this type of immunotherapy, immature DCs are extracted from the patient, cultured *ex vivo*, and loaded with tumor-associated antigens to become sensitized. Once sensitized and thereby activated, DCs are then injected back into the patient, where they migrate to

the lymphoid organs via the bloodstream. Within the lymphoid organs, the activated (mature) DCs interact with the naive cytotoxic T lymphocytes (CTLs), activating them and instructing them to proliferate. These activated CTLs, otherwise known as effector cells, travel to the tumor, where they mount a fight against cells expressing the tumor-associated antigen. The cancer cells and the immunosuppressive environment of the tumor are able to inactivate CTLs or induce CTL apoptosis, and the activated CTLs in turn kill the tumor cells (Aerts and Hegmans, 2013). The immune system retains a memory response to these formerly encountered antigens through the existence of memory CTLs, leading to the long-term impacts of immunotherapies.

Human clinical trials involving DC-based vaccines commenced in the 1990s, yielding positive results for patients with melanoma (Nestle *et al.*, 1998), prostate cancer (Tjoa *et al.*, 1999), and B-cell lymphoma (Hsu *et al.*, 1996). Over 400 clinical trials evaluating DC vaccines are currently being carried out in the United States, of which 237 are Phase II and 11 are Phase III (U.S. National Library of Medicine, 2018). Since the beginnings of DC-based vaccine-related clinical trials, a number of malignancies have been tested with the immunotherapy, including intracranial tumors (Liau *et al.*, 2000), multiple myeloma (Ridgway, 2003), renal cell carcinoma (Wierecky *et al.*, 2006), colorectal cancer (Fong *et al.*, 2001), and cervical cancer (Ferrara *et al.*, 2003). Furthermore, various treatment strategies, including prophylactic (pre-exposure) dosing, have been studied. Prolonged survival and limited side effects have been observed in patients with a vast array of tumor types treated with DC-based vaccines (Ridgway, 2003). Prophylactic dosing with DC-based vaccines, useful for patients with a high risk of developing cancer, has been observed to effectively inhibit certain types of cancers when studied *in vivo* (Markov *et al.*, 2015). However, the most effective use of the DC vaccine has been shown with combination treatments. The low toxicity of the DC vaccine greatly adds to its appeal as part

of a combination therapy and, as such, DC vaccines are often tested in conjunction with other treatments, such as chemotherapy, immune checkpoint inhibitors, and radiotherapy (van Gulijk *et al.*, 2018). Mathematical models allow for a deeper look into the behavior of the vaccine and an exploration into what mechanisms lead to treatment success or failure during these clinical trials, consequently motivating and informing new clinical trials. Once a greater understanding of the monotherapy is established, clear extensions would involve incorporating combination treatments to better comprehend the synergy. Additional insights into these key mechanisms decidedly prove valuable when designing combination therapies.

In this chapter, we explore the dynamics underlying the tumor-immune interactions following continuous and intermittent administration of dendritic cell therapy. We determine thresholds for tumor existence or eradication. We investigate the existence of a backward bifurcation, Hopf bifurcation, and Bogdanov-Takens bifurcation. We conduct a sensitivity analysis to determine which parameters most strongly influence the dendritic cell therapy efficacy, followed by a brief identifiability analysis. Some of the work contained in this chapter has been accepted for publication, with co-author and journal permissions found in Appendix A and Appendix B respectively.

2.3 Previous and Proposed Models

Immunotherapy treatments, particularly DC vaccines, have been a recent focus of mathematical modeling efforts. Within the last 15 years, a number of researchers have examined optimal DC treatment protocols by studying systems of ordinary differential equations (ODEs) through the lens of various optimal control strategies (Burden *et al.*, 2004; Cappuccio *et al.*, 2007; Castiglione and Piccoli, 2006; de Pillis *et al.*, 2007; Ghaffari and Naserifar, 2010). Furthermore, ODEs have been employed recently in working towards the goal of precision medicine. Gevertz and Wares (2018) sought to

find a simpler form of an ODE model that would better allow for personalization of the parameters and individualized fitting, while still maintaining the ability to describe the data and key biological features for cancer treatment of DC injections and viruses engineered to infect and kill cancer cells. Additionally, models exploring DC therapy for melanoma have tested differing dosing strategies using delay differential equations (DDEs) (Castillo-Montiel *et al.*, 2015; de Pillis *et al.*, 2013; Ludewig *et al.*, 2004). In hopes of using *in silico* tests to reduce the economic burden of searching for and experimenting with new protocols, Castillo-Montiel *et al.* (2015) studied the question of how to improve the efficacy of DC treatment through simulating various treatment strategies and evaluating the sensitivity to changes in parameters.

In studying the effects of DC injections in mice, Ludewig *et al.* (2004) developed a delay differential compartment model representing DC and CTL trafficking. In 2013, de Pillis *et al.* proposed an extension of the Ludewig *et al.* (2004) model to explore tumor response to treatment. We discuss the formulation and main findings of these two papers. Our proposed model modifies the de Pillis *et al.* (2013) model, with several key changes.

2.3.1 Ludewig et al. *(2004) Model*

The Ludewig *et al.* (2004) model was developed to describe the kinetics of the DC-CTL interaction. Their model formulation considered three main areas: (i) initial DC distribution, (ii) DC-CTL interaction in the spleen, and (iii) CTL recirculation between the spleen, blood, and liver. Variables consisted of DCs concentration in the blood, spleen, liver, and lung ($D_{Blood}, D_{Spleen}, D_{Liver}, D_{Lung}$), DC density in the spleen (D), activated CTL (E_a), quiescent 'memory' CTL (E_m), and CTL densities in the blood, spleen, and liver ($E_i^{Blood}, E_i^{Spleen}, E_i^{Liver}$), where $i = a$ denotes activated CTL and $i = m$ denotes memory CTL. The following equations from Ludewig *et al.*

(2004) reflect (i) initial DC distribution:

$$\frac{d}{dt}D_{Blood} = -\underbrace{(\mu_{BS} + \mu_{BLi} + \mu_{BLu} + \mu_{BO})D_{Blood}}_{\text{migration}}, \tag{2.3.1a}$$

$$\frac{d}{dt}D_{Spleen} = \underbrace{\mu_{BS}\frac{Q_{Blood}}{Q_{Spleen}}D_{Blood}}_{\text{migration}}, \tag{2.3.1b}$$

$$\frac{d}{dt}D_{Liver} = \underbrace{\mu_{BLi}\frac{Q_{Blood}}{Q_{Liver}}D_{Blood}}_{\text{migration}}, \tag{2.3.1c}$$

$$\frac{d}{dt}D_{Lung} = \underbrace{\mu_{BLu}\frac{Q_{Blood}}{Q_{Lung}}D_{Blood}}_{\text{migration}} - \underbrace{\mu_{LuO}D_{Lung}}_{\text{elimination}}. \tag{2.3.1d}$$

To consider (ii) DC-CTL interaction in the spleen, Ludewig *et al.* (2004) models as follows:

$$\frac{d}{dt}D = \underbrace{\mu_{BS}\frac{Q_{Blood}}{Q_{Spleen}}D_{Blood}}_{\text{migration}} - \underbrace{a_D D}_{\text{death}} - \underbrace{b_{DE}E_a D}_{\text{death by CTL}}, \tag{2.3.2a}$$

$$\frac{d}{dt}E_a = \underbrace{a_{E_a}(E^{naive} - E_a)}_{\text{homeostasis of naive CTL}} + \underbrace{b_p\frac{D(t-\tau_d)E_a(t-\tau_d)}{\theta_D + D(t-\tau_d)}}_{\text{proliferation}} - \underbrace{r_{am}E_a}_{\text{becoming memory}}$$

$$+ \underbrace{b_a D E_m}_{\text{activation}}, \tag{2.3.2b}$$

$$\frac{d}{dt}E_m = \underbrace{r_{am}E_a}_{\text{becoming memory}} - \underbrace{a_{E_m}E_m}_{\text{death}} - \underbrace{b_a D E_m}_{\text{activation}}. \tag{2.3.2c}$$

To reflect (iii) recirculation of the CTL, Ludewig *et al.* (2004) employs the subsequent equations denoted in vector notation:

$$\frac{d}{dt}\mathbf{E}_i = \underbrace{\mathbf{M}^{(E_i)}\mathbf{E}_i}_{\text{migration}} + \underbrace{\mathbf{I}_i}_{\text{DC-induced CTL response in spleen}} \tag{2.3.3a}$$

with the densities of the CTL subsets given by

$$\mathbf{E}_i(t) = \left[E_i^{Blood}(t), E_i^{Spleen}(t), E_i^{Liver}(t)\right]^T, \quad i = (a, m),$$

and the CTL transfer rates represented by the compartmental matrix

$$\mathbf{M}^{E_i} = \begin{pmatrix} -\mu_{BB} & \mu_{SB}(D_{Spleen}) & \mu_{LB} \\ \mu_{BS} & -\mu_{SB}(D_{Spleen}) & 0 \\ \mu_{BL} & 0 & -\mu_{LB} \end{pmatrix}.$$

Furthermore, Ludewig *et al.* (2004) defines

$$\mu_{SB}(D_{Spleen}) = \mu^*_{SB} + \frac{\Delta\mu}{1 + \frac{D_{Spleen}(t)}{\theta_{shut}}},$$

and the vector-function $I_i(t) = [0, (division - death)_{Spleen}, 0]^T$.

The initial DC distributions are primarily governed by migration. In modeling the DC-CTL interaction in the spleen, DCs are governed by migration from the blood compartment, natural death, and CTL-mediated killing, which is hypothesized to contribute to the downregulation of adaptive immune responses (Ronchese and Hermans, 2001). The activated CTLs are governed by homeostasis, DC-induced proliferation, differentiation to a memory CTL, and activation of memory cells. The memory CTLs are then governed by differentiation to become a memory CTL, natural death, and DC-induced activation. The recirculation of the CTL subsets is modeled by the migration between compartments and, for the spleen compartment, the DC-induced response. The function $\mu_{SB}(D_{Spleen})$ allows for the capture of a DC-induced 'trapping' effect in the spleen, where the retention of T cells in lymph nodes is dependent on the presence of DCs. Numerical simulations in conjunction with data fitting helped in identifying influential parameters in the DC-CTL interaction.

2.3.2 de Pillis et al. *(2013) Model*

In 2013, de Pillis *et al.* proposed a modification and extension of the Ludewig *et al.* (2004) model, most notably by the addition of a tumor compartment. DC therapy seeks to eradicate tumor cells by exciting a tailored immune response. The

de Pillis *et al.* (2013) model captures the dynamics of immune system excitement in the spleen compartment and the dynamics of eradication in the tumor compartment. The blood compartment captures transport between the other two. Their model of 9 DDEs and ODEs consisted of DCs in the blood, tumor, and spleen, activated CTLs in the blood, tumor, and spleen, memory CTLs in the blood and spleen, and tumor cells. The governing equations of the de Pillis *et al.* (2013) model are as follows:

$$\frac{d}{dt}D_{blood} = -\underbrace{\mu_B D_{blood}}_{\text{migration}} + \underbrace{\mu_{TB} D_{tumor}}_{\text{migration}} + \underbrace{v_{blood}(t)}_{\text{injection}} \tag{2.3.4a}$$

$$\frac{d}{dt}E^a_{blood} = \underbrace{\mu_{SB}(D_{spleen})E^a_{spleen}}_{\text{migration}} - \underbrace{\mu_{BB}E^a_{blood}}_{\text{clearance/extravasation}} \tag{2.3.4b}$$

$$\frac{d}{dt}E^m_{blood} = \underbrace{\mu_{SB}(D_{spleen})E^m_{spleen}}_{\text{migration}} - \underbrace{\mu_{BB}E^m_{blood}}_{\text{clearance/extravasation}} \tag{2.3.4c}$$

$$\frac{d}{dt}D_{spleen} = \underbrace{MaxD\left(1 - e^{\left(\frac{-\mu_{BS}D_{blood}}{MaxD}\right)}\right)}_{\text{migration}} - \underbrace{a_D D_{spleen}}_{\text{death}} - \underbrace{b_{DE}E^a_{spleen}D_{spleen}}_{\text{death by CTL}} \tag{2.3.4d}$$

$$\begin{aligned}\frac{d}{dt}E^a_{spleen} = {} & \underbrace{\mu_{BSE}E^a_{blood}}_{\text{migration}} - \underbrace{\mu_{SB}(D_{spleen})E^a_{spleen}}_{\text{migration}} + \underbrace{b_a D_{spleen}E^m_{spleen}}_{\text{activation}} \\ & + \underbrace{a_{E_aS}DC_{on}E_{naive}}_{\text{activation}} - \underbrace{a_{E_aS}E^a_{spleen}}_{\text{death}} - \underbrace{r_{am}E^a_{spleen}}_{\text{becoming memory}} \\ & + \underbrace{b_p\frac{D_{spleen}(t-\tau_D)E^a_{spleen}(t-\tau_D)}{\theta_D + D_{spleen}(t-\tau_D)}}_{\text{proliferation}}\end{aligned} \tag{2.3.4e}$$

$$\begin{aligned}\frac{d}{dt}E^m_{spleen} = {} & \underbrace{r_{am}E^a_{spleen}}_{\text{becoming memory}} - \underbrace{a_{E_m}E^m_{spleen}}_{\text{death}} - \underbrace{b_a D_{spleen}E^m_{spleen}}_{\text{activation}} + \underbrace{\mu_{BSE}E^m_{blood}}_{\text{migration}} \\ & - \underbrace{\mu_{SB}(D_{spleen})E^m_{spleen}}_{\text{migration}}\end{aligned} \tag{2.3.4f}$$

$$\frac{d}{dt}E^a_{tumor} = \underbrace{\mu_{BB}\frac{T}{\alpha + T}E^a_{blood}}_{\text{tumor recruitment}} - \underbrace{a_{E_aT}E^a_{tumor}}_{\text{death}} - \underbrace{cE^a_{tumor}T}_{\text{inactivation by tumor}} \tag{2.3.4g}$$

$$\frac{d}{dt}T = \underbrace{rT\left(1-\frac{T}{k}\right)}_{\text{growth}} - \underbrace{d\frac{\left(\frac{E^a_{tumor}}{T}\right)^l}{s+\left(\frac{E^a_{tumor}}{T}\right)^l}T}_{\text{death by CTL}} \tag{2.3.4h}$$

$$\frac{d}{dt}D_{tumor} = \underbrace{\frac{mT}{q+T}}_{\text{tumor recruitment}} - \underbrace{\mu_{TB}D_{tumor}}_{\text{migration}} - \underbrace{a_D D_{tumor}}_{\text{death}} + \underbrace{v_{tumor}(t)}_{\text{injection}} \tag{2.3.4i}$$

Murine melanoma data from Lee *et al.* (2007) was used in calibrating model parameters. Simulations of tumor growth were validated against the data, then explored through various dosing strategies. They concluded that even with the most aggressive dosing regimen, regardless of whether an intratumoral or intravenous injection, DC treatment could not completely eradicate the tumor after the tumor had already presented itself. However, if DC treatment was administered before the tumor challenge, with the fractional tumor kill rate by CTLs sufficiently large, the tumor was able to be eradicated. Due to the complexity of the model, they were limited in their ability to do mathematical analysis.

2.3.3 Our Model

Our model is based on the de Pillis *et al.* (2013) model with several main modifications. The de Pillis *et al.* (2013) model captures the interactions between DCs, activated and memory CTLs, and tumor cells in spleen, blood and tumor compartments. DC therapy consists of injecting activated DC cells intravenously or intratumorally. DCs then travel through the blood to the spleen where they stimulate the activation of CTLs, which in turn travel through the blood back to the tumor to eradicate tumor cells. In the de Pillis *et al.* (2013) model, the blood is a means of transport for dendritic cells and effector cells between the spleen and the tumor. The primary focus of their work involved examining optimal hypothetical DC treatments. From the perspective of the tumor, the treatment has the net effect of changing the flow of DCs

and active CTLs into the tumor. Since we are chiefly interested in the effectiveness of the therapy, it is reasonable to model some of the interactions away from the tumor compartment implicitly, rather than explicitly. To that end, we introduce a delay to account for the history of the DCs and CTLs as they travel through the blood to the spleen. This allows us to model the activation of naive and memory CTLs in the blood, while implicitly accounting for the fact that activation actually takes place in the spleen. Our first reduced model (intermediate model) of 6 DDEs and ODEs captures the movement between two compartments: the blood and the tumor. In retaining the tumor compartment, the dynamics of excitement and eradication are thus still accounted for. The model consists of DCs in the blood (D_b), DCs in the tumor (D_t), tumor cells (T), memory CTLs in the blood (E_b^m), activated CTLs in the blood (E_b^a), and activated CTLs in the tumor (E_t^a), all of which are represented by the circles in Figure 2.1. We additionally incorporate the effect of competition for space within the tumor compartment by adding negative feedback on the tumor cell growth from activated CTLs and DCs, as also shown in Figure 2.1.

The other major change is the choice of functional response for the interactions between CTLs and DCs. The de Pillis *et al.* (2013) model assumes naive cells are activated at a constant rate when DCs are present. To reflect the biology of the cell-cell interactions better, we instead allow Michaelis-Menten kinetics to govern the interaction between naive CTLs and DCs. Finally, we assume a constant influx of activated CTLs from the spleen to the blood. We refer to the resulting model as the intermediate model. Figure 2.1 provides a diagram of the intermediate model.

The intermediate model is given by the following system:

$$\frac{dD_b}{dt} = \underbrace{v_b(t)}_{\text{injection}} + \underbrace{\mu_{TB} D_t}_{\text{migration}} - \underbrace{\mu_{BT} D_b \frac{T}{K_T + T}}_{\text{tumor recruitment}} - \underbrace{\delta_D D_b}_{\text{death}}, \tag{2.3.5a}$$

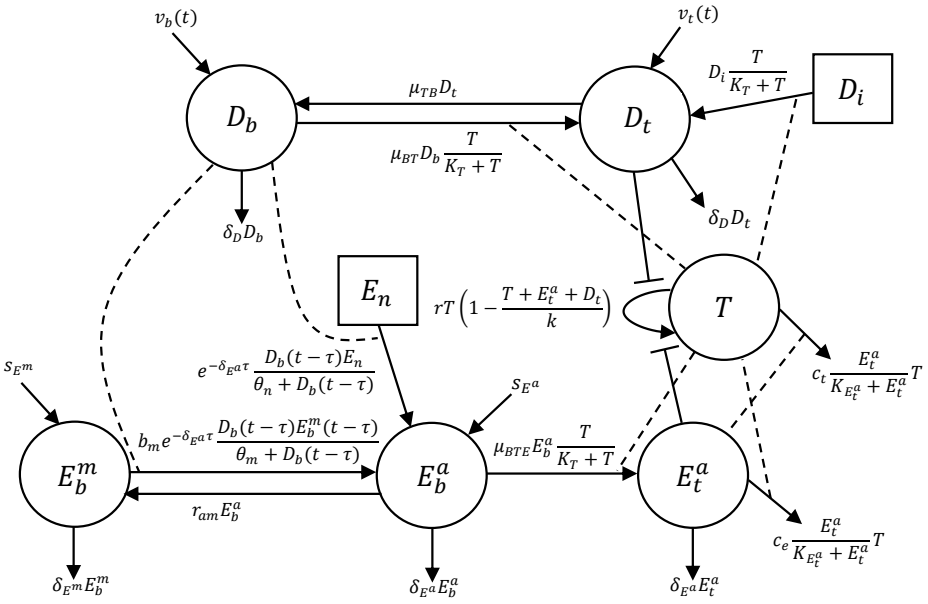

Figure 2.1: The Interactions Governing (2.3.5). Dashed Lines Represent a Catalytic Effect, Flat-Headed Arrows Represent an Inhibitory Effect, and Straight Arrows Connecting Populations Represent Movement Between Populations, Whether Through Entering a New Compartment or Becoming Activated/Inactivated. The Circles Represent the Variables of the System, While Squares Represent Cell Populations Per Day Assumed to Be Constant. $D_b, D_t, E_b^m, E_b^a, E_t^a, T, E_n$, and D_i Represent DCs in the Blood, DCs in the Tumor, Memory CTLs in the Blood, Activated CTLs in the Blood, Activated CTLs in the Tumor, Tumor Cells, the Number of Naive CTLs Activated/Proliferating Per Day, and the Number of Immature DCs Being Activated Per Day. The μ Parameters Represent Maximum Transfer Rates Between Compartments, δ Parameters Reflect Death of the Cell Populations, and s Parameters Act As Source Terms. Intratumoral and Intravenous DC Injections Are Given by $v_t(t)$ and $v_b(t)$ Respectively. r, k, c_t, c_e, b_m, and r_{am} Reflect the Tumor Cell Growth Rate, Tumor Cell Carrying Capacity, Maximum Rate Activated CTLs Kill the Tumor Cells, Maximum Rate Tumor Cells Inactivate CTLs, Maximum Activation/Proliferation Rate of Memory CTLs by DCs, and Natural Inactivation Rate of Activated CTLs. All Parameter Values and Descriptions Are Listed in Table C.1.

$$\frac{dD_t}{dt} = \underbrace{v_t(t)}_{\text{injection}} + \underbrace{D_i \frac{T}{K_T + T}}_{\text{activation}} + \underbrace{\mu_{BT} D_b \frac{T}{K_T + T}}_{\text{tumor recruitment}} - \underbrace{\mu_{TB} D_t}_{\text{migration}} - \underbrace{\delta_D D_t}_{\text{death}}, \tag{2.3.5b}$$

$$\frac{dE_b^a}{dt} = \underbrace{s_{E^a}}_{\text{source}} + \underbrace{e^{-\delta_{E^a}\tau} \frac{D_b(t-\tau)E_n}{\theta_n + D_b(t-\tau)}}_{\text{activation/proliferation}} + \underbrace{b_m e^{-\delta_{E^a}\tau} \frac{D_b(t-\tau)E_b^m(t-\tau)}{\theta_m + D_b(t-\tau)}}_{\text{activation/proliferation}}$$

$$- \underbrace{r_{am} E_b^a}_{\text{becoming memory}} - \underbrace{\mu_{BTE} E_b^a \frac{T}{K_T + T}}_{\text{migration}} - \underbrace{\delta_{E^a} E_b^a}_{\text{death}}, \tag{2.3.5c}$$

$$\frac{dE_t^a}{dt} = \underbrace{\mu_{BTE} E_b^a \frac{T}{K_T + T}}_{\text{migration}} - \underbrace{c_e \frac{E_t^a}{K_{E_t^a} + E_t^a} T}_{\text{inactivation by tumor}} - \underbrace{\delta_{E^a} E_t^a}_{\text{death}}, \tag{2.3.5d}$$

$$\frac{dE_b^m}{dt} = \underbrace{s_{E^m}}_{\text{source}} - \underbrace{b_m e^{-\delta_{E^a}\tau} \frac{D_b(t-\tau)E_b^m(t-\tau)}{\theta_m + D_b(t-\tau)}}_{\text{activation/proliferation}} + \underbrace{r_{am} E_b^a}_{\text{becoming memory}} - \underbrace{\delta_{E^m} E_b^m}_{\text{death}}, \tag{2.3.5e}$$

$$\frac{dT}{dt} = \underbrace{rT\left(1 - \frac{T + E_t^a + D_t}{k}\right)}_{\text{growth}} - \underbrace{c_t \frac{E_t^a}{K_{E_t^a} + E_t^a} T}_{\text{death by CTL}}. \tag{2.3.5f}$$

A description of the model parameters, their values for fitting along with the related sources from the literature are given in Table C.1. The parameters unable to be found in literature were fixed using melanoma data from Lee *et al.* (2007).

The behavior of the DCs moving between the blood and tumor compartments is captured through Equations (2.3.5a) and (2.3.5b) respectively. The functions $v_b(t)$ and $v_t(t)$ are source terms modeling intravenous and intratumoral DC injections. As functions of time, these source terms allow for numerical testing of dosing strategies. DC transfer from the blood to the tumor occurs at a maximum rate of μ_{BT}, with the population of tumor cells catalyzing the movement. Once the DCs are sensitized and loaded with tumor antigens, they leave the tumor to migrate towards the lymphoid organs via the blood at a maximum rate of μ_{TB} to interact with the CTLs. A daily number of immature DCs, D_i, become sensitized and activated as they interact with

the tumor cells. Following standard practice as in Kirschner and Panetta (1998), the model assumes Michaelis-Menten kinetics in all immune and tumor-immune interactions. The Michaelis-Menten kinetics allow for a representation of saturated immune responses and can also capture the effects of only portions of the tumor being able to interact with the immune cells at a time.

The activated CTLs migrate between the blood and tumor compartments as given by Equations (2.3.5c) and (2.3.5d). The prolonged interaction between DCs and CTLs required for activation and the time accounting for their travel from the lymphoid organs are represented by a delay in interactions between memory and naive CTLs and DCs. Through these interactions with the DCs, the naive and memory CTLs are instructed to multiply at maximum rates b_n and b_m respectively. Following an absence of contact with the tumor-associated antigen, activated CTLs in the blood return to a resting memory state at rate r_{am} (Berard and Tough, 2002). We assume a constant influx s_{E^a} of activated CTLs from the spleen to the blood. The presence of the tumor helps to catalyze the migration of the activated CTLs from the blood to the tumor at a maximum rate of μ_{BTE}. Once in the tumor, the activated CTLs interact with the tumor, becoming inactivated by the tumor cells at a rate of c_e.

Equation (2.3.5e) governs the dynamics of the memory CTLs in the blood. We assume a constant influx s_{E^m} of memory CTLs from the spleen to the blood. Additionally, the activation of memory CTLs acts as a loss, and inactivation of E_b^a acts as a source term.

The first term of the right-hand side of Equation (2.3.5f) accounts for tumor growth. In a variety of models, tumor growth has been modeled with a logistic (de Pillis *et al.*, 2013; Nikolopoulou *et al.*, 2018), exponential (Portz and Kuang, 2013), power law (Dethlefsen *et al.*, 1968), or Gompertzian (Castillo-Montiel *et al.*, 2015; Norton, 1988) approach. We assume competition for space from the activated

CTLs and DCs in the tumor compartment negatively impacts the tumor growth. The activated CTLs kill the tumor cells at rate c_t. By using Michaelis-Menten kinetics to govern the killing of the tumor cells, we are able to capture the effects of melanoma being a solid tumor, where immune cells can only contact fractions of the tumor at a time.

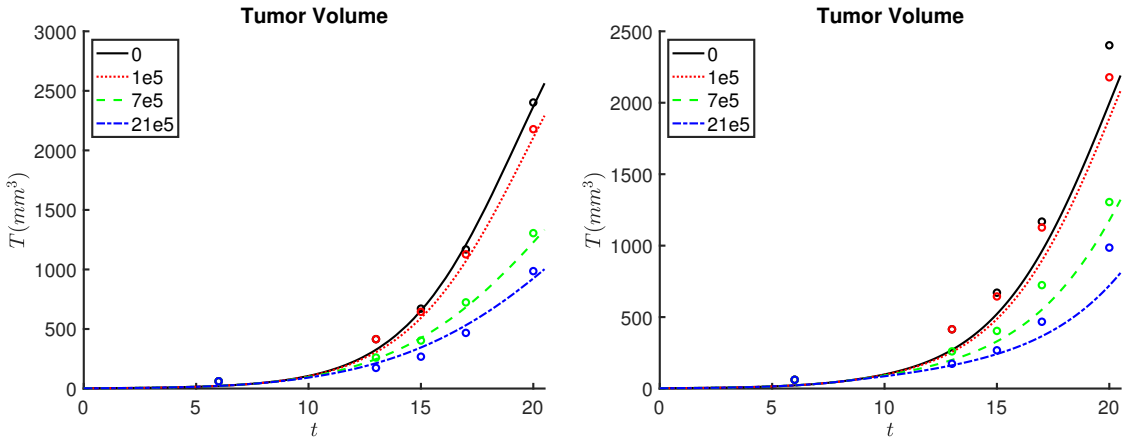

(a) Intermediate Model (2.3.5) (b) de Pillis *et al.* (2013) Model

Figure 2.2: The Fit to the Data from Lee *et al.* (2007) with (a) the Intermediate DDE and ODE Model (2.3.5), and (b) the de Pillis *et al.* (2013) Model. Mean Relative Errors for the Fits Are Given in Table 2.3.

To determine the validity of our biological assumptions and simplifications, we compare our model to the de Pillis *et al.* (2013) model using the clinical data in Lee *et al.* (2007), extracted by means of WebPlotDigitizer (Rohatgi, 2019). The mice experiments in Lee *et al.* (2007) examine the tumor volume with and without DC treatment. All mice were injected with 5×10^5 B16-F10 cells to induce malignant melanomas. Intratumoral doses ranging from 0 to 21×10^5 DCs were administered 6, 8, and 10 days following the B16-F10 cell inoculation. In computing tumor volume, we assume tumor cells are spherical. We approximate the diameters to be 20 μm, in accordance with the mean B16-F10 cell diameter recorded in recent measurements

(Polo-Parada *et al.*, 2017).

The MATLAB solver ODE15S is employed in numerically solving the system to produce Figure 2.2, as well as all figures in this chapter, unless otherwise explicitly noted. The Nelder-Mead simplex algorithm (Lagarias *et al.*, 1998) is used to find the free parameters that minimize the mean squared error (MSE) between the model simulations and the mice data. From Figure 2.2a, we observe our intermediate model can closely reproduce the experimentally observed tumor reductions from various doses of DCs. While fitting data does not necessarily validate mathematical models, the ability of our model to describe clinical data does help justify incorporating our additional biological details and simplifications. Additionally, we note that even though the intermediate model is simpler than the de Pillis *et al.* (2013) model, it is comparable in terms of fitting, as outlined in Table 2.3 and demonstrated in Figure 2.2.

The solutions of system (2.3.5) should remain non-negative and bounded, as the model captures the cell populations over time. We establish these properties in the following.

Proposition 2.3.1 *Suppose that $v_b(t)$ and $v_t(t)$ are smooth, bounded functions of t, with $v_b(t) + v_t(t) \leq v$. All solutions in $\mathbb{R}^6_+$ exist for all $t > 0$ and are attracted by the forward invariant compact set*

$$\mathcal{O} = \{(D_b, D_t, E_b^a, E_t^a, E_b^m, T) \in \mathbb{R}^6_+ : D_b + D_t \leq \frac{v + D_i}{\delta_D}, E_b^a + E_t^a \leq C_0,$$
$$E_b^m \leq \frac{s_E^m + r_{am} C_0}{\delta_E^m}, T \leq k\},$$

where $C_0 = (s_E^a + s_E^m + E_n e^{-\delta_E^a \tau})/\delta_E^m$.

Proof. We first show $\mathbb{R}^6_+$ is positively invariant. If not, there exists some $t_1 > 0$ such that $D_b(t_1) = 0, D_t(t_1) = 0, E_b^a(t_1) = 0, E_b^m(t_1) = 0$, or $T(t_1) = 0$. Since (2.3.5f)

takes the form $\dot{T} = TF(E_t^a, D_t, T)$, then

$$T(t_1) = T(0)\exp\left(\int_0^{t_1} F(E_t^a(s), D_t(s), T(s)\right) ds > 0,$$

a contradiction. We then examine the case where $E_t^a(t_1) = 0$. Then $\dot{E}_t^a(t) \geq -\delta_E^a E_t^a$, $\forall t \in [0, t_1]$. Thus, $E_t^a(t_1) \geq E_t^a(0)e^{-\delta_E^a t_1} > 0$, a contradiction. Similar arguments extend to the remaining variables, and $\mathbb{R}_+^6$ is forward invariant.

By (2.3.5f), it follows that $\dot{T} \leq rT(1 - \frac{T}{k})$. Then $\limsup_{t\to+\infty} T(t) \leq k$. Let $D = D_b + D_t$. Since v_b and v_t are bounded, there exists a positive constant v such that $\dot{D} \leq v + D_i - \delta_D D$. Therefore, $\limsup_{t\to+\infty}(D_b(t) + D_t(t)) \leq \frac{v+D_i}{\delta_D}$. Take $E_b = E_b^a + E_b^m$, and let $C_0 = \frac{s_E^a + s_E^m + E_n e^{-\delta_E^a \tau}}{\delta_E^m}$. Since we always have that $\delta_E^a \geq \delta_E^m$ by definition, $\dot{E}_b \leq s_E^m + s_E^a + E_n e^{-\delta_E^a \tau} - \delta_E^m E_b$, and $\limsup_{t\to+\infty}(E_b^a(t) + E_b^m(t)) \leq C_0$. As $E_b^a \leq C_0$, then $\dot{E}_b^m \leq s_E^m + r_{am}C_0 - \delta_E^m E_b^m$. Hence $\limsup_{t\to+\infty} E_b^m(t) \leq \frac{s_E^m + r_{am}C_0}{\delta_E^m}$. As long as the solutions to system (2.3.5) exist, the inequalities hold. The boundedness implies the solution exists for all $t > 0$, and the proof is complete. □

Having formulated the intermediate model, we go on to make several simplifying assumptions supported by biological observations. Through studying a variety of species, including both mice (Tough and Sprent, 1994) and humans (Michie *et al.*, 1992; McCune *et al.*, 2000), the memory T cells have been found to turn over faster than the naive T cells. We assume this turnover is happening rapidly such that the memory CTLs are at a quasi-steady state. Additionally, since the model is only intended to assess treatment for a short period of time, we can reasonably assume the DC movement between the blood and tumor compartments is independent of the tumor size during the brief period being considered. We simplify the representation of cell-cell interactions by supposing mass action kinetics as opposed to Michaelis-Menten. We assume that the proportion of activated CTLs in the tumor, $\frac{E_t^a}{E_t^a + E_b^a}$, is approximately constant. This constant ratio allows us to combine (2.3.5c) and

(2.3.5d) into a single equation for the effector cells, given by (2.3.6c). These assumptions lead to further model reductions and the formulation of the reduced model (2.3.6), which is analytically tractable.

Table 2.1: Variables of the Simplified Model (in cells)

Variable	Description
D_b	Dendritic cells in the blood
D_t	Dendritic cells in the tumor
E	Activated CTLs
T	Tumor cells

The variables of the simplified model, their meanings, and their units are listed in Table 2.1. Parameter values are outlined in Table C.2. The simplified system takes the following form:

$$\frac{dD_b}{dt} = v_b(t) - \mu_{BT} D_b + \mu_{TB} D_t - \delta_D D_b \tag{2.3.6a}$$

$$\frac{dD_t}{dt} = v_t(t) + D_i T + \mu_{BT} D_b - \mu_{TB} D_t - \delta_D D_t \tag{2.3.6b}$$

$$\frac{dE}{dt} = s_E + cD_b - c_e ET - (r_{am} + \delta_E)E \tag{2.3.6c}$$

$$\frac{dT}{dt} = rT\left(1 - \frac{T + E + D_t}{k}\right) - c_t ET \tag{2.3.6d}$$

The assumptions that lead to the reduced model are further justified by a fit to clinical data, as displayed in Figure 2.3.

Despite the reductions made, the model remains able to describe the data from all four trials with a single set of fixed, biologically reasonable parameters. As the simplified model is comparable in terms of fitting to both the de Pillis *et al.* (2013) model and the intermediate model, as outlined in Table 2.2 and Figures 2.2 and 2.3, it is worth mathematically studying to extract insights since the complexity of the

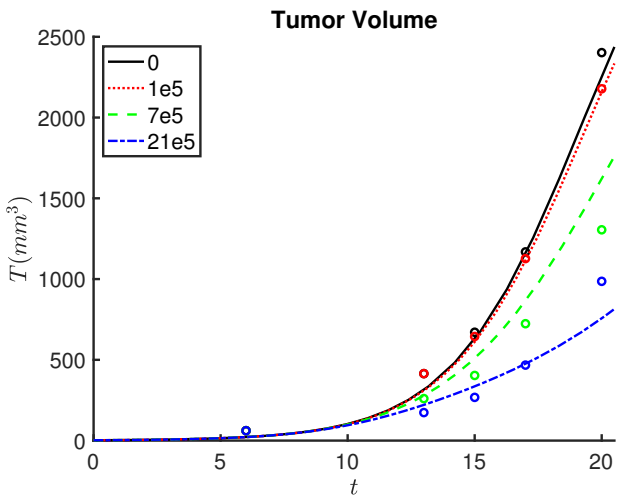

Figure 2.3: The Fit to the Data From Lee *et al.* (2007) with the Simplified ODE Model (2.3.6). The Mean Relative Error for the Fit Is Given in Table 2.3.

other models allows for far less analysis.

Table 2.2: Mean Relative Errors for Various Model Formulations

Model	**Mean Relative Error**
System (2.3.5): Intermediate Model (DDE and ODE)	0.204766
System (2.3.6): Simplified Model (ODE)	0.230647
de Pillis *et al.* (2013) Model	0.291335

2.4 Preliminary Analysis

The analysis that follows is based on the reduced model given by system (2.3.6). In this Section, we establish basic results of the model like well-posedness, dissipativity, and the existence of equilibria. In addition, we determine the basic reproduction number $\mathcal{R}_0$. Unless otherwise stated, we assume that all of the parameters of (2.3.6) are positive.

Proposition 2.4.1 *Suppose that $v_b(t)$ and $v_t(t)$ are smooth, bounded functions of t. Then system* (2.3.6) *is well-posed and point dissipative.*

Proof. Let $x = (D_b, D_t, E, T)$ and let ϕ_t be the flow of (2.3.6). Writing (2.3.6) as the vector equation $x = f(t, x)$, since $v_b(t)$ and $v_t(t)$ are smooth, we have that f is continuously differentiable and $x = f(t, x)$ is well-posed. By examining the flow on the boundary, we see that for $i = 1, 2, 3$, if $x_i = 0$ then $(\phi_t(x))_i > 0$ for $t > 0$. The subspace $\{x \in \mathbb{R}^4 | T = 0\}$ is fully invariant. By the previous arguments, the restriction of this fully invariant to its intersection with the non-negative orthant is forward invariant. By Grönwall's inequality, if $x_4 > 0$, then $(\phi_t(x))_4 > 0$.

It follows that $\dot{T} \leq rT(1 - \frac{T}{k})$. Given $T(0) \geq 0$, given $\varepsilon > 0$, there exists t_0 such that $T(t) < k + \varepsilon$ for all $t > t_0$. Since v_b and v_t are bounded, there exist positive constants C_1 and C_2 such that if $D = D_b + D_t$, then $\dot{D} < C_1 - C_2 D$ for $t > t_0$. It follows that given $\varepsilon > 0$, there exists $t_1 > t_0$ such that $D(t) = D_b(t) + D_t(t) < \frac{C_1}{C_2} + \varepsilon$ for all $t > t_1$. Taken together, there exists positive constants C_3 and C_4 such that $\dot{E} < C_3 - C_4 E$ for $t > t_1$. Given $\varepsilon > 0$, there exists $t_2 > t_1$ such that $E(t) < \frac{C_3}{C_4} + \varepsilon$ for all $t > t_2$. Fix $\varepsilon > 0$ and let $C_5 = \max(k, \frac{C_1}{C_2}, \frac{C_3}{C_4}) + \varepsilon$. For any non-negative initial condition x, there exists $t_2 > 0$ such that $\phi_{t+t_2}(x) \in [0, C_5]^4$ for all $t > 0$. Thus, system (2.3.6) is point dissipative. □

For the purpose of simplifying the mathematical analysis we make the assumption that $v_b(t) = v_b$ and $v_t(t) = v_t$ are constant and non-negative, modeling as if a continuous dose is being administered through an IV. The next result is the existence and uniqueness of a tumor-free equilibrium.

Proposition 2.4.2 *Let $v_b(t) = v_b$ and $v_t(t) = v_t$ be constant and non-negative. System* (2.3.6) *admits the unique tumor-free equilibrium $E_0 = (D_{b*}, D_{t*}, E_*, 0)$.*

Proof. Suppose $T = 0$, then $\dot{T} = 0$, and (2.3.6a) and (2.3.6b) decouple from (2.3.6)

to form the planar cooperative system:

$$\begin{aligned} \dot{D}_b &= v_b - \delta_D D_b - \mu_{BT} D_b + \mu_{TB} D_t \\ \dot{D}_t &= v_t - \delta_D D_t + \mu_{BT} D_b - \mu_{TB} D_t, \end{aligned} \tag{2.4.7}$$

which admits the unique equilibrium (D_{b*}, D_{t*}) given by

$$D_{b*} = \frac{\mu_{TB} v_t + (\delta_D + \mu_{TB}) v_b}{\delta_D(\delta_D + \mu_{BT} + \mu_{TB})}; \quad D_{t*} = \frac{(\delta_D + \mu_{BT}) v_t + \mu_{BT} v_b}{\delta_D(\delta_D + \mu_{BT} + \mu_{TB})}.$$

Substituting $T = 0$ and $D_b = D_{b*}$ into (2.3.6c) yields

$$E_* = \frac{s_e + c D_{b*}}{\widetilde{\delta}_E}.$$

□

The treatment we are considering involves tailoring the immune system to launch an enhanced response targeting tumor cells. From the perspective of the immune system in this context, tumor cells can be viewed as similar to an infectious disease. We borrow the notion of the basic reproduction number from the study of infectious disease dynamics. The basic reproduction number, denoted $\mathcal{R}_0$, is defined as the average number of secondary infections generated by a single infectious individual in a totally susceptible population during the lifetime of the infectious individual. In the present context, the basic reproduction number can be viewed as a ratio of the proliferation potential of a tumor cell to the strength of a combination of the immune response and crowding effects. The basic reproduction number can be calculated using the next generation matrix approach (Diekmann *et al.*, 1990; van den Driessche and Watmough, 2002).

Proposition 2.4.3 *Let $v_b(t) = v_b$ and $v_t(t) = v_t$ be constant and non-negative. The basic reproduction number $\mathcal{R}_0$ is given by*

$$\mathcal{R}_0 = \frac{k}{\left(1 + \frac{k c_t}{r}\right) E_* + D_{t*}}. \tag{2.4.8}$$

Proof. Note $\dot{T} = \mathcal{F}(D_b, D_t, E, T) - \mathcal{V}(D_b, D_t, E, T)$, where $\mathcal{F}$ represents the new infections (tumor cells) and $\mathcal{V}$ represents the rate of tumor cells leaving the system. We can then decouple (2.3.6d) from the rest of (2.3.6) when close to the disease-free equilibrium, E_0. Thus $\frac{dT}{dt} = (F - V)T$. We then have:

$$F = \left(\frac{\partial \mathcal{F}}{\partial T}\right)\Bigg|_{E_0} = r; \qquad V = \left(\frac{\partial \mathcal{V}}{\partial T}\right)\Bigg|_{E_0} = \frac{r}{k}(E_* + D_{t*}) + c_t E_*.$$

Now the next generation operator $FV^{-1} = \frac{k}{\left(1+\frac{kc_t}{r}\right)E_* + D_{t*}}$. Therefore,

$$\mathcal{R}_0 = \frac{k}{\left(1 + \frac{kc_t}{r}\right) E_* + D_{t*}}, \tag{2.4.9}$$

where E_* and D_{t*} correspond to the steady states of the activated CTLs and DCs in the tumor when the system is tumor-free. □

Remark 2.4.4 *Suppose that r is the dominant eigenvalue of the Jacobian of* (2.3.6) *evaluated at E_0. Then r and $\mathcal{R}_0 - 1$ have the same sign. In models of infectious disease dynamics, it is common that the disease-free equilibrium undergoes a trans-critical bifurcation as $\mathcal{R}_0$ increases through the critical value $\mathcal{R}_0 = 1$ resulting in the emergence of a unique positive equilibrium. However, system* (2.3.6) *produces more complicated dynamics. While it is indeed the case that* (2.3.6) *admits a unique positive equilibrium when $\mathcal{R}_0 > 1$, it may admit two positive equilibria when $\mathcal{R}_0 < 1$. We will see that the existence of these two positive equilibria is the result of a backward bifurcation in Section 2.5.*

Proposition 2.4.5 *Let $v_b(t) = v_b$ and $v_t(t) = v_t$ be constant and non-negative. If $\mathcal{R}_0 \geq 1$, then there exists a unique positive equilibrium, E_1. For k sufficiently large, there exists constants C_6 and $\mathcal{R}_{crit}$ such that if $c_e > C_6$ and $\mathcal{R}_{crit} < \mathcal{R}_0 < 1$, then in addition to E_1, there exists an additional positive equilibrium, E_2.*

Proof. Suppose $T^* > 0$. From (2.3.6a),

$$D_b^* = \frac{\mu_{TB}}{\delta_D + \mu_{BT}} D_t^* + \frac{v_b}{\delta_D + \mu_{BT}}. \tag{2.4.10}$$

From $\dot{D}_t = 0$, we have

$$D_t^* = \frac{D_i(\delta_D + \mu_{BT})}{\delta_D(\delta_D + \mu_{BT} + \mu_{TB})} T^* + \frac{v_t(\delta_D + \mu_{BT}) + v_b\mu_{BT}}{\delta_D(\delta_D + \mu_{BT} + \mu_{TB})} = c_4 T^* + D_{t*}. \tag{2.4.11}$$

Combining (2.4.10) and (2.4.11) yields

$$D_b^* = \frac{D_i\mu_{TB}}{\delta_D(\delta_D + \mu_{BT} + \mu_{TB})} T^* + \frac{v_t\mu_{TB} + v_b(\delta_D + \mu_{TB})}{\delta_D(\delta_D + \mu_{BT} + \mu_{TB})} = c_3 T^* + D_{b*}. \tag{2.4.12}$$

From $\dot{T} = 0$, $T^* = 0$ or

$$E^* = -\frac{(1 + c_4)}{1 + \frac{kc_t}{r}} T^* + \frac{k - D_{t*}}{1 + \frac{kc_t}{r}}. \tag{2.4.13}$$

Recall that for $T(0) > 0$, after finite time we have $0 < T < k + \varepsilon$. Therefore, $(\dot{D}_b, \dot{D}_t)^T$ is greater than the monotone planar system (2.4.7). It follows that $D_b^* > D_{b*} - \varepsilon$ in finite time. Therefore, after finite time $\dot{E} > s_E + cD_{b*} - (\widetilde{\delta}_E + k)E$. Thus, we must have that $E^* > 0$.

Substituting (2.4.12) and (2.4.13) into $\dot{E} = 0$ yields $g(T) = \mathcal{A}_0 T^2 + \mathcal{A}_1 T + \mathcal{A}_2 = 0$ where:

$$\mathcal{A}_0 = \frac{c_e(1 + c_4)}{1 + \frac{kc_t}{r}}, \tag{2.4.14a}$$

$$\mathcal{A}_1 = cc_3 + \frac{\widetilde{\delta}_E(1 + c_4)}{1 + \frac{kc_t}{r}} - \frac{c_e(k - D_{t*})}{1 + \frac{kc_t}{r}}, \tag{2.4.14b}$$

$$\mathcal{A}_2 = \frac{\widetilde{\delta}_E}{1 + \frac{kc_t}{r}} \left[\left(1 + \frac{kc_t}{r}\right) \frac{s_E + cD_{b*}}{\widetilde{\delta}_E} + D_{t*} - k \right]. \tag{2.4.14c}$$

Note that $\operatorname{sgn}(\mathcal{A}_2) = \operatorname{sgn}(1 - \mathcal{R}_0)$. If $\mathcal{R}_0 > 1$, then $\mathcal{A}_2 < 0$ and $g(T)$ is a concave up parabola with $g(0) < 0$. Therefore, there exists a unique positive solution, T_1^* of $g(T) = 0$ when $\mathcal{R}_0 > 1$. In light of equations (2.4.12), (2.4.11) and (2.4.13),

$E_1 = (D_b^*(T_1^*), D_t^*(T_1), E^*(T_1^*), T_1^*)$ is the unique positive equilibrium of (2.3.6) when $\mathcal{R}_0 > 1$.

Now, $\mathcal{R}_0$ is monotonically decreasing in s_E with $\lim_{s_E \to \infty} \mathcal{R}_0 = 0$. Rewriting $\mathcal{A}_2 = s_E + cD_{b*} - \tilde{\delta}_E \frac{k - D_{t*}}{1 + \frac{kc_t}{r}}$, it is clear that $\lim_{s_E \to \infty} \mathcal{A}_2 = +\infty$. Suppose that initially $\mathcal{R}_0 > 1$, as in the previous case. We increase s_E until $\mathcal{R}_0 = 1$. Then $\mathcal{A}_2 = 0$ and $g(T^*)$ has two real roots, $T^* = 0$ and $T^* = \frac{-\mathcal{A}_1}{\mathcal{A}_0}$. If

$$c_e > C_6 = \frac{1 + \frac{kc_t}{r}}{k - D_{t*}} \left(\tilde{\delta}_E \frac{1 + c_4}{1 + \frac{kc_t}{r}} + cc_3 \right), \tag{2.4.15}$$

then $\mathcal{A}_1 < 0$ and $T^* = \frac{-\mathcal{A}_1}{\mathcal{A}_0} > 0$. By continuity, there exists $\delta > 0$ such that $g(T^*)$ has two real distinct positive roots for $1 - \delta < \mathcal{R}_0 < 1$. Now consider the discriminant, $\mathscr{D} = \mathcal{A}_1^2 - 4\mathcal{A}_0\mathcal{A}_2$, of g. If $\mathcal{R}_0 = 1$, then $\mathscr{D} = \mathcal{A}_1^2 > 0$. Since $\mathcal{A}_2$ monotonically increases from zero as we decrease $\mathcal{R}_0$ (say by increasing s_E), there exists a unique s_1 such that if $s_E = s_1$, then $\mathcal{A}_2 = \frac{\mathcal{A}_1^2}{4\mathcal{A}_0}$ which implies that $\mathscr{D} = 0$. Let

$$\mathcal{R}_{crit} = \frac{k}{(1 + \frac{kc_t}{r}) \frac{s_1 + cD_{b*}}{\tilde{\delta}_E} + D_{t*}}. \tag{2.4.16}$$

It follows that if $c_e > C_6$, then $g(T^*)$ has two positive roots $T_1^* > T_2^*$ for $\mathcal{R}_{crit} < \mathcal{R}_0 < 1$. Setting $E_i = (D_b^*(T_i^*), D_t^*(T_i), E^*(T_i^*), T_i^*)$ for $i = 1, 2$ completes the proof. □

The next two results are related to the stability of the tumor-free equilibrium, E_0. It was noted in the proof of Proposition 2.4.1 that the subspace $\{(D_b, D_t, E, T) \in \mathbb{R}^4 | T = 0\}$ is fully invariant. Let X_2 be the intersection of this fully invariant subspace with the non-negative orthant. From examination of the flow on the boundary, it follows that X_2 is forward invariant. The following result deals with the stability of the tumor-free equilibria in X_2. At first glance, this result may appear to lack biological relevance. However, it is critical ground work for later results regarding the existence or eradication of the tumor.

Proposition 2.4.6 *Let $v_b(t) = v_b$ and $v_t(t) = v_t$ be constant and non-negative. The tumor-free equilibrium is globally asymptotically stable* (G.A.S.) *in the forward invariant boundary subspace X_2.*

Proof. As noted in the proof of Proposition 2.4.2, when $T = 0$, (2.3.6a) and (2.3.6b) decouple from system (2.3.6) to form the monotone planar system (2.4.7) which admits the equilibrium (D_{b*}, D_{t*}). Let $D = D_b + D_t$. Then $\dot{D} = \dot{D}_b + \dot{D}_t = v - \delta_D D$, where $v = v_b + v_t$. Thus, for any $D(0) \geq 0$,

$$\lim_{t\to\infty} D(t) = \lim_{t\to\infty} D_b(t) + D_t(t) = \frac{v}{\delta_D}.$$

It follows from application of Theorem 2.2 of Smith (1995), that solutions of (2.4.7) with non-negative initial conditions converge to (D_{b*}, D_{t*}). Therefore, for any $\epsilon > 0$, solutions of (2.4.7) with non-negative initial conditions enter $\{(D_b, D_t) : |D_b - D_{b*}| < \epsilon\}$ in finite time.

The remaining equation describing the flow in X_2 is given by

$$\dot{E} = s_E + cD_b - \widetilde{\delta}_E E,$$

where $\widetilde{\delta}_E = r_{am} + \delta_E$. For any $\epsilon > 0$, for any initial data in X_2, after finite time

$$s_E + c(D_{b*} - \epsilon) - \widetilde{\delta}_E E < \dot{E} < s_E + c(D_{b*} + \epsilon) - \widetilde{\delta}_E E.$$

The result follows by the comparison principle. □

Next we consider the stability of E_0 in the in the full space $\bar{\mathbb{R}}^4_+$. At this stage, we are limited to local stability analysis.

Proposition 2.4.7 *Let $v_b(t) = v_b$ and $v_t(t) = v_t$ be constant and non-negative. $E_0 = (D_{b*}, D_{t*}, E_*, 0)$ is locally asymptotically stable when $\mathcal{R}_0 < 1$ and unstable when $\mathcal{R}_0 > 1$.*

Proof. The Jacobian of system (2.3.6) evaluated at the tumor-free equilibrium E_0 is given by

$$\mathbf{J}|_{E_0} = \begin{pmatrix} -\mu_{BT} - \delta_D & \mu_{TB} & 0 & 0 \\ \mu_{BT} & -\mu_{TB} - \delta_D & 0 & D_i \\ c & 0 & -\widetilde{\delta}_E & -c_e E_* \\ 0 & 0 & 0 & r\left(1 - \frac{1}{\mathcal{R}_0}\right) \end{pmatrix}, \tag{2.4.17}$$

which admits eigenvalues

$$\lambda_1 = r\left(1 - \frac{1}{\mathcal{R}_0}\right); \lambda_2 = -\widetilde{\delta}_E; \lambda_3 = -\delta_D; \lambda_4 = -(\delta_D + \mu_{TB} + \mu_{BT}).$$

Thus, E_0 is locally asymptotically stable when $\mathcal{R}_0 < 1$. E_0 is unstable when $\mathcal{R}_0 > 1$. □

2.5 Backward Bifurcation and Bistability

In this section we return attention to the possibility of the existence of two positive equilibria described in Proposition 2.4.5. In Remark 2.4.4 we allude to the fact that, in epidemiological models, it is typical for a disease-free equilibrium to undergo a transcritical bifurcation with a unique positive equilibrium as $\mathcal{R}_0$ increases through the critical value of 1. Another possibility is that of a backward bifurcation. Backward bifurcations in epidemiological models have been associated with modeling assumptions that lead to loops among infected and susceptible classes as a result of reinfection or waning immunity, for example. Our next result is a proof of the existence of a backward bifurcation in system (2.3.6), via analysis of the center manifold and Theorem 4.1 of Castillo-Chavez and Song (2004), reproduced below for convenience. Interestingly, this backward bifurcation relies on the rate that activated CTLs are inactivated as a result of interacting with tumor cells. One feature of backward bifurcations in epidemiological models is that they can generally be eliminated by

assuming mass action, rather than frequency-dependent functional response. Similar to a tuberculosis model outlined in Gumel (2012), it is possible to exhibit backward bifurcation in models with mass action functional response, and system (2.3.6) is an example of that.

Theorem 1 (Castillo-Chavez and Song (2004)) *Consider the following general system of ODEs with a parameter* ϕ :

$$\frac{dx}{dt} = f(x, \phi), \qquad f : \mathbb{R}^n \times \mathbb{R} \to \mathbb{R} \text{ and } f \in \mathbb{C}^2(\mathbb{R}^n \times \mathbb{R}), \tag{2.5.18}$$

where 0 *is an equilibrium point of the system (that is,* $f(0, \phi) \equiv 0$ *for all* ϕ*) and assume*

A1: $A = D_x f(0,0) = \left(\frac{\partial f_i}{\partial x_j}(0,0)\right)$ *is the linearization matrix of system* (2.5.18) *around the equilibrium* 0 *with* ϕ *evaluated at* 0*. Zero is a simple eigenvalue of* A *and all other eigenvalues of* A *have negative real parts;*

A2: Matrix A *has a nonnegative right eigenvector* w *and a left eigenvector* v *corresponding to the zero eigenvalue.*

Let f_k *be the* k*th component of* f *and*

$$a = \sum_{k,i,j=1}^{n} v_k w_i w_j \frac{\partial^2 f_k}{\partial x_i \partial x_j}(0,0), \tag{2.5.19}$$

$$b = \sum_{k,i=1}^{n} v_k w_i \frac{\partial^2 f_k}{\partial x_i \partial \phi}(0,0). \tag{2.5.20}$$

The local dynamics of (2.5.18) *around* 0 *are totally determined by* a *and* b*.*

i. $a > 0, b > 0$*. When* $\phi < 0$ *with* $|\phi| \ll 1, 0$ *is locally asymptotically stable, and there exists a positive unstable equilibrium; when* $0 < \phi \ll 1, 0$ *is unstable and there exists a negative and locally asymptotically stable equilibrium;*

ii. $a < 0, b < 0$. *When* $\phi < 0$ *with* $|\phi| \ll 1, 0$ *is unstable; when* $0 < \phi \ll 1, 0$ *is locally asymptotically stable, and there exists a positive unstable equilibrium;*

iii. $a > 0, b < 0$. *When* $\phi < 0$ *with* $|\phi| \ll 1, 0$ *is unstable, and there exists a locally asymptotically stable negative equilibrium; when* $0 < \phi \ll 1, 0$ *is stable, and a positive unstable equilibrium appears;*

iv. $a < 0, b > 0$. *When* ϕ *changes from negative to positive,* 0 *changes its stability from stable to unstable. Correspondingly a negative unstable equilibrium becomes positive and locally asymptotically stable.*

Particularly, if $a > 0$ *and* $b > 0$*, then a backward bifurcation occurs at* $\phi = 0$.

Rearranging (2.4.9), it follows that

$$\operatorname{sgn}(\mathcal{R}_0 - 1) = \operatorname{sgn}\left(k - \frac{E_* + D_{t*}}{1 - \frac{c_t}{r}E_*}\right).$$

It is always possible make $1 - \frac{c_t}{r}E_* > 0$, by making c_t sufficiently small. That is, if

$$c_t < C_7 = \frac{r}{E_*} \tag{2.5.21}$$

then there exists unique $k^* > 0$ such that $k = k^*$ implies that $\mathcal{R}_0 = 1$. In applying the above theorem, we use k^* as the bifurcation parameter in place of ϕ.

Theorem 2 *Let* $v_b(t) = v_b$ *and* $v_t(t) = v_t$ *be constant and non-negative. If* $\mathcal{R}_0 = 1$ *and* $c_t < C_7$*, then there exists* $C_8 > 0$ *such that system* (2.3.6) *undergoes a backward bifurcation at* E_0 *as* c_e *increases through* C_8.

Proof. We first recall the Jacobian, J, of (2.3.6) evaluated at the disease-free equilibrium, E_0, is given by (2.4.17) where $j_{44} = r\left(1 - \frac{1}{\mathcal{R}_0}\right)$ is the only non-zero entry of J in the fourth row. Since $c_t < C_7$, $\exists! k^* > 0$ such that $k = k^*$ implies $\mathcal{R}_0 = 1$. Setting $k = k^*$, we have that zero is a simple eigenvalue of J, and all

other eigenvalues have negative real part. Hence, we apply center manifold theory to analyze the dynamics near $k = k^*$. The right eigenvector of J associated with the eigenvalue 0 is given by

$$w = \left[c_3, c_4, \frac{cc_3 - c_e E_*}{\widetilde{\delta}_E}, 1\right]^T,$$

where c_3 and c_4 are given in (2.4.12) and (2.4.11), respectively. The left eigenvector associated to the eigenvalue 0 is given by

$$v = [0, 0, 0, 1].$$

Rewrite (2.3.6) as $\dot{x} = f(x, \phi)$, where x and $f(x, \phi)$ are vectors in $\mathbb{R}^4$ and $\phi = k$. Following Castillo-Chavez and Song (2004), we compute the following sums:

$$a = \sum_{k,i,j=1}^{n} v_k w_i w_j \frac{\partial^2 f_k}{\partial x_i \partial x_j}(E_0, k^*); \qquad b = \sum_{k,i=1}^{n} v_k w_i \frac{\partial^2 f_k}{\partial x_i \partial \phi}(E_0, k^*).$$

Since $v = [0, 0, 0, 1]$, we need only consider the partial derivatives of $f_4(x)$. We then calculate:

$$\begin{aligned}
\frac{\partial f_4}{\partial x_1} &= 0, \\
\frac{\partial f_4}{\partial x_2} &= -\frac{r}{k}T, \\
\frac{\partial f_4}{\partial x_3} &= -\frac{r}{k}T - c_t T, \\
\frac{\partial f_4}{\partial x_4} &= r\left(1 - \frac{T + \left(1 + \frac{kc_t}{r}\right)E + D_t}{k}\right) - \frac{r}{k}T.
\end{aligned}$$

Evaluated at (E_0, k^*), the nonzero second order partial derivatives are as follows:

$$\begin{aligned}
\frac{\partial^2 f_4}{\partial x_4 \partial x_2}(E_0, k^*) &= \frac{\partial^2 f_4}{\partial x_2 \partial x_4}(E_0, k^*) = -\frac{r}{k}, \\
\frac{\partial^2 f_4}{\partial x_4 \partial x_3}(E_0, k^*) &= \frac{\partial^2 f_4}{\partial x_3 \partial x_4}(E_0, k^*) = -\left(\frac{r}{k} + c_t\right), \\
\frac{\partial^2 f_4}{\partial x_4^2}(E_0, k^*) &= -2\frac{r}{k}.
\end{aligned}$$

It then follows that

$$\begin{aligned} a &= w_4 w_2 \frac{\partial^2 f_4}{\partial x_4 \partial x_2} + w_4 w_3 \frac{\partial^2 f_4}{\partial x_4 \partial x_3} + w_2 w_4 \frac{\partial^2 f_4}{\partial x_2 \partial x_4} + w_3 w_4 \frac{\partial^2 f_4}{\partial x_3 \partial x_4} + w_4^2 \frac{\partial^2 f_4}{\partial x_4^2} \\ &= -c_4 \frac{r}{k} - \left(\frac{cc_3 - c_e E_*}{\widetilde{\delta}_E} \right) \left(\frac{r}{k} + c_t \right) - c_4 \frac{r}{k} - \left(\frac{cc_3 - c_e E_*}{\widetilde{\delta}_E} \right) \left(\frac{r}{k} + c_t \right) - 2\frac{r}{k}. \end{aligned}$$

To evaluate b, we first compute

$$\frac{\partial f_4}{\partial \phi} = \frac{rT(T + E + D_t)}{k^2}.$$

We then find

$$\begin{aligned} \frac{\partial^2 f_4}{\partial x_i \partial \phi}(E_0, k^*) &= 0, \quad i = 1, 2, 3, \\ \frac{\partial^2 f_4}{\partial x_4 \partial \phi}(E_0, k^*) &= \frac{r(E_* + D_{t*})}{k^2}. \end{aligned}$$

Thus direct calculation reveals that

$$\begin{aligned} a &= -2\frac{r}{k}(c_4 + 1) - 2\left(\frac{r}{k} + c_t \right) \left(\frac{cc_3 - c_e E_*}{\widetilde{\delta}_E} \right), \\ b &= \frac{r(E_* + D_{t*})}{k^2}. \end{aligned}$$

Then b is always positive and $a > 0$ if and only if

$$c_e > C_8 = \frac{1}{E_*} \left(\widetilde{\delta}_E \left(\frac{1 + c_4}{1 + \frac{c_t k}{r}} \right) + cc_3 \right). \tag{2.5.22}$$

The statement follows from application of Theorem 4.1 in Castillo-Chavez and Song (2004), given in Theorem 1. □

This backward bifurcation consists of two codimension-one bifurcations, a saddle node bifurcation together with a transcritical bifurcation. By tuning the vertex of the degree 2 polynomial for T^*, we can reduce the region of bistability associated with the backward bifurcation and even eliminate it by making the saddle node and transcritical bifurcation points to coincide. In this case, we have a pitchfork-like

bifurcation. We may further perturb the vertex into the infeasible region, $T^* < 0$, where bistability exists in a mathematical sense, but has no biological meaning. The critical value where the two bifurcation points collide and result in a pitchfork-like bifurcation corresponds to making $\mathcal{A}_1 = 0$. From (2.4.14b) $\mathcal{A}_1 = 0$ if and only if

$$cc_3 + \frac{\widetilde{\delta}_E(1+c_4)}{1+\frac{kc_t}{r}} - \frac{c_e(k-D_{t*})}{1+\frac{kc_t}{r}} = 0,$$

which, when $\mathcal{R}_0 = 1$, is equivalent to

$$cc_3 + \frac{\widetilde{\delta}_E(1+c_4)}{1+\frac{kc_t}{r}} - c_e E_* = 0 \iff a = 0.$$

Figure 2.4 illustrates the cases where $a > 0$, $a = 0$ and $a < 0$.

Each bifurcation diagram is produced in MATLAB, examining the stability of the analytical solutions for the equilibria by way of the Jacobian. The parameter v_b is varied to produce a range of $\mathcal{R}_0$ and explore corresponding stability switches. The diagrams are found in agreement with results generated by the bifurcation analysis software package XPPAUT (Ermentrout, 2002). The stability of the various branches of equilibria is determined by Theorem 4.1 of Castillo-Chavez and Song (2004). Since,

$$\frac{k-D_{t*}}{1+\frac{kc_t}{r}} = \frac{\left(\left(1+\frac{kc_t}{r}\right)E_* + D_{t*}\right)\mathcal{R}_0 - D_{t*}}{1+\frac{kc_t}{r}},$$

we may view C_6 as a decreasing function of $\mathcal{R}_0$ with $C_6|_{\mathcal{R}_0=1} = C_8$ and $C_6 > C_8$ when $\mathcal{R}_0 < 1$. Then $\mathcal{R}_0 = \mathcal{R}_{crit}$ corresponds to the saddle node bifurcation point and $\mathcal{R}_0 = 1$ corresponds to the transcritical bifurcation point. Together this results in the following Corollary. Figure 2.5 illustrates the bistability indicated in the Corollary.

Corollary 2.5.1 *Suppose the assumptions of Theorem 2 hold. Then system* (2.3.6) *exhibits bistability for* $\mathcal{R}_{crit} < \mathcal{R}_0 < 1$.

The next result describes the conditions for the global stability of the tumor-free equilibrium. We only consider the case in which the system exhibits a backward bifurcation and a pair of positive equilibria for $\mathcal{R}_{crit} < \mathcal{R}_0 < 1$.

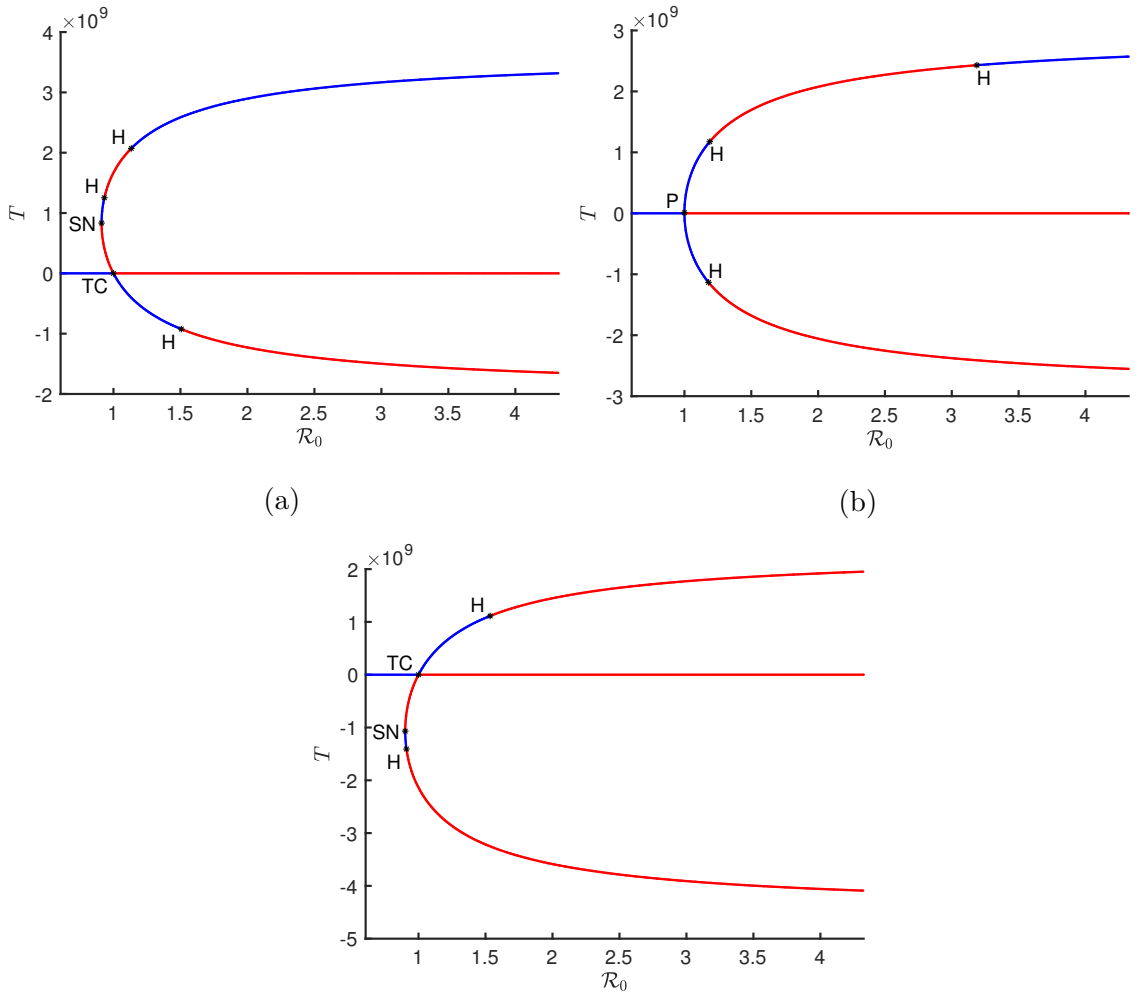

Figure 2.4: Backward Bifurcation (a), Pitchfork-Like Bifurcation (b) and Transcritical Bifurcation (c) of the Tumor-Free Equilibrium E_0, with H: Hopf Bifurcation, SN: Saddle-Node Bifurcation, TC: Transcritical Bifurcation, and P: Pitchfork-Like Bifurcation. The Blue Lines Represent Stable Equilibria, While the Red Lines Represent Unstable Equilibria.

Theorem 3 *Suppose that the conditions of Theorem 2 hold. Then there exists* $C_9 > 0$ *such that if* $\mathcal{R}_0 < C_9$, *then the tumor-free equilibrium is G.A.S.*

Proof. By hypothesis, Corollary 2.5.1 implies that system (2.3.6) admits two distinct positive equilibria for $\mathcal{R}_{crit} < \mathcal{R}_0 < 1$. By construction, the choice of s_1

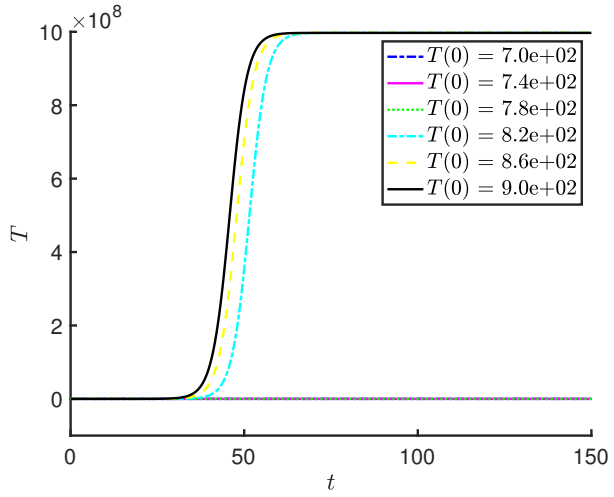

Figure 2.5: Bistability Exhibited As Initial Tumor Burden Increases with a Fixed $v_b = 6.2 \times 10^3$. We Take $v_t = 0, \mu_{BT} = 9.826 \times 10^{-9}, \mu_{TB} = 0.0011, \delta_D = 0.34, D_i = 0.001, s_E = 0.1, c = 3.205, c_e = 10^{-4}, r_{am} = 0.01, \delta_E = 0.1155, r = 0.3994, k = 10^9, c_t = 3.5 \times 10^{-6}$, Satisfying the Condition (2.5.22) Needed for a Backward Bifurcation.

used to formulate $\mathcal{R}_{crit}$ in (2.4.16) guarantees that when $\mathcal{R}_0 = \mathcal{R}_{crit}$, the discriminant $\mathscr{D} = \mathcal{A}_1^2 - 4\mathcal{A}_0\mathcal{A}_2 = 0$. Thus, if $\mathcal{R}_0 < \mathcal{R}_{crit}$, or equivalently, $s_E > s_1$, then E_0 is the only equilibrium of (2.3.6). We will proceed using comparison arguments. To that end, it is necessary to assume that

$$s_E > s_2 = \left(\widetilde{\delta}_E + c_e k\right) \frac{k - D_{t*}}{1 + \frac{kc_t}{r}} - cD_{b*}. \tag{2.5.23}$$

Let $s_E^* = \max(s_1, s_2)$

$$C_9 = \frac{k}{(1 + \frac{kc_t}{r})\frac{s_E^* + cD_{b*}}{\widetilde{\delta}_E} + D_{t*}}. \tag{2.5.24}$$

Now consider the flow of (2.3.6) when $T(0) > 0$. From (2d), $\dot{T} < rT\left(1 - \frac{T}{k}\right)$. Therefore, for any $\varepsilon > 0$, there exists $t_0 > 0$ such that $T(t) < k + \varepsilon$, for all $t > t_0$. Similarly, equations (2.3.6a) and (2.3.6b) are greater than or equal to the planar system (2.4.7) so that for any $\varepsilon > 0$, there exists $t_1 > t_0$ such that $D_b(t) > D_{b*} - \varepsilon$

and $D_t(t) > D_{t*} - \varepsilon$, for all $t > t_1$. It follows that, for any $\varepsilon > 0$, for $t > t_1$,

$$\dot{E} > s_E + c(D_{b*} - \varepsilon) - E(\widetilde{\delta}_E + c_e(k + \varepsilon)).$$

For $\varepsilon > 0$, the equilibrium of the linear equation on the right hand side of the inequality is

$$\frac{s_e + c(D_{b*} - \varepsilon)}{\widetilde{\delta}_E + c_e(k + \varepsilon)}.$$

Thus, for $\varepsilon > 0$, there exists $t_2 > t_1$ such that

$$E(t) > \frac{s_E + cD_{b*}}{\widetilde{\delta}_E + c_e k} - \varepsilon,$$

for all $t > t_2$.

Since $\mathcal{R}_0 < C_9$, we have $s_E > s_E^*$ and $\frac{(1+\frac{kc_t}{r})\frac{s_E+cD_{b*}}{\widetilde{\delta}_E+c_e k}+D_{t*}}{k} > 1$. Fix

$$\varepsilon_1 = \frac{1}{2}\left[\frac{(1+\frac{kc_t}{r})\frac{s_E+cD_{b*}}{\widetilde{\delta}_E+c_e k}+D_{t*}}{2+\frac{kc_t}{r}} - \frac{k}{2+\frac{kc_t}{r}}\right].$$

Then, for $t > t_2$,

$$\dot{T} < rT\left(1 - \frac{T + (1+\frac{kc_t}{r})\left[\frac{s_E+cD_{b*}}{\widetilde{\delta}_E+c_e k} - \varepsilon_1\right] + D_{t*} - \varepsilon_1}{k}\right) < 0.$$

For $t > t_2$, $T(t)$ is decreasing and bounded below. Thus, $\lim_{t\to\infty} T(t) = \alpha < \infty$. By Barbalat's Lemma, $\lim_{t\to\infty} \dot{T} = 0$. Since $s_E > s_E^* \geq s_1$, the only possibility is $\alpha = 0$. The omega limit set of the initial point x_0 with $T(0) > 0$ contains a point in the forward invariant boundary set, X_2, described in the comments preceding Proposition 2.4.6. By the Proposition 2.4.6, the omega limit set of any point in X_2 is the singleton $\{E_0\}$, so $\{E_0\} \subset \omega(x_0)$. If $\omega(x_0)$ contains a point other than E_0, then it would have to have $T > 0$, since E_0 is G.A.S in X_2. However, this is a contradiction of the fact that $\lim_{t\to\infty} T(t) = 0$. Thus, $\omega(x_0) = \{E_0\}$. □

Remark 2.5.2 *By the definition of* s_E^**, we have* $C_9 \leq \mathcal{R}_{crit}$*, with equality when* $s_1 \geq s_2$*. Conditions for the positivity of* $(s_1 - s_2)$ *have proven elusive. The difficulty is in the requirement that* $c_e > C_6$*, since* C_6 *depends on all of the remaining parameters, either directly or through dependence on* c_3 *and* c_4*. In the case that* $s_1 < s_2$*, we have* $C_9 < \mathcal{R}_{crit}$*, suggesting that perhaps* $\mathcal{R}_{crit}$ *is not a sharp threshold. However, numerical experiments suggest the stability of* E_0 *for* $\mathcal{R}_0 < \mathcal{R}_{crit}$ *even when* $s_1 < s_2$*. It remains an open question to close the gap between* C_9 *and* $\mathcal{R}_{crit}$ *in the case that* $s_1 < s_2$*.*

An important clinical consideration resulting from a backward bifurcation is its implication for treatment strategies. As Theorem 3 implies, in the case of a backward bifurcation, more aggressive intervention strategies are required to eradicate the tumor. Namely, if the conditions of Theorem 2 hold and a conservative treatment strategy is designed to have the effect of reducing $\mathcal{R}_0$ below 1, the tumor will not be eradicated. However, D_{b*} and D_{t*} are monotonically increasing in both v_b and v_t. If we view these constants as the average load of injected DCs, this implies more aggressive treatment strategies can reduce $\mathcal{R}_0$ below any positive threshold.

It has been found clinically that response rates for DC vaccines are two to three times higher in the adjuvant setting when compared to the metastatic setting (Bol *et al.*, 2016a). In an adjuvant setting, the tumor burden is already lessened by previous treatments. Additionally, it has been observed that DCs are insufficient as a monotherapy in treating advanced melanoma, yielding $< 10\%$ improvements in objective response rates. This behavior corresponds qualitatively to what might be expected in the bistable region described above.

2.6 Numerical Analysis

2.6.1 Hopf Bifurcation and Periodic Solutions

In addition to a backward bifurcation, numerical experiments indicate the existence of Hopf bifurcations leading to periodic solutions to system (2.3.6). First, fix our choice of parameters. If we view $\mathcal{R}_0$ as a function of r, then it is an increasing function of r, since

$$\frac{d}{dr}\mathcal{R}_0(r) = \frac{k^2 c_t E_*}{((r + kc_t)E_* + D_{t*})^2} > 0.$$

Next, we numerically compute the eigenvalues of the Jacobian evaluated at E_1. We do this as we vary r from 0.005 to 7 by increments of 1×10^{-3}.

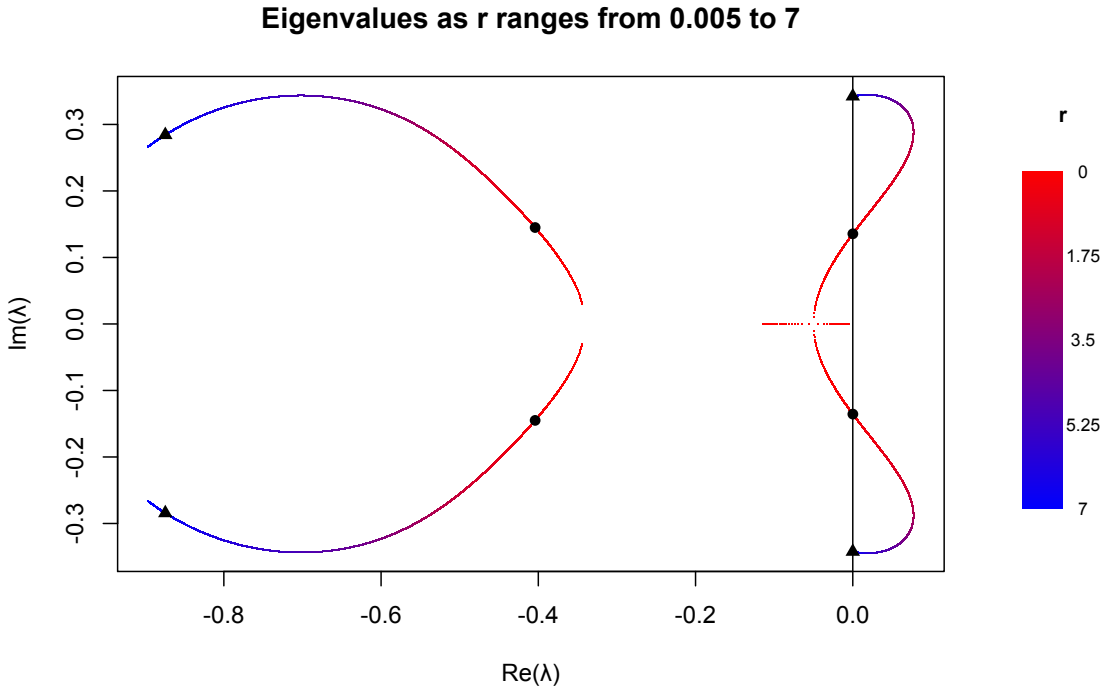

Figure 2.6: Eigenvalues of the Jacobian of (2.3.6) Evaluated at E_1 As r Varies from 0.005 to 7 in Increments of 0.001 with $v_b = v_t = 0, \mu_{BT} = 1.272 \times 10^{-5}, \mu_{TB} = 0.0011, \delta_D = 0.34, D_i = 0.00126, s_E = 0.01189, c = 0.127, c_e = 9.42 \times 10^{-14}, \widetilde{\delta}_E = 0.1255, k = 10^9$, and $c_t = 0.0035$.

Plotting the eigenvalues in the complex plane we see that a complex conjugate pair crosses from the left half-plane to the right half-plane at approximately $r = 0.233$. This indicates a supercritical Hopf which we can detect via numerical integration of (2.3.6). The same conjugate pair of eigenvalues cross back at approximately $r = 6.806$. Thus, the periodic orbit either disappears, or there is a second subcritical Hopf. The plot of the eigenvalues as we vary r is generated in R and presented in Figure 2.6. While the existence of purely imaginary eigenvalues shown in Figure 2.6 is necessary for the existence of a Hopf bifurcation, the numerical proof of a Hopf bifurcation is established by the confirmation of Figure 2.4 through XPPAUT's continuation package, AUTO (Ermentrout, 2002). An analytical proof of the Hopf bifurcation for system (2.3.6) remains an open question.

Remark 2.6.1 (Bogdanov-Takens bifurcation) *Recall the pitchfork-like bifurcation illustrated in Figure 2.4. The bifurcation on the branch equilibria with $T < 0$ is a Hopf bifurcation. The close proximity of a pitchfork-like bifurcation and Hopf bifurcation in the parameter space suggests the possibility of a Bogdanov-Takens (BT) bifurcation. Since we insist that all parameters other than v_b and v_t are strictly positive, the Jacobian evaluated at E_0, given in* (2.4.17)*, can have at most a single zero eigenvalue. However, if we let $\widetilde{\delta}_E = 0$, J admits a double zero eigenvalue. In the case of a BT, the magnitude of periodic orbits around equilibria on the positive and negative branches increase until the birth of homoclinic connections form from the equilbrium at $T = 0$. Then a periodic orbit appears which contains all three equilibria in its interior (in normal form with interior in the sense of a Jordan curve, cf. Kuznetsov (1998, p. 329)). However, in our system, the equilibrium with $T = 0$ is in the fully invariant set $\{(D_b, D_t, E, T) \in \mathbb{R}^4 | T = 0\}$. Therefore, once homoclinic orbits appear, they persist even as the magnitude of oscillations continues to increase. Some*

numerical experiments, as in Figure 2.7, suggest the presence of a homoclinic connection from E_0 to itself as the magnitude of oscillatory solutions increases. In order to study the BT, we must consider the limit as $\widetilde{\delta}_E \to 0$. However, $\lim_{\widetilde{\delta}_E \to 0} E_* = \infty$. It may be possible to make a change of variables ($\frac{1}{E_*} \to 0$ as $\widetilde{\delta}_E \to 0$). A full analysis of a possible BT bifurcation is beyond the scope of this chapter.

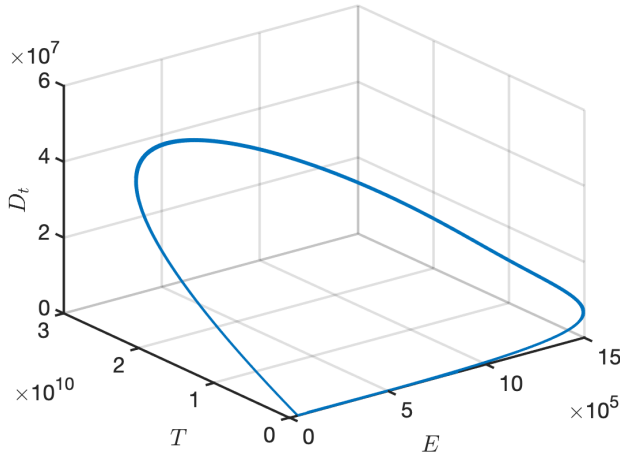

Figure 2.7: Projection of Limit Cycle in $\mathbb{R}^3$ When $v_b = 0, v_t = 0, \mu_{BT} = 9.826 \times 10^{-9}, \mu_{TB} = 0.0011, \delta_D = 0.34, D_i = 0.001, s_E = 5 \times 10^3, c = 3.205, c_e = 9.42 \times 10^{-14}, r_{am} = 0.01, \delta_E = 0.1155, r = 0.9, k = 5 \times 10^{12}$, and $c_t = 3.5 \times 10^{-6}$. Simulations Run for $t = 2000$ Days.

Oscillatory dynamics between the tumor and the immune system suggest periodic relapses in the tumor approximately every few months given r, the tumor growth rate, sufficiently high. Biologically, naturally occurring periodic oscillations in tumor size have been seen in various types of cancers (Fortin and Mackey, 1999). In Figure 2.7, the dynamics are shown to slow down as the periodic limit cycle approaches the tumor-free saddle E_0. Administering an appropriate amount of DC treatment during the period of an increasing tumor can sufficiently perturb the DC and CTL populations to shift to the decreasing tumor phase of the limit cycle. Dosing schedules could then be designed to perturb the system every few months to maintain the tumor

at low levels.

2.6.2 Dosing Strategies

To consider a clinically relevant treatment, we consider a discrete treatment case by running simulations up to 600 days. We first standardize the time between injections while varying the dose amount, followed by standardizing the total dosage amount while varying the frequency of injection. Figure 2.8a displays the tumor cell response to various dose amounts given every 100 days over the course of 600 days, with DC doses ranging from 2×10^7 to 8×10^7 cells. Larger doses respond more positively, increasing the periods of tumor remission. With a large enough dose, tumor eradication is possible. Figure 2.8b depicts the amount of tumor cells when the total intravenous DC dose given over the 600 days is 4.5×10^8 with injections ranging from every day to every 150 days. If the entire dose is given on Day 1, without a follow-up treatment, the tumor aggressively grows to carrying capacity, as shown in Figure 2.8c.

Together our simulations suggest larger, less frequent doses are more efficient in eradicating the tumor compared to the smaller, more frequent doses, though follow-up treatment is necessary to maintain control of the tumor. Unlike the majority of cancer treatments, toxicity has been determined to be a minimal issue for DC treatments, as flu-like symptoms are often the most adverse effect of DC vaccines. The low toxicity of DC vaccines allows higher, less frequent doses suggested by our model to be feasible in practice.

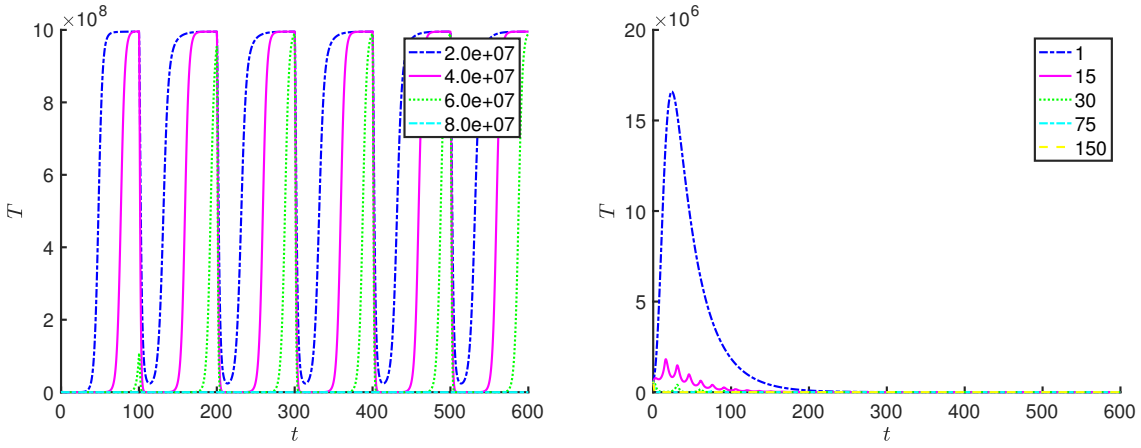

(a) Tumor with Fixed Timing, Varying Dose (b) Tumor with Fixed Dose, Varying Timing

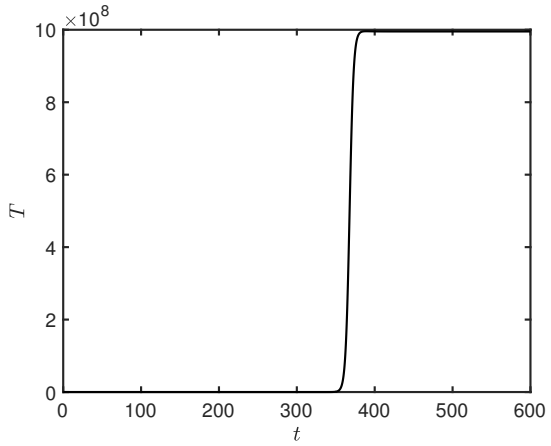

(c) Entire Dose of 4.5×10^8 DCs on Day 1

Figure 2.8: Tumor Response Shown with Respect to Various Doses and Timings. (a) Intravenous Injections of 2×10^7 to 8×10^7 Cells Given Every 100 Days for 600 Days. (b) Total DC Dose of 4.5×10^8 Injected Intravenously over 600 Days, with Injection Times from Every Day to Every 150 Days. (c) Entire DC Dose Injected Intravenously on Day 1.

2.7 Sensitivity and Identifiability Analysis

2.7.1 PRCC

To better understand the main drivers of $\mathcal{R}_0$ and its sensitivity to parameter uncertainties, as it is a critical value in determining tumor eradication or escape,

we utilize the Partial Rank Correlation Coefficient (PRCC) method, where 1,000,000 Latin hypercube samples (LHS) are taken for each parameter distribution. As there is uncertainty in parameter estimates, we assume a uniform distribution for all the ranges given in Table C.2. For the parameters without ranges, we consider uniform distributions for ranges around 10^{-3} to 10^{3} times the fixed values. In Figure 2.9a, we employ uniform sampling for all parameters. To avoid under-sampling in intervals where the parameter values are very small, we use a log-uniform distribution, thus sampling on a logarithmic scale when the max/min $> 10^3$, with results shown in Figure 2.9b. All codes for generating the PRCC plots are written in MATLAB.

The PRCC method reflects the correlation between $\mathcal{R}_0$ and parameters. PRCC values range from -1 to 1, where -1 indicates the parameter is highly negatively correlated with $\mathcal{R}_0$, and 1 signifies the parameter is highly positively correlated with $\mathcal{R}_0$. Figure 2.9a gives the principal parameters influencing $\mathcal{R}_0$ to be v_b, r_{am}, c_t, and c. The natural inactivation rate of CTLs (r_{am}) has the most significant positive effect on $\mathcal{R}_0$, while the intravenous dose amount (v_b), kill rate of tumor cells by activated CTLs (c_t), and the activation/proliferation rate of CTLs (c) are similarly negatively correlated. The different methods of sampling lead to different results, as Figure 2.9b shows c_t, v_t and v_b to be most significant, thus losing r_{am} and c and gaining v_t, the intratumoral dose amount. Combining results, r_{am}, v_b, c_t, c, and v_t are significant, where r_{am} is positively correlated with $\mathcal{R}_0$, and v_b, c_t, c, and v_t are negatively correlated.

Thus, for $\mathcal{R}_0$ to be low enough such that the tumor-free equilibrium is the only stable equilibrium, a high DC dosage amount, whether intravenous v_b or intratumoral v_t, or treatments targeting a decrease in r_{am} or an increase in c_t or c would be most effective. In particular, this suggests a treatment to prolong the activation period for exhausted cells or to reactive exhausted effector cells, such as an immune checkpoint

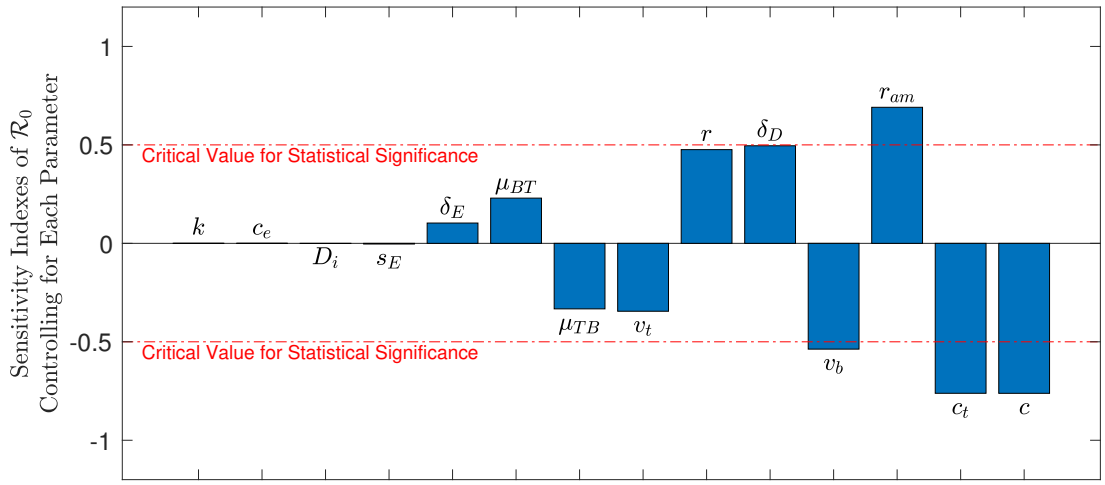

(a) Uniform Sampling of Parameter Distributions

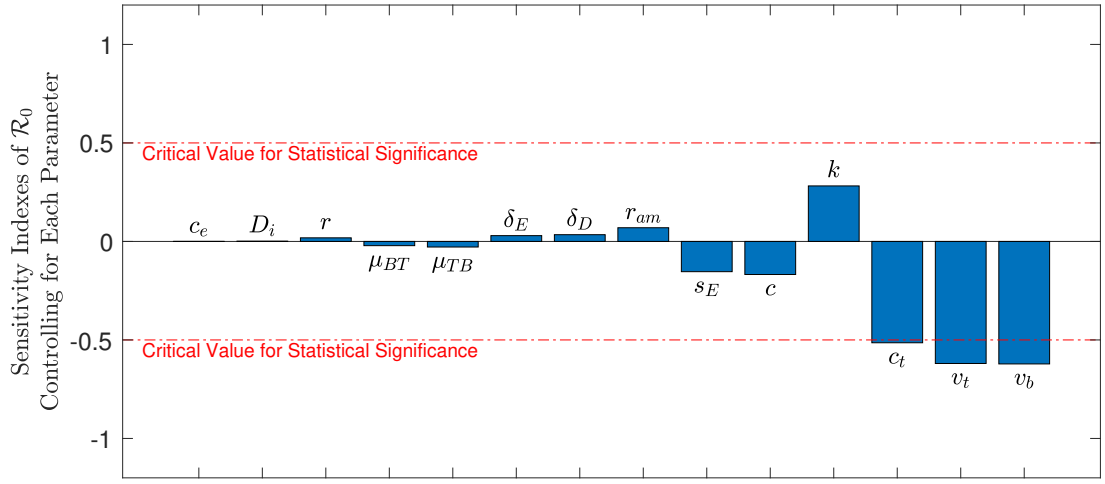

(b) Log-Uniform Sampling of Parameter Distributions (Log Scale If Max/Min $> 10^3$)

Figure 2.9: Sensitivity Analysis Is Conducted Using the PRCC Method, Where 1,000,000 Latin Hypercube Samples Are Taken for Each (a) Uniform and (b) Log-Uniform Parameter Distributions. Combining Results, r_{am}, v_b, c_t, c, and v_t Are Significant, Where r_{am} Is Positively Correlated with $\mathcal{R}_0$.

blockade, would be advantageous to combine with DC therapy. A rising interest in this combination over the last decade has led to the conception of various Phase I/II clinical trials researching a combined DC vaccine with an immune checkpoint

blockade, with results still being awaited (Versteven *et al.*, 2018).

2.7.2 Parameter Identifiability

Effective parameter identification is necessary in enhancing the predictive capability of any model. As often the case for mechanistic models, our model is limited by its many parameters and sparse data. While the PRCC provides an initial glimpse into the sensitivity of model output to parameters, it is necessary to conduct an identifiability analysis to understand fully the impact of the parameterization. Identifiability analysis is widely discussed in literature (Raue *et al.*, 2009; Brun *et al.*, 2001) and addresses two main problems: parameter identification given the data and model structure selection. As with most mechanistic models, available clinical or laboratory data poses a challenge in identifying model parameters. Identifiability analysis answers the question of whether it is possible to determine the values of unknown parameters and is categorized into two classes: structural and practical identifiability. Structural non-identifiability occurs when a unique optimal value for the parameter cannot be estimated, indicating a problem in the model structure selection. Problems with the type and quality of data are addressed when studying practical identifiability.

A first assessment of identifiability is done by examining the correlation between model parameters with a correlation matrix, an approach proposed by Rodriguez-Fernandez *et al.* (2006) for testing practical identifiability in nonlinear dynamic models. The correlation matrix provides a sense of the pairwise relationships between model parameters. A high correlation between two parameters indicates that the change to model output resulting from a change in a model parameter can nearly be compensated when the other parameter is appropriately changed, thus suggesting the two parameters cannot be separately estimated. The correlation matrix of the

parameter estimates takes the form of the following symmetric matrix:

$$R = \begin{bmatrix} r_{11}(\hat{\theta}_1, \hat{\theta}_1) & r_{12}(\hat{\theta}_1, \hat{\theta}_2) & \dots & r_{1m}(\hat{\theta}_1, \hat{\theta}_m) \\ r_{21}(\hat{\theta}_2, \hat{\theta}_1) & r_{22}(\hat{\theta}_2, \hat{\theta}_2) & \dots & r_{1m}(\hat{\theta}_2, \hat{\theta}_m) \\ \vdots & & & \\ r_{m1}(\hat{\theta}_m, \hat{\theta}_1) & r_{m2}(\hat{\theta}_m, \hat{\theta}_2) & \dots & r_{mm}(\hat{\theta}_m, \hat{\theta}_m) \end{bmatrix},$$

where r_{ij} $(i, j = 1, 2, \dots, m$ and $-1 \leq r_{ij} \leq 1)$ is the correlation coefficient between parameter estimates $\hat{\theta}_i$ and $\hat{\theta}_j$, with the parameter estimates $\theta = [\hat{\theta}_1, \hat{\theta}_2, \dots, \hat{\theta}_m]^T$ following from fitting the model to data.

Despite providing a quantitatively good fit to the data, the correlation matrix of the estimates given in Figure 2.10 suggests the model parameters are all poorly identifiable, as the magnitude of each correlation coefficient is above 0.8. It is important to note that Figure 2.10 displays rounded values, and the only pairs of parameters with a correlation coefficient of exactly 1 or -1 are c_t and c, c_t and D_i, c_t and μ_{TB}, μ_{BT} and δ_D, and c and μ_{TB}, indicating a need to fix these parameters prior to estimation or to reparameterize the model. Though the correlation matrix provides a glimpse into the identifiability of the parameters, a clear drawback is in its assessment of strictly pairs of parameters.

There then remains a need to understand interactions between all possible parameter combinations, which can be accomplished by way of the collinearity indices, as proposed by Brun *et al.* (2001). To do so, we first construct a dimensionless sensitivity matrix $S = \{s_{ij}\}$ with

$$s_{ij} = \frac{\partial y_i}{\partial \theta_j} \cdot \frac{w_{\theta_j}}{w_{y_i}}, \quad i = 1, 2, \dots, n \quad j = 1, 2, \dots, m.$$

with y_i as an output variable, θ_j a parameter, w_{y_i} the scaling of y_i, and w_{θ_j} the scaling of θ_j. The normalized matrix $\bar{S}$ contains the sensitivity matrix columns corresponding

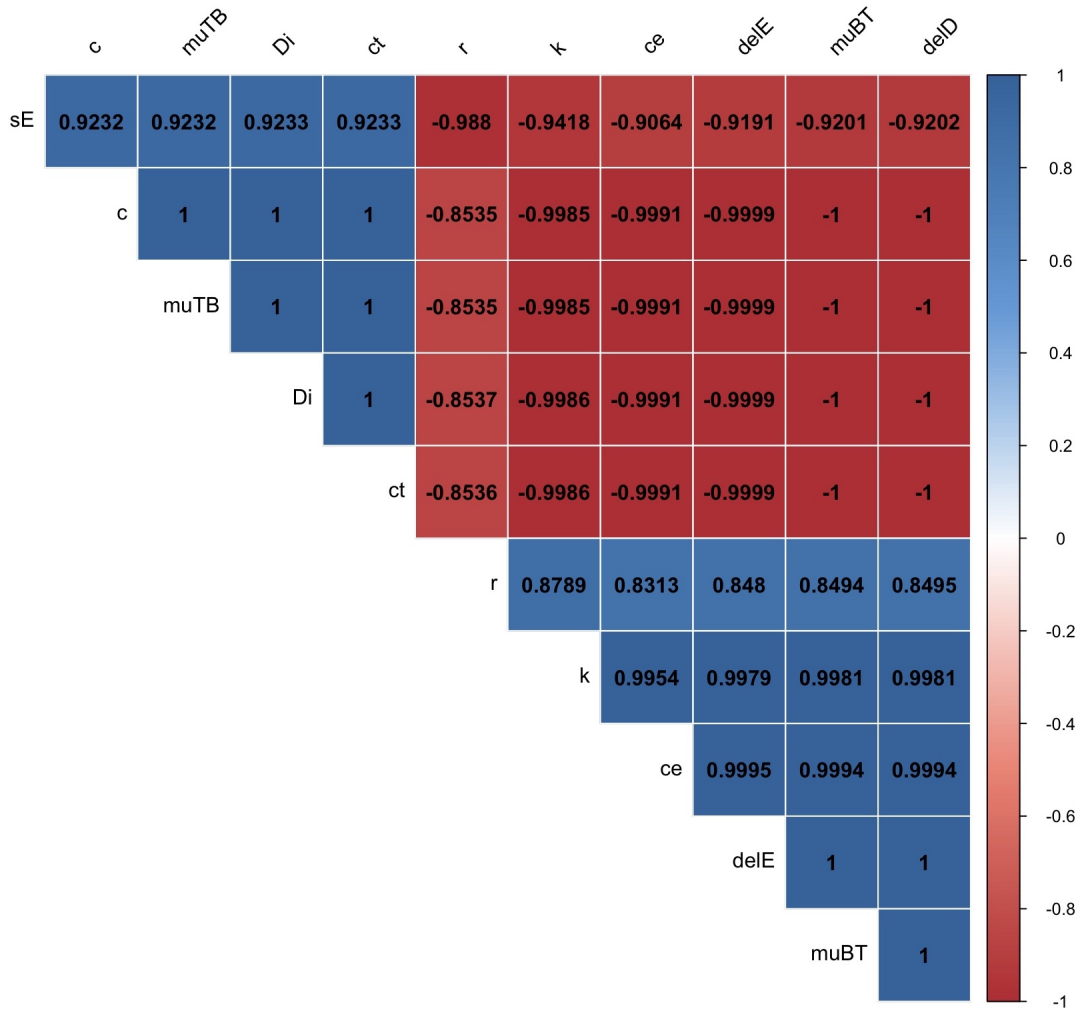

Figure 2.10: Correlation Matrix for All Parameters.

to the parameters in the subset and has its columns defined as

$$\bar{s}_j = \frac{s_j}{||s_j||}, \quad j = 1, 2, \ldots, m.$$

The collinearity index γ assesses the degree of linear dependence of $k \leq m$ columns of $\bar{S}$ and is defined as

$$\gamma = \frac{1}{\sqrt{\lambda_k}},$$

with λ given as the smallest eigenvalue of ${\bar{S}_k}^T \bar{S}_k$ and $\bar{S}_k$ being an $n \times k$ submatrix of $\bar{S}$ with its columns as the parameters in the subset of interest (Brun *et al.*, 2001).

In addition to allowing for analysis of all parameter combinations, the collinearity index yields itself to a clear interpretation of how parameters can compensate for changes made by other parameters. Omlin *et al.* (2001) outlines how the collinearity index γ indicates $1-1/\gamma$ of the model output changes caused by shifting one parameter can be compensated by an appropriate change of the other parameters. Thus, the threshold of 20 indicates 95% of the change in results caused by shifting one parameter can be compensated by appropriately changing the other parameters. High values of the collinearity index indicate poor practical identifiability of the parameter set. Both the collinearity plot and correlation matrix are produced using the R package Flexible Modeling Environment (FME) (Soetaert and Petzoldt, 2010).

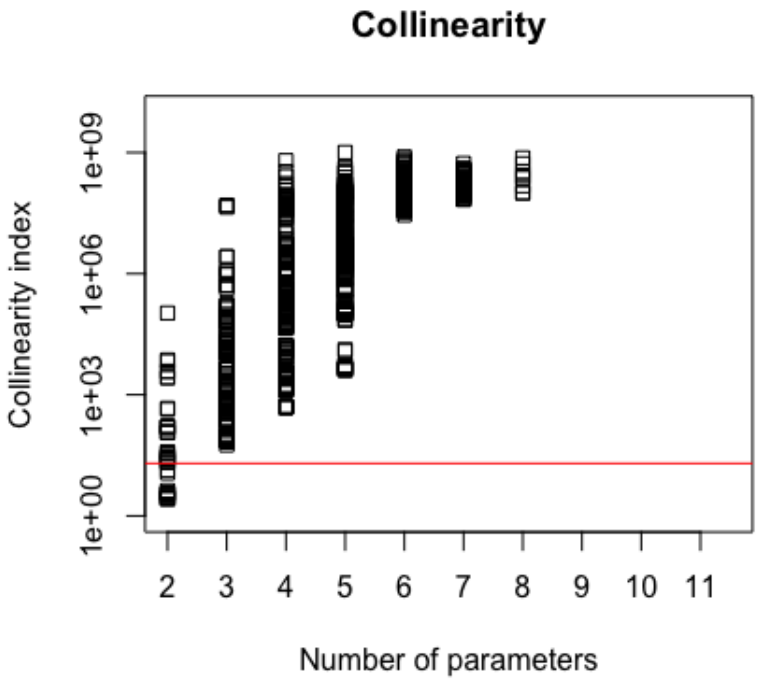

Figure 2.11: Collinearity Plot for All Parameters. The Red Line Corresponds to a Threshold of 20 for the Collinearity Index.

Figure 2.11 displays the collinearity indices for all sizes of parameter subsets, in-

cluding the parameters fixed during the original parameter estimation, and indicates a subset larger than two parameters cannot be identified strictly on the available tumor volume data. When testing the full set of 11 parameters, taking $r_{am} + \delta_E = \tilde{\delta}_E$, the collinearity is too large to fit all the parameters to data. Subsets that are identifiable, setting the threshold of 20 for the collinearity indices, are listed in Table 2.3. From the list, we observe that each parameter is represented in an identifiable subset. As Brun *et al.* (2001) similarly concludes, the collinearity indices then suggest that a pairwise correlation matrix alone is insufficient for making conclusions regarding identifiability, as we would have naively concluded that all parameters were poorly identifiable. When coupled with the collinearity indices, it is revealed that the high collinearity of the triples and the full parameter set lead to high elements of the correlation matrix, not merely the pairwise relationship between parameters.

Within the pairs, the highest collinearity indices are given as follows: c and μ_{TB} (105405.0), c_t and D_i (7343.9), μ_{BT} and δ_D (4264.2), μ_{TB} and c_t (3850.1), c_t and c (3717.2), D_i and μ_{TB} (2698.1), and c and D_i (2630.8). Adding c_t, D_i, or μ_{TB} to a parameter set has the effect of dramatically increasing the collinearity index. The index for $\{r, \tilde{\delta}_E\}$ is 2.747, which increases to 482.41 for $\{r, \tilde{\delta}_E, c_t\}$. By the PRCC, we additionally know the model output is highly sensitive to c_t. Fixing this parameter prior to parameter estimation will lead to more consistent parameter estimates.

Though many of the model parameters are significantly correlated, these parameters do not necessarily have a strong biological relationship. Instead, this indicates changes need to be made to the formulation of the model or estimation to reflect their separate impacts on the data. If separate, significant impacts of these model parameters are biologically known, the identifiability analysis indicates collecting data regarding the CTL or DC populations would be beneficial in decorrelating the parameters, as the available tumor volume data is insufficient for capturing the separate

Table 2.3: Collinearity Indices for Identifiable Parameter Subsets

Parameter Subset	γ_K
s_E, D_i	3.665217
s_E, μ_{BT}	3.582261
s_E, c	3.660364
s_E, δ_D	3.584072
s_E, c_e	3.262577
$s_E, \tilde{\delta}_E$	3.555876
s_E, c_t	3.663904
s_E, μ_{TB}	3.660485
s_E, k	4.244452
s_E, r	11.601526
r, D_i	2.810441
r, μ_{BT}	2.762569
r, c	2.807659
r, δ_D	2.763618
r, c_e	2.572128
$r, \tilde{\delta}_E$	2.747225
r, c_t	2.809711
r, μ_{TB}	2.807729
r, k	3.129791
c_e, k	13.563424

effects of parameters. Further work in overcoming the non-identifiability of model parameters is outlined in Chapter 4.

2.8 Discussion

We present a simple, autonomous, biologically meaningful mathematical model which accounts for observations found in the clinical setting. The reduced model is analytically tractable and admits rich dynamics. We have proven the existence of a backward bifurcation, given numerical evidence of a Hopf bifurcation, and given thresholds, C_9 and 1, for the combination parameter, $\mathcal{R}_0$, that guarantee the elimination ($\mathcal{R}_0 < C_9$) or existence ($\mathcal{R}_0 > 1$) of the tumor in the case of a continuous treatment. Since $\mathcal{R}_0$ decreases asymptotically to 0 as the treatment intensity (captured by v_b and v_t) increases, our model suggests that there is some level of treatment that will eradicate the tumor. Now $\mathcal{R}_0$ increases without bound with the proliferation rate of tumor cells. Therefore, our model suggests, if treatment is limited, aggressive cancers will continue to exist. In a subspace of the parameter space, the model exhibits bistability in the region $\mathcal{R}_{crit} < \mathcal{R}_0 < 1$. This suggests that more aggressive treatment strategies may be required than would be expected in the absence of the bistability.

As noted in Remark 5.1, there exists a double zero eigenvalue if we allow $\widetilde{\delta}_E = 0$. This suggests the possibility of a Bogdanov-Takens (BT) bifurcation. The close proximity of pitchfork-like and Hopf bifurcations illustrated by numerical simulations and shown in Figure 2.4 provide further evidence of a possible BT bifurcation. It is known that a BT bifurcation may give rise to a homoclinic orbit. For our analysis, we assume that v_t and v_b are non-negative and all other parameters are positive. Therefore, there is no BT in the relevant parameter space. Nevertheless, simulations suggest that system (2.3.6) admits a homoclinic orbit connecting the tumor-free equilibrium to itself. In the absence of this homoclinic connection, it is possible to show that the system is uniformly strongly persistent when $\mathcal{R}_0 > 1$. However, an analytic proof of the ex-

istence of this homoclinic connection and precise conditions for its existence remain open questions.

A sensitivity analysis using the PRCC method via LHS reveals the main drivers of $\mathcal{R}_0$ that will most effectively lower $\mathcal{R}_0$, thereby improving the efficacy of the treatment. We conclude the natural inactivation rate of CTLs (r_{am}) is most positively correlated with $\mathcal{R}_0$, while the intravenous dose amount (v_b), intratumoral dose amount (v_t), kill rate of tumor cells by activated CTLs (c_t), and the activation/proliferation rate of CTLs (c) are negatively correlated. An increased DC treatment, whether intratumoral or intravenous, in conjunction with a treatment targeting a decrease in r_{am} or an increase in c_t or c would yield optimal results. Analysis regarding the critical sub-threshold of $\mathcal{R}_0$, $\mathcal{R}_{\text{crit}}$, reveals the tumor inactivation rate of CTLs (c_e) is important in the threshold sufficient for tumor eradication. Treatments to decrease c_e would similarly prove beneficial as a combination treatment. Immune checkpoint blockades would act to decrease r_{am} and their combination with DC therapies is the subject of many ongoing clinical trials.

Chapter 3

DELAY DIFFERENTIAL EQUATION MODEL

3.1 Abstract

We formulate a tumor-immune interaction model with constant delay to capture the behavior following application of a dendritic cell therapy. The model is validated using experimental data from melanoma-induced mice. Through theoretical and numerical analysis, the model is shown to produce rich dynamics, such as a Hopf bifurcation and bistability. We provide thresholds for tumor existence and, in a special case, tumor elimination. Our work indicates a sensitivity in model outcomes to the immune response time. We provide a stability analysis for the high tumor equilibrium. For small delays in response, the tumor and immune system coexist at a low level. Large delays give rise to fatally high tumor levels. Our computational and theoretical work reveals there exists an intermediate region of delay that generates complex oscillatory, even chaotic, behavior. The model then reflects uncertainty in treatment outcomes for varying initial tumor burdens, as well as tumor dormancy followed by uncontrolled growth to a lethal size, a phenomenon seen *in vivo*. Analytic analysis suggests efficacious treatments to use in conjunction with the dendritic cell vaccine. Additional analysis of a highly aggressive tumor additionally confirms the importance of representation with a time delay, as periodic solutions are strictly able to be generated when a delay is present.

3.2 Introduction

Since their landmark discovery by Steinman and Cohn (1973), dendritic cells (DCs) have been hailed as the most potent antigen-presenting cells with the singularly efficient ability to initiate and coordinate immune responses. Their critical role in linking the adaptive and innate immune responses has made DCs an attractive candidate in cancer treatments. The first clinical trial testing a DC-based immunotherapy was published in 1996, in which four patients with follicular B-cell lymphoma were infused with antigen-pulsed DCs (Hsu *et al.*, 1996). As a result of patients responding in measurably favorable manners, a substantial number of clinical trials studying DC vaccines have been and continue to be conducted. In this form of immunotherapy, DCs are extracted from the patient and sensitized with tumor-associated antigens. The activated DCs are injected into the patient, where they interact with and activate naive and memory T cells in the lymphoid organs. Following exposure to the tumor-associated antigen, the T cells become activated and differentiate into cytotoxic T lymphocytes (CTLs), also known as effector cells, which migrate to the tumor and mount a fight.

DC vaccination studies have recently resulted in the approval of new government-approved cancer treatments. In 2010, sipuleucel-T (Provenge®) became the first DC-based therapy approved by the FDA (Kantoff *et al.*, 2010). Sipuleucel-T was shown to yield an increase in overall survival of 4.1 months and an improvement of 8.7% in the 3-year survival probability for men with metastatic castration-resistant prostate cancer. Seven years later, the Indian government agency (CDSCO - Central Drugs Standard Control Organization) approved the DC-based vaccine APCEDEN® for treatment of prostate, ovarian, non-small cell lung carcinoma, and colorectal cancer (Kumar *et al.*, 2017). The recent federal approval of these DC vaccines rekindled interest in

DC research, though excitement waned as the clinical results proved unsatisfactory. Much of the ineffective behavior has been attributed to the immunosuppressive tumor microenvironment (Bol *et al.*, 2016b). Interest in enhancing the immune response of DC vaccines has given rise to many clinical trials and mathematical modeling efforts (Castillo-Montiel *et al.*, 2015; Gevertz and Wares, 2018; Kronik *et al.*, 2010; Ludewig *et al.*, 2004; Portz and Kuang, 2013; Rutter and Kuang, 2017).

Ordinary differential equations (ODEs) are extensively used in mathematical modeling to better understand various life processes, such as cell interactions (Kuznetsov *et al.*, 1994; Nikolopoulou *et al.*, 2018), disease transmission (Korobeinikov, 2006; Li *et al.*, 2001), and predator-prey relationships (Hsu, 1978; Kuang and Beretta, 1998). Implicit in ODE models is the assumption that reaction times are instantaneous. As such, these models are often unable to capture much of nature's true complexity, as they are approximations of reality. Delay differential equations (DDEs) reflect naturally occurring delays, such as the binding time required for cell activation, and thus exhibit more interesting and realistic dynamics.

In Chapter 2, we formulated and analyzed a system of four ODEs describing the interactions between DCs in the blood, DCs in the tumor, effector cells, and tumor cells as DC therapy was administered. This model system was motivated and based on the earlier work of de Pillis *et al.* (2013). The simplified system in Chapter 2 is given by

$$\dot{D}_b = v_b(t) - \mu_{BT} D_b + \mu_{TB} D_t - \delta_D D_b, \tag{3.2.1a}$$

$$\dot{D}_t = v_t(t) + D_i T + \mu_{BT} D_b - \mu_{TB} D_t - \delta_D D_t, \tag{3.2.1b}$$

$$\dot{E} = s_E + c D_b - c_e E T - (r_{am} + \delta_E) E, \tag{3.2.1c}$$

$$\dot{T} = rT(1 - (T + E + D_t)/k) - c_t E T, \tag{3.2.1d}$$

where D_b, D_t, E, and T respectively denote DCs in the blood, DCs in the tumor,

effector cells, and tumor cells. The μ parameters reflect transport between compartments, while v_b and v_t reflect intravenous and intratumoral dosing. The meanings of the remainder of the parameters are reflected in Table C.2.

Though strictly consisting of ODEs, our model was able to produce complex dynamics, including oscillatory behavior and bistability. The existence of bistability suggested more aggressive treatments were needed than would otherwise be expected, and the mathematical analysis revealed thresholds that guaranteed tumor elimination or existence. Motivated by this work, we seek to gain additional insights by further reducing the system and introducing delay.

The primary aim of this chapter is to investigate how incorporating the more realistic delay in interactions influences the dynamics of the system. In doing so, (3.2.1) is first reduced in two stages. By assuming a constant proportion of DCs in the blood, we collapse the DCs in the blood and tumor into a single equation. Through the introduction of delay, we account for the time it takes for activated CTLs to become effective in killing tumor cells. Numerical experiments, including a justification using clinical data and bifurcation diagrams, reveal the model remains capable of representing complex tumor-immune behavior. A quasi-steady state assumption is employed to further reduce the model to a system of two DDEs. The model is again justified using clinical data. Following non-dimensionalization, mathematical analysis reveals the existence of periodic solutions and stability switches. Numerical experiments confirm the results of the mathematical analysis and demonstrate the sensitivity to the immune system response time. The limiting case when the immunosuppressive tumor environment is neutralized is analytically explored. Furthermore, the limiting case in which the death rate of effector cells by tumor cell interactions far exceeds the natural death rate is analyzed both numerically and analytically.

The chapter is organized in the following manner. A description of the intermedi-

ate model formulation along with supporting numerical experiments and preliminary analysis is given in Section 3.3. The formulation and preliminary analysis of the reduced model is provided in Section 3.4. A thorough analysis of the interior equilibria stability and corresponding numerical experiments are provided in Section 3.5. The stability of the boundary equilibria is provided in Section 3.6. The special case when the tumor is highly aggressive is explored in Section 3.7. The main results are outlined and discussed in Section 3.9.

3.3 Intermediate Model

In order to better study the effect of a delayed immune response, we make several simplifying assumptions to reduce system (3.2.1) and allow for a more mathematically tractable model. Since our focus is no longer on different dosing techniques, there is no longer a need to represent the intratumoral and intravenous dosing as separate terms. We collapse the DCs into a single equation, assuming the proportion of DCs in the blood, $\frac{D_b}{D_b+D_t}$ is approximated by the constant α. Additionally, we assume the DC therapy takes τ units of time to become effective, i.e. the effector cells take τ units of time following activation to kill tumor cells. Thus, the activation of naive and memory effector cells is assumed to occur at time $t-\tau$. Since activated effector cells die at a rate of $\tilde{\delta}_E$, the probability of survival for the effector cells is given by $e^{-\tilde{\delta}_E\tau}$ during this period of delay. The assumptions give rise to the following model:

$$\dot{D} = v(t) + D_i T - \delta_D D, \tag{3.3.2a}$$

$$\dot{E} = s_E + \tilde{c}e^{-\tilde{\delta}_E\tau} D(t-\tau) - c_e ET - \tilde{\delta}_E E, \tag{3.3.2b}$$

$$\dot{T} = rT\left(1 - \frac{T+E+(1-\alpha)D}{k}\right) - c_t ET, \tag{3.3.2c}$$

where $\tilde{c} = c\alpha$ and we assume the initial values are

$$E(0) \geq 0, T(0) > 0, D(\theta) \geq 0 \text{ for } \theta \in [-\tau, 0]. \tag{3.3.3}$$

Parameter values of system (3.3.2) are specified in Table 3.1.

Table 3.1: Parameters of System (3.3.2)

Para.	Description	Value	Ref.
D_i	Rate of immature DCs being activated by tumor	3.4946×10^{-4}/day	Fitted
δ_D	Natural death rate of DCs	0.34/day [.116,.5]	Dickman *et al.* (2020)
s_E	Source of activated CTLs	2.83×10^{-3}cells/day	Fitted
c	Activation/proliferation rate of CTLs	0.016001/day	Fitted
α	Proportion of DCs in blood	0.2778	Fitted
r_{am}	Inactivation rate of activated CTLs	0.002/day $[4 \times 10^{-4} - 1.2]$	Dickman *et al.* (2020)
δ_E	Natural death rate of activated CTLs	0.1155/day	Dickman *et al.* (2020)
τ	Time from activation to killing tumor cells	0.744912 days	Fitted
c_e	Max inactivation rate of activated CTLs by tumor cells	5.539×10^{-14}/(cells×day) $[9.42 \times 10^{-14} - 10^{-3}]$	Dickman *et al.* (2020)
r	Tumor cell growth rate	0.39/day $[0.17 - 0.69]$	Dickman *et al.* (2020)
k	Tumor cell carrying capacity	10^9 cells	Dickman *et al.* (2020)

c_t	Max rate activated CTLs kill tumor cells	$3.5 \times 10^{-5}/(\text{cells}\times\text{day})$ $[0-1]$	Dickman *et al.* (2020)

The biological assumptions are justified by the fit to clinical data displayed in Figure 3.1, as system (3.3.2) is capable of capturing the behavior of the melanoma-induced mice data from Lee *et al.* (2007) with a single set of biologically reasonable parameters. Data from Lee *et al.* (2007) reflects the average tumor volume of melanoma-induced mice treated with $0, 1 \times 10^5, 7 \times 10^5$, or 21×10^5 DCs on days 6, 8, and 10. The fit to the data remains comparable to that of Chapter 2. Numerical experiments seen in Figure 3.2 indicate the reduced model continues to give rise to interesting dynamics, such as oscillatory behavior and the presence of a singular Hopf bifurcation, as in the original ODE model given by (3.2.1). Figure 3.2 and the remainder of the figures in this chapter are generated using MATLAB's built-in dde solver DDE23.

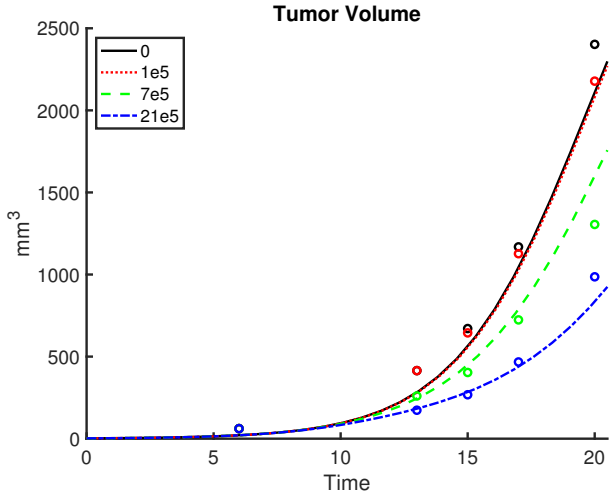

Figure 3.1: Fit to Lee *et al.* (2007) Data for (3.3.2).

In this section, we confirm the solutions to system (3.3.2) are biologically meaningful through establishing positivity and boundedness given appropriate initial con-

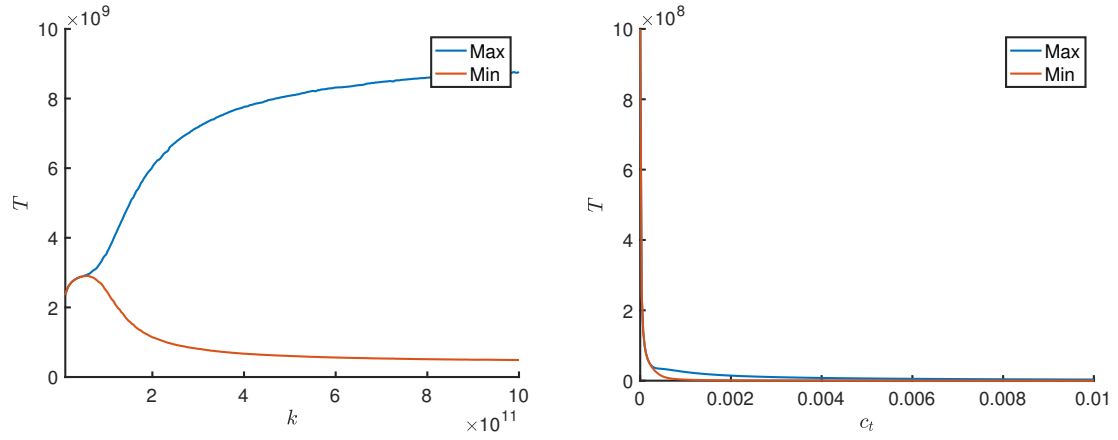

(a) $k \in [10^{10}, 10^{12}]$ (b) $c_t \in [0, 0.01]$

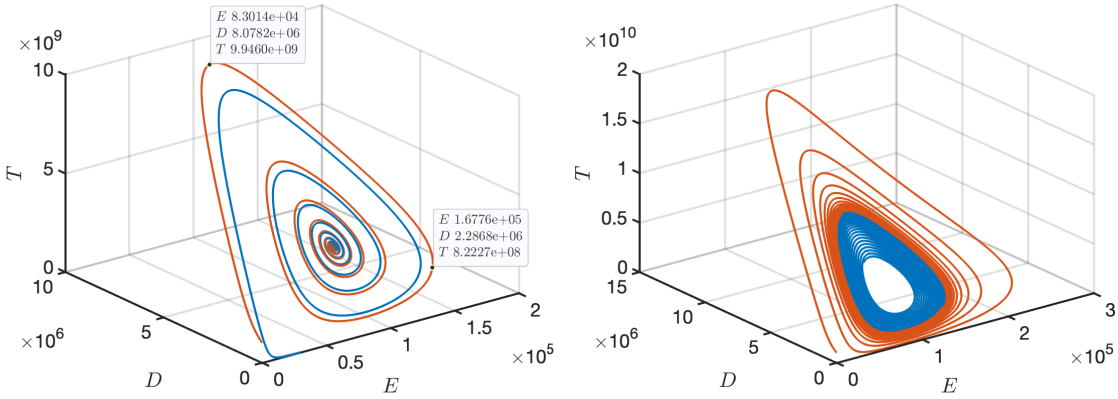

(c) $k = 3 \times 10^{10}$ (d) $k = 5 \times 10^{11}$

Figure 3.2: Bifurcation Diagrams and Phase Portraits for Intermediate Model (3.3.2), Consistent with Behavior Seen in Dickman *et al.* (2020) and Reflection of Oscillatory Behavior and Hopf Bifurcation.

ditions.

Proposition 3.3.1 *Every solution of system* (3.3.2) *with initial conditions* (3.3.3) *is positive and bounded.*

Proof. Suppose there exists t_0 such that $T(t_0) = 0$ and $T(t) > 0$ for $t \in [0, t_0)$. By

(3.3.2c), we have

$$T(t_0) = T(0)\exp\left(\int_0^{t_0} F(E(s), T(s))ds\right) > 0,$$

a contradiction. Thus, $T(t) > 0$ for $t \in [0, \infty)$. Similarly, suppose there exists t_1 such that $D(t_1) = 0$ and $\dot{D}(t_1) \leq 0$. Then (3.3.2a) gives $\dot{D}(t_1) = v(t) + D_i T(t_1) > 0$, and a time t_1 assuredly does not exist. Hence, $D(t) > 0$ for all $t > 0$. The positivity of E similarly follows.

By (3.3.2c), it follows that $\dot{T} \leq rT(1 - \frac{T}{k})$. Then $\limsup_{t\to\infty} T(t) \leq k$. Given $\epsilon > 0$, there exists $t_2 > 0$ such that $T(t) < k + \epsilon$ for all $t > t_2$. By (3.3.2a), we have that $\dot{D} < v(t) + D_i k - \delta_D D$ for $t > t_2$. Therefore $\limsup_{t\to\infty} D(t) \leq C_1$, where $C_1 := \max\{D(0), (v(t) + D_i k)/\delta_D\}$. Given $\epsilon > 0$, there exists $t_3 > t_2$ such that $D(t) < C_1 + \epsilon$ for all $t > t_3$. For $t > t_3 + \tau$, (3.3.2b) gives

$$\begin{aligned}\dot{E} &\leq \tilde{c}e^{-\tilde{\delta}_E \tau}(C_1 + \epsilon) - c_e E(k + \epsilon) - \tilde{\delta}_E E \\ &\leq \tilde{c}e^{-\tilde{\delta}_E \tau}(C_1 + \epsilon) - \tilde{\delta}_E E.\end{aligned}$$

Hence, $\limsup_{t\to\infty} E(t) \leq C_2$, where

$$C_2 := \max\{E(0), \tilde{c}e^{-\tilde{\delta}_E \tau}(C_1 + \epsilon)/\tilde{\delta}_E\}.$$

Given $\epsilon > 0$, there exists $t_4 > t_3 + \tau$ such that $E(t) < C_2 + \epsilon$ for all $t > t_4$. □

3.4 Preliminary Analysis: Simplified Model

As the turnover for dendritic cells is much quicker than that of the effector cells (Granucci and Zanoni, 2009; Ludewig *et al.*, 2004), a quasi-steady state assumption can be applied to D. The system (3.3.2) then reduces to the simpler system given by

$$\dot{E} = s_E + \tilde{c}e^{-\tilde{\delta}_E \tau}(\tilde{v} + \tilde{D}_i T(t - \tau)) - c_e E T - \tilde{\delta}_E E, \tag{3.4.4a}$$

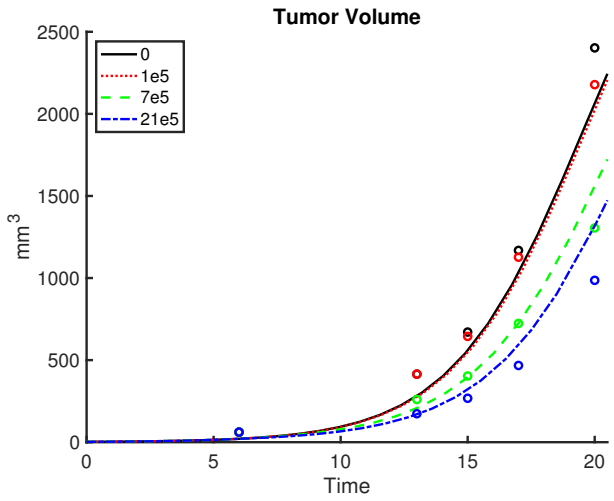

Figure 3.3: Fit to Lee *et al.* (2007) Data for (3.4.4).

$$\dot{T} = rT\left(1 - \frac{T + E + (1-\alpha)(\tilde{v} + \tilde{D}_i T)}{k}\right) - c_t ET, \tag{3.4.4b}$$

where $\tilde{v} = \frac{v}{\delta_D}, \tilde{D}_i = \frac{D_i}{\delta_D}$. The simplifications can again be justified through the fit to the Lee *et al.* (2007) data, as shown in Figure 3.3, where the fitting is comparable to all previous model formulations.

Non-dimensionalization, taking $\bar{t} = rt, \bar{E} = \frac{E}{k}, \bar{T} = \frac{T}{k}$, mathematically reduces the number of parameters. In the remainder of the paper, we will then consider the dimensionless system

$$\dot{E} = \beta + e^{-\delta\tau}(\gamma + \rho T(t-\tau)) - \eta_e ET - \delta E, \tag{3.4.5a}$$

$$\dot{T} = T(1 - (T + E + \nu + \mu T)) - \eta_t ET, \tag{3.4.5b}$$

where $\beta = \frac{s_E}{rk}, \gamma = \frac{\tilde{c}\tilde{v}}{rk}, \delta = \frac{\tilde{\delta}_E}{r}, \rho = \frac{\tilde{c}\tilde{D}_i}{r}, \eta_e = \frac{c_e k}{r}, \nu = \frac{(1-\alpha)\tilde{v}}{k}, \mu = (1-\alpha)\tilde{D}_i, \eta_t = \frac{c_t k}{r}, \bar{\tau} = r\tau$ are the dimensionless, positive parameters (with the exception of $\gamma = \nu = 0$ when no DC therapy is administered), and we drop the bars from variables and parameters. Values of the dimensionless parameters computed from the parameters of system (3.4.4) are given in Table 3.2.

Table 3.2: Parameters of System (3.4.4)

Parameter	Value
β	7.39×10^{-12}
δ	0.3277
ρ	1.45×10^{-5}
η_e	2.46×10^{-4}
μ	6.46×10^{-4}
η_t	9138.38
τ	0.382

Positivity and boundedness of the dimensionless system (3.5.11) can similarly be proven as before. The tumor-free equilibrium is given by $(E_0, T_0) = ((\beta+\gamma e^{-\delta\tau})/\delta, 0)$. Through the next generation matrix approach (Diekmann *et al.*, 1990; van den Driessche and Watmough, 2002), the basic reproduction number can be calculated as

$$\mathcal{R}_0 = \frac{1}{(1+\eta_t)E_0 + \nu}, \tag{3.4.6}$$

viewing the tumor cells as an infectious disease, as in Chapter 2. Biologically, the basic reproduction can be interpreted as the ratio of the proliferation potential of a tumor cell to the strength of the immune response and crowding effects. We will see that the system (3.5.11) admits two positive equilibria when $\mathcal{R}_0 < 1$, thus remaining consistent with the existence of a backward bifurcation observed in the Chapter 2.

Proposition 3.4.1 *If $\mathcal{R}_0 \geq 1$, then there exists a unique positive equilibrium, E_1. For ν sufficiently small, there exist constants C_3 and $\mathcal{R}_{crit}$ such that if $\eta_e > C_3$ and $\mathcal{R}_{crit} < \mathcal{R}_0 < 1$, then there exists a positive equilibrium E_2, in addition to E_1.*

Proof. Suppose $T^* > 0$. From $\dot{T} = 0$, we have $T^* = 0$ or

$$E^* = -\frac{1+\mu}{1+\eta_t}T^* + \frac{1-\nu}{1+\eta_t}. \tag{3.4.7}$$

Recall that when $T(0) > 0$, we have $0 < T < \frac{1}{1+\mu} + \epsilon$ after finite time. Thus,

$$\dot{E} > \beta + e^{-\delta\tau}\Big(\gamma + \frac{\rho}{1+\mu}\Big) - \Big(\frac{\eta_e}{1+\mu} + \delta\Big)E$$

after finite time, and it must follow that $E^* > 0$.

Substituting (3.4.7) in $\dot{E} = 0$ yields $g(T) = \mathcal{A}_0T^2 + \mathcal{A}_1T + \mathcal{A}_2 = 0$ where

$$\begin{cases} \mathcal{A}_0 = \dfrac{\eta_e(1+\mu)}{1+\eta_t}, \\ \mathcal{A}_1 = \rho e^{-\delta\tau} - \dfrac{\eta_e(1-\nu) - \delta(1+\mu)}{1+\eta_t}, \\ \mathcal{A}_2 = \beta + \gamma e^{-\delta\tau} - \dfrac{\delta(1-\nu)}{1+\eta_t}. \end{cases} \tag{3.4.8}$$

Given all parameters are positive, clearly $\mathcal{A}_0 > 0$. Additionally, we note that $\text{sgn}(\mathcal{A}_2)$ $= \text{sgn}(1-\mathcal{R}_0)$. By Descartes' Rule of Signs, there exists a unique positive solution, T_1^* of $g(T) = 0$ when $\mathcal{R}_0 > 1$. Thus, the system (3.4.5) has a unique positive equilibrium $E_1 = (E^*(T_1^*), T_1^*)$ when $\mathcal{R}_0 > 1$.

When $\mathcal{R}_0 < 1$, there is the possibility of having a second interior equilibrium, $E_2 = (E^*(T_2^*), T_2^*)$. In order for there to be two interior equilibria, as shown in Figure 3.5, we must have $\mathcal{R}_0 < 1$ and $\mathcal{A}_1 < 0$. By Descartes' Rule of Signs, there exists either two positive equilibria or zero. For two positive equilibria to exist, it is necessary to have $\mathcal{A}_1 < 0$ and $\mathcal{A}_1^2 - 4\mathcal{A}_0\mathcal{A}_2 > 0$. Similar to the 4D system (3.2.1) given in Dickman *et al.* (2020), η_e can be chosen sufficiently large, taking

$$\eta_e > C_3 = \frac{\rho(1+\eta_t) + \delta(1+\mu)}{1-\nu}, \tag{3.4.9}$$

such that $\mathcal{A}_1 < 0$ for all $\tau \geq 0$. When $\mathcal{R}_0 = 1$, then $\mathcal{A}_2 = 0$, and $g(T^*)$ has two real roots, $T^* = 0$ and $T^* = -\frac{\mathcal{A}_1}{\mathcal{A}_0}$. By continuity, there exists a $\delta > 0$ such that

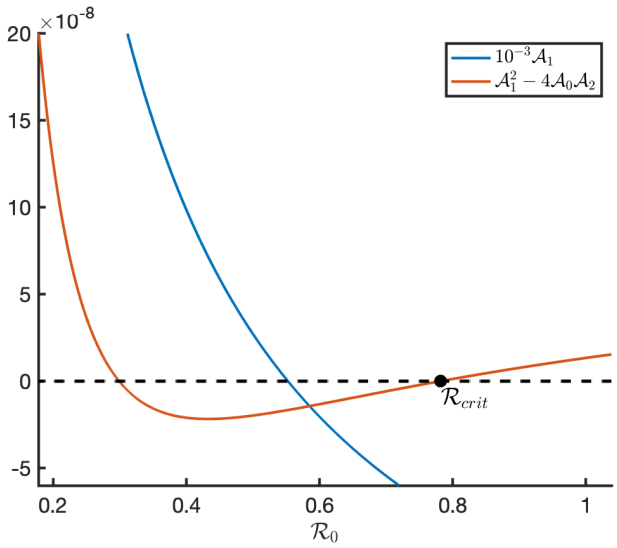

Figure 3.4: Discriminant and a Scaled $\mathcal{A}_1$ As a Function of $\mathcal{R}_0$. As Necessary for the Existence of Both E_1 and E_2, the Discriminant Is Positive and $\mathcal{A}_1 < 0$ for a Range of $\mathcal{R}_0 \in (\mathcal{R}_{crit}, 1)$.

$g(T^*)$ admits two real distinct positive roots for a range of $\mathcal{R}_0 \in (1-\delta, 1)$. Now, $\mathcal{R}_0$ is monotonically decreasing in β, and $\mathcal{A}_2$ is monotonically increasing in β. Then there exists a unique β^* such that when $\beta = \beta^*$, then $\mathcal{A}_2 = \frac{\mathcal{A}_1^2}{4\mathcal{A}_0}$ and the discriminant $\mathcal{A}_1^2 - 4\mathcal{A}_0\mathcal{A}_2$ is zero. Let

$$\mathcal{R}_{crit} = \frac{1}{(1+\eta_t)\frac{\beta^*+\gamma e^{-\delta\tau}}{\delta} + \nu}. \tag{3.4.10}$$

Then if $\eta_e > C_3$, $g(T^*)$ admits two positive roots $T_1^* > T_2^*$ for $\mathcal{R}_0 \in (\mathcal{R}_{crit}, 1)$. Denote $E_i = (E^*(T_i^*), T_i^*)$ for $i = 1, 2$. □

Figure 3.4 confirms the analytical findings, since both conditions necessary for the existence of two positive equilibria hold. With η_e chosen sufficiently large then $\mathcal{A}_1 < 0$, and $\mathcal{A}_1^2 - 4\mathcal{A}_0\mathcal{A}_2 > 0$ holds when $\mathcal{R}_0 \in (\mathcal{R}_{crit}, 1)$.

Figure 3.5 clearly illustrates how the interior equilibria both depend on τ. For lower τ, E_0 exists, but neither interior equilibria are feasible. Increasing τ shifts the E nullcline down and allows for the existence of the interior equilibria E_1 and E_2. A

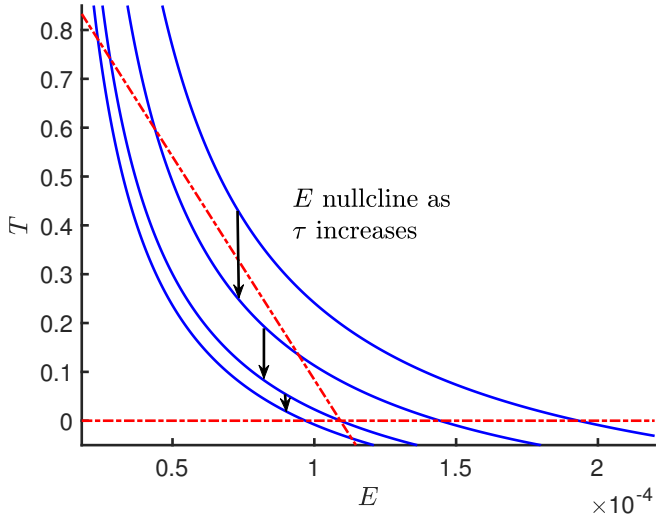

Figure 3.5: The E (Blue) and T (Red) Nullclines of (3.4.5) as τ Increases. As τ Increases, the Value of $\mathcal{R}_0$ Falls in the Following Ranges: $\mathcal{R}_0 < \mathcal{R}_{crit}, \mathcal{R}_{crit} < \mathcal{R}_0 < 1, \mathcal{R}_0 = 1$, and $\mathcal{R}_0 > 1$.

further increase to the delay causes the intermediate equilibrium E_2 to coincide with E_0 at a finite τ, corresponding to $\mathcal{R}_0 = 1$. The condition $\mathcal{R}_{crit} < \mathcal{R}_0 < 1$ required for two equilibria is thus shown to only be satisfied for finite τ. Though E_2 is not feasible for a higher value of τ, the interior equilibrium E_1 remains feasible as $\tau \to +\infty$.

Thus, for η_e sufficiently large such that $\eta_e > C_3$, there always exists at least one positive equilibrium root when $\mathcal{R}_0 \geq \mathcal{R}_{crit}$. Additionally, the second interior equilibrium only exists when the delay τ and other parameters are chosen such that $\mathcal{R}_{crit} < \mathcal{R}_0 < 1$. When conducting analysis, it will therefore be critical to keep track of how the feasibility of interior equilibria changes as τ or other parameters vary.

3.5 Stability of Interior Equilibria

3.5.1 No Delay

To understand the effects of delay on system (3.4.5), we first establish the stability of the equilibria when there is no delay. Without delay, the system is given as follows:

$$\dot{E} = \gamma_\beta + \rho T - \eta_e ET - \delta E, \tag{3.5.11a}$$

$$\dot{T} = T(1 - (T + E + \nu + \mu T)) - \eta_t ET, \tag{3.5.11b}$$

where $\gamma_\beta = \gamma + \beta$. Figure 3.6 depicts the nullclines and equilibria when the conditions $\mathcal{R}_{crit} < \mathcal{R}_0 < 1$ and $\mathcal{A}_1 < 0$ are satisfied for the existence of two interior equilibria.

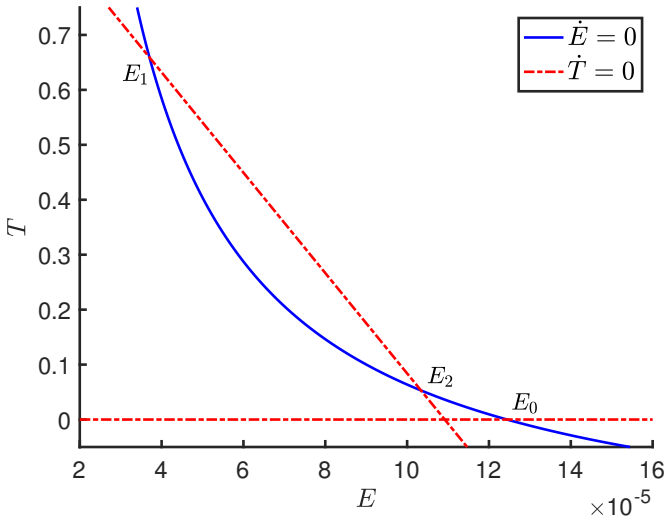

Figure 3.6: The E (Blue) and T (Red) Nullclines of (3.5.11), Where $\mathcal{R}_{crit} < \mathcal{R}_0 < 1$ and $\mathcal{A}_1 < 0$. Parameter Values Are Taken to Follow from Calculations Using Table 3.2, with the Exception of $\gamma = 4.621 \times 10^{-5}, \rho = 5.56 \times 10^{-6}, \eta_e = 1.3055$, and $\nu = 0.00206$.

We determine the local stability of the interior equilibria through a geometric approach.

Theorem 4 *If $\mathcal{R}_{crit} < \mathcal{R}_0 < 1$ and $\eta_e > C_3$ are satisfied for the existence of E_1 and E_2 (the intermediate tumor), the interior equilibria of* (3.5.11)*, then E_1 is stable, and E_2 is unstable.*

Proof. Through geometric arguments, we can deduce the signs of the Jacobians evaluated at E_1 and E_2 respectively as:

$$J_1 = \mathbf{J}|_{E_1} = \begin{pmatrix} - & - \\ & \\ - & - \end{pmatrix} \qquad J_2 = \mathbf{J}|_{E_2} = \begin{pmatrix} - & - \\ & \\ - & - \end{pmatrix}$$

Thus $tr(J_1) < 0$ and $tr(J_2) < 0$, and we need to determine the signs of the determinants. Let $\dot{E} \equiv g(E,T)$ and $\dot{T} \equiv h(E,T)$. Implicitly differentiating $g(E,T) = 0$ and $h(E,T) = 0$, we can respectively conclude $\frac{dT}{dE} = -\frac{g_E}{g_T}$ and $\frac{dT}{dE} = -\frac{h_E}{h_T}$. Since the slope of the T nullcline is greater than the slope of the E nullcline at E_1, then $-\frac{h_E}{h_T} > -\frac{g_E}{g_T}$. We know $\det = g_E h_T - g_T h_E$. We can then conclude $\det(J_1) > 0$. Similarly, since the slope of the E nullcline is greater than the slope of the T nullcline at E_2, then $-\frac{h_E}{h_T} < -\frac{g_E}{g_T}$, and $\det(J_2) < 0$. □

More aggressive treatment than standard is then required to decrease $\mathcal{R}_0$ sufficiently outside the region of bistability. Reducing the strength of the immunosuppressive microenvironment would increase the efficacy of the DC vaccines, as η_e is derived from the inactivation rate of CTLs by the tumor (c_e), and sufficient reduction of η_e eliminates the region of bistability. Agents to inhibit immunosuppressive factors, such as anti-interleukin-10 (anti-IL-10) and anti-transforming growth factor-β (anti-TGF-β), would then be suitable candidates for combination therapies (Cheever and Higano, 2011).

3.5.2 Linear Stability of Interior Equilibria

In this section, we study the linear stability of the interior equilibria, E_1, E_2, assuming the conditions $\eta_e > C_3$ and $\mathcal{R}_{crit} < \mathcal{R}_0 < 1$ hold such that both interior equilibria, are feasible. However, we again note that the condition $\mathcal{R}_{crit} < \mathcal{R}_0 < 1$ can only be satisfied up to a finite value of τ, as $\mathcal{R}_0$ monotonically increases in τ, thereby causing the intermediate equilibrium E_2 to lose its feasibility, as depicted in Figure 3.5. Hence, it is necessary to keep track of the feasibility of the equilibria during any analysis.

Let us first linearize (3.4.5) at the interior equilibrium (E^*, T^*). Setting $x = E - E^*, y = T - T^*$, where x, y are small, gives

$$x' = \rho e^{-\delta\tau} y(t-\tau) - (\eta_e T^* + \delta)x - \eta_e E^* y, \tag{3.5.12a}$$

$$\begin{aligned} y' = {} & (1 - (T^* + E^* + \nu + \mu T^*))y - (1+\eta_t)T^* x \\ & - (1+\mu)T^* y - \eta_t E^* y. \end{aligned} \tag{3.5.12b}$$

If we take solutions to be of the form $(x, y) = (c_1, c_2)e^{\lambda t}$, then non-trivial solutions exist if and only if the characteristic equation $F(\lambda, \tau) = 0$, where

$$\begin{aligned} F(\lambda,\tau) = \lambda^2 + ((\mu + \eta_e + 1)T^* + \delta)\lambda + ((\mu+1)(\eta_e T^* \\ + \delta) + (\eta_t + 1)(\rho e^{-(\delta+\lambda)\tau} - \eta_e E^*))T^*. \end{aligned} \tag{3.5.13}$$

The characteristic equation (3.5.13) can alternatively be expressed in the following form:

$$P(\lambda,\tau) + Q(\lambda,\tau)e^{-\lambda\tau} = 0, \tag{3.5.14}$$

where $P(\lambda,\tau) = \lambda^2 + \mathcal{A}(\tau)\lambda + \mathcal{C}(\tau)$ and $Q(\lambda,\tau) = \mathcal{B}(\tau)\lambda + \mathcal{D}(\tau)$ with

$$\mathcal{A} = (\mu + \eta_e + 1)T^* + \delta, \tag{3.5.15a}$$

$$\mathcal{B} = 0, \tag{3.5.15b}$$

$$\mathcal{C} = ((\mu+1)(\eta_e T^* + \delta) - (\eta_t + 1)\eta_e E^*)T^*, \tag{3.5.15c}$$

$$\mathcal{D} = (\eta_t + 1)\rho e^{-\delta\tau} T^*. \tag{3.5.15d}$$

Note that the characteristic equation (3.5.14) involves delay not just in the $e^{-\lambda\tau}$ term, but in several other places as well, since T^* and E^* depend on τ. Since our model (3.4.5) has delay dependent parameters, there is increased complexity in analyzing the system. Analytical results for systems with delay independent parameters have been thoroughly studied (Kuang, 1993) and result in clean, explicit calculations, such as the exact values of τ where stability switches occur. We apply the approach from Beretta and Kuang (2002) for studying these challenging characteristic equations which analyzes the stability switches via computational means, as exact values of τ where these switches occur cannot be analytically found.

In order to apply the technique of Beretta and Kuang (2002), we must verify the following properties hold for all $\tau \in \mathbb{R}_+$:

(i) $P(0,\tau) + Q(0,\tau) \neq 0, \forall \tau \in \mathbb{R}_{+0}$;

(ii) If $\lambda = i\omega$, $\omega \in \mathbb{R}$, then $P(i\omega,\tau) + Q(i\omega,\tau) \neq 0, \tau \in \mathbb{R}$;

(iii) $\limsup_{|\lambda|\to\infty} \left|\frac{Q(\lambda,\tau)}{P(\lambda,\tau)}\right| : |\lambda| \to \infty, \mathrm{Re}\lambda \geq 0\} < 1$ for any τ;

(iv) $F(\omega,\tau) := |P(i\omega,\tau)|^2 - |Q(i\omega,\tau)|^2$ for each τ has a finite number of zeros.

(v) Each positive root $\omega(\tau)$ of $D(\omega,\tau) = 0$ is continuous and differentiable in τ whenever it exists.

We first have $P(0,\tau) + Q(0,\tau) = \mathcal{C} + \mathcal{D}$. By assumption, property (i) is established, implying $\lambda = 0$ is not a root of (3.5.13). Now $P(i\omega,\tau) + Q(i\omega,\tau) = -\omega^2 + i\omega(\mathcal{A} + \mathcal{B}) + \mathcal{C} + \mathcal{D} \neq 0$, satisfying property (ii). Clearly property (iii)

holds, as $\limsup_{|\lambda|\to\infty}\left|\frac{Q|(\lambda,\tau)}{P(\lambda,\tau)}\right| = 0$. Additionally, we can clearly see that $F(\omega,\tau) := |P(i\omega,\tau)|^2 - |Q(i\omega,\tau)|^2$ has a maximum of four roots, since

$$|P(i\omega,\tau)|^2 = \omega^4 + (\mathcal{A}(\tau)^2 - 2\mathcal{C}(\tau))\omega^2 + \mathcal{C}(\tau)^2,$$
$$|Q(i\omega,\tau)|^2 = \mathcal{B}(\tau)^2\omega^2 + \mathcal{D}(\tau)^2,$$

thus satisfying property (iv). Let (ω_0,τ_0) be an arbitrary point in its domain such that $F(\omega_0,\tau_0) = 0$. Then we see that F_ω and F_τ exist and are continuous in a neighborhood of (ω_0,τ_0). Additionally, $F_\tau(\omega_0,\tau_0) \neq 0$. Then by the Implicit Function Theorem, we have property (v) holds. Since the five properties hold, we can then apply the results from Beretta and Kuang (2002).

As the roots of the characteristic equations are functions of delays, a stability switch may occur, where the stability of the equilibrium changes as the delay increases. If a stability switch occurs, we know (3.4.4) has a pair of conjugate pure imaginary roots $\lambda(\tau) = \pm i\omega(\tau), \omega(\tau) \in \mathbb{R}^+$ which crosses the imaginary axis at some $\tau = \tau^*$, and a Hopf bifurcation occurs.

To find the value of τ^* where a stability switch may occur, without loss of generality, we let $\lambda(\tau) = i\omega(\tau)$. Substitution of $\lambda = i\omega$ into (3.5.13) yields the following:

$$\begin{aligned} -\omega^2 + ((\mu+\eta_e+1)T^* + \delta)i\omega + ((\mu+1)(\eta_e T^* + \delta) \\ + (\eta_t+1)(\rho e^{-(\delta+i\omega)\tau} - \eta_e E^*))T^* = 0. \end{aligned} \tag{3.5.16}$$

By using Euler's formula $e^{i\theta} = \cos\theta + i\sin\theta$, we simplify and solve for the real and imaginary parts to obtain

$$\begin{cases} -\omega^2 + ((\mu+1)(\eta_e T^* + \delta) - (\eta_t+1)\eta_e E^*)T^* \\ \quad = -(\eta_t+1)\rho e^{-\delta\tau}\cos(\omega\tau)T^*, \\ \omega((\mu+\eta_e+1)T^* + \delta) = (\eta_t+1)\rho e^{-\delta\tau}\sin(\omega\tau)T^*. \end{cases} \tag{3.5.17}$$

Then ω must be a solution of

$$\begin{aligned}\omega^4 + \omega^2((\eta_e^2 + (\mu+1)^2)T^{*2} + 2\eta_e(\eta_t+1)E^* + \delta)T^* \\ + \delta^2) + ((\mu+1)(\eta_e T^* + \delta) - (\eta_t+1)\eta_e E^*)^2 T^{*2} \\ = ((\eta_t+1)\rho e^{-\delta\tau} T^*)^2.\end{aligned} \tag{3.5.18}$$

Using (3.5.15) to rewrite (3.5.18), we reach

$$F(\omega, \tau) := \omega^4 + \omega^2(\mathcal{A}^2 - 2\mathcal{C}) + (\mathcal{C}^2 - \mathcal{D}^2) = 0, \tag{3.5.19}$$

with its roots as

$$w_\pm^2 = \frac{1}{2}\{(2\mathcal{C} - \mathcal{A}^2) \pm \Delta^{1/2}\}, \tag{3.5.20}$$

where $\Delta = (2\mathcal{C} - \mathcal{A}^2)^2 - 4(\mathcal{C}^2 - \mathcal{D}^2)$. We know ω_-^2 is always negative, as

$$\mathcal{A}^2 - 2\mathcal{C} = (\mu+1)T^{*2} + (\eta_e T^* + \delta)^2 + 2(\eta_t+1)\eta_e E^* T^* > 0.$$

If $\omega_+^2 < 0$, a real ω does not exist and there are no stability switches. We can see there exists one real solution $\omega > 0$ if and only if

$$(\mathcal{C} + \mathcal{D})(\mathcal{C} - \mathcal{D}) < 0. \tag{3.5.21}$$

By Theorem 4, $\mathcal{C} + \mathcal{D} > 0$ at E_1 and $\mathcal{C} + \mathcal{D} < 0$ at E_2. Since $\mathcal{D} \geq 0$, we can deduce $\mathcal{C} < 0$ at E_2, making $\mathcal{C} - \mathcal{D} < 0$ at E_2. Thus, a real ω does not exist, and there are no stability switches for E_2. It then follows that E_2 is unstable for all $\tau \geq 0$. The sign of $\mathcal{C} - \mathcal{D}$ proves more challenging to evaluate for E_1. Therefore, for a stability switch to exist for E_1, the following additional condition is needed:

$$\mathcal{C} - \mathcal{D} < 0. \tag{3.5.22}$$

Since a real ω exists for E_1 when $\mathcal{C} - \mathcal{D} < 0$, the characteristic equation (3.5.13) has a pair of simple and conjugate pure imaginary roots $\lambda = \pm i\omega$. By application of Theorem 4.1 of Beretta and Kuang (2002), we prove this complex conjugate pair

of eigenvalues crosses the imaginary axis, ensuring a stability switch for E_1 when $\mathcal{C} - \mathcal{D} < 0$.

Assume $I \subseteq \mathbb{R}_{+0}$ is the set where $\omega(\tau) > 0$ is a root of (3.5.19). For any $\tau \in I$, we use (3.5.17) to define the angle $\theta(\tau) \in [0, 2\pi]$ as follows:

$$\sin\theta(\tau) = \frac{\omega\mathcal{A}}{\mathcal{D}}, \qquad \cos\theta(\tau) = \frac{\omega^2 - \mathcal{C}}{\mathcal{D}}. \tag{3.5.23}$$

For $\tau \in I$, we have the relationship

$$\omega(\tau)\tau = \theta(\tau) + 2n\pi, n \in \mathbb{N}_0.$$

From (3.5.23), we see

$$\theta(\tau) = \operatorname{arccot}\left(\frac{\omega^2 - \mathcal{C}}{\omega\mathcal{A}}\right). \tag{3.5.24}$$

If the conditions hold for an imaginary solution to exist, making ω feasible for $\tau \in I$, then we have the continuous and differentiable sequence of functions $I \to \mathbb{R}$:

$$S_n(\tau) = \tau - \frac{\theta(\tau) + 2n\pi}{\omega(\tau)}. \tag{3.5.25}$$

The characteristic equation (3.5.13) has a pair of simple conjugate pure imaginary roots $\lambda = \pm i\omega(\tau^*)$ at $\tau^* \in I$ when $S_n(\tau^*) = \tau^* - \tau_n(\tau^*) = 0$ for some $n \in \mathbb{N}_0$. By application of Theorem 4.1 in Beretta and Kuang (2002), the following theorem then holds.

Theorem 5 *Suppose $\eta_e > C_3$ and $\mathcal{R}_{crit} < \mathcal{R}_0 < 1$. For each interior equilibrium (E^*, T^*), define $\mathcal{C} = ((\mu+1)(\eta_e T^* + \delta) - (\eta_t + 1)\eta_e E^*)T^*$ and $\mathcal{D} = (\eta_t + 1)\rho e^{-\delta\tau}T^*$. Assume $\mathcal{C} + \mathcal{D} \neq 0$. Then E_2 is unstable for all $\tau \geq 0$. If $\mathcal{C} < \mathcal{D}$, the characteristic equation about E_1 admits a pair of simple conjugate pure imaginary roots $\lambda(\tau^*) = \pm i\omega(\tau^*)$ at $\tau^* \in I, I \subseteq \mathbb{R}_{+0}$, which crosses the imaginary axis from left to right if $\delta(\tau^*) > 0$ and from right to left if $\delta(\tau^*) < 0$, where*

$$\delta(\tau^*) := sgn\left\{\frac{dRe\ \lambda}{d\tau}\bigg|_{\lambda = i\omega(\tau^*)}\right\} = sgn\left\{\frac{dS_n(\tau)}{d\tau}\bigg|_{\tau=\tau^*}\right\}, \tag{3.5.26}$$

and $S_n(\tau^*) = 0$ *for some* $n \in \mathbb{N}_0$.

We determine the direction of the roots crossing the imaginary axis by evaluating

$$\delta(\tau^*) := \operatorname{sgn}\left\{ \frac{d\text{Re }\lambda}{d\tau}\bigg|_{\lambda=i\omega(\tau^*)} \right\} = \operatorname{sgn}\left\{ \text{Re}\left(\frac{d\lambda}{d\tau}\right)^{-1}\bigg|_{\lambda=i\omega(\tau^*)} \right\}.$$

We compute

$$\left(\frac{d\lambda}{d\tau}\right)^{-1} = \frac{2\lambda + \mathcal{A} - \mathcal{D}\tau e^{-\lambda\tau}}{\mathcal{D}\lambda e^{-\lambda\tau} - \mathcal{D}' e^{-\lambda\tau} - (\mathcal{A}'\lambda + \mathcal{C}')}. \tag{3.5.27}$$

By the characteristic equation (3.5.14), we have

$$e^{-\lambda\tau} = -\frac{\lambda^2 + \mathcal{A}\lambda + \mathcal{C}}{D}. \tag{3.5.28}$$

Substituting (3.5.28) into (3.5.27) yields

$$\left(\frac{d\lambda}{d\tau}\right)^{-1} = \frac{-\frac{2\lambda+\mathcal{A}}{\lambda^2+\mathcal{A}+\mathcal{C}} - \tau}{\lambda + \frac{\mathcal{A}'\lambda+\mathcal{C}'}{\lambda^2+\mathcal{A}\lambda+\mathcal{C}} - \frac{D'}{D}}.$$

Evaluating at $\lambda = i\omega(\tau^*)$, we have

$$\begin{aligned}
&\operatorname{sgn}\left\{ \text{Re}\left(\frac{d\lambda}{d\tau}\right)^{-1}\bigg|_{\lambda=i\omega(\tau^*)} \right\} \\
&= \operatorname{sgn}\Big\{ \omega^2[\mathcal{D}^2 + \mathcal{A}'(\mathcal{C} - \omega^2) - \mathcal{A}\mathcal{C}'] + \omega\omega'[\mathcal{D}^2\tau^* + \mathcal{A}(\mathcal{C} - \omega^2) + 2\omega^2\mathcal{A}] \Big\}.
\end{aligned}$$

As the sign is complex to determine analytically, we computationally determine whether the roots cross the imaginary axis and a stability switch for E_1 exists as τ increases, recalling the relationship

$$\operatorname{sgn}\left\{ \text{Re}\left(\frac{d\lambda}{d\tau}\right)^{-1}\bigg|_{\lambda=i\omega(\tau^*)} \right\} = \operatorname{sgn}\left\{ \frac{dS_n(\tau)}{d\tau}\bigg|_{\tau=\tau^*} \right\}.$$

by Theorem 5.

We consider two scenarios to demonstrate the impacts of the delay τ and ρ on E_1. Recall ρ is the only parameter in system (3.4.5) that is dependent on c, the activation/proliferation rate of CTLs, when there is not a constant DC dose applied ($v = 0$).

The stability of the system is demonstrated when the CTL activation/proliferation rate is low, intermediate, and high. Figure 3.7, Figure 3.10, and Figure 3.12 depict the functions $S_0(\tau), S_1(\tau)$, and $S_2(\tau)$ as defined above. For both scenarios, $\mathcal{C} - \mathcal{D} < 0$ up to a finite τ, such that real ω exists and Theorem 5 can be applied.

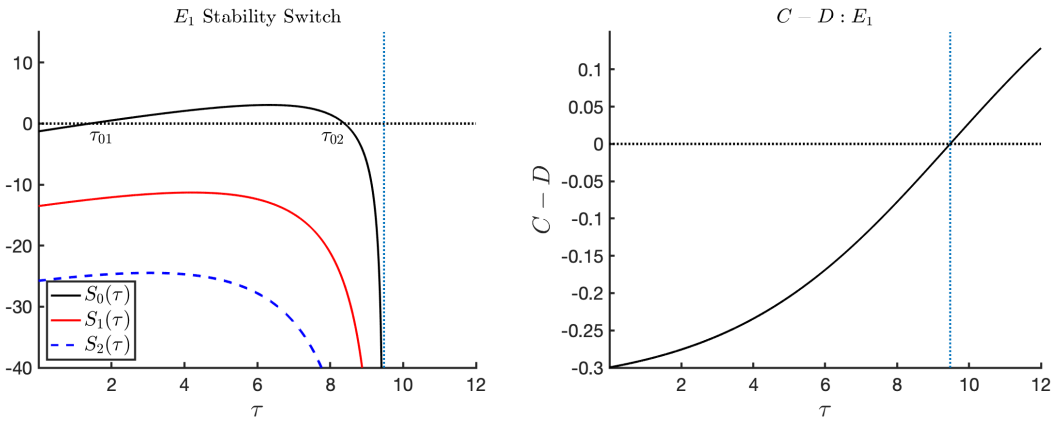

Figure 3.7: Plots of $S_0(\tau), S_1(\tau)$, and $S_2(\tau)$ When $\rho = 8 \times 10^{-4}$ and All Other Parameters Are Given As in Table 3.2. The Vertical Line Provides the Endpoint for the Existence Interval for $S_0(\tau)$, When $\mathcal{C} - \mathcal{D} < 0$ Is No Longer Satisfied. E_1 Is Asymptotically Stable for $\tau \in [0, \tau_{01}) \cup (\tau_{02}, \infty)$ and Unstable for $\tau \in (\tau_{01}, \tau_{02})$.

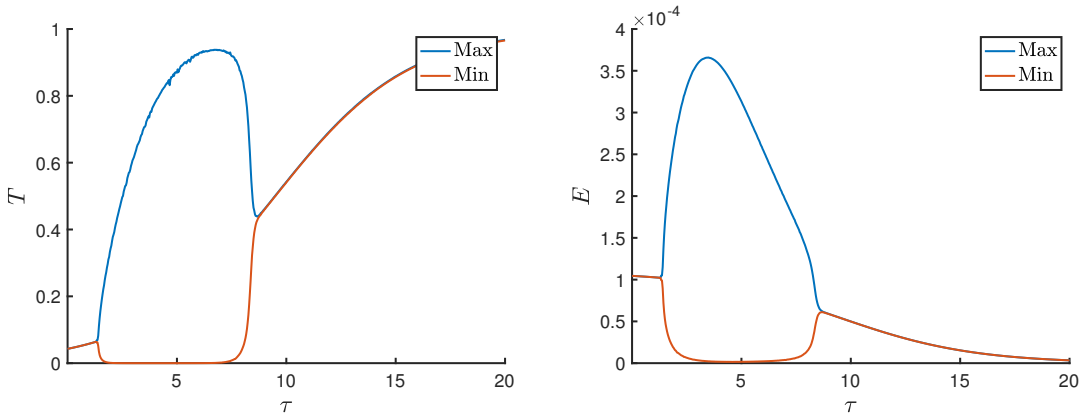

Figure 3.8: Bifurcation Diagrams for System (3.4.5), with Parameters As in Figure 3.7.

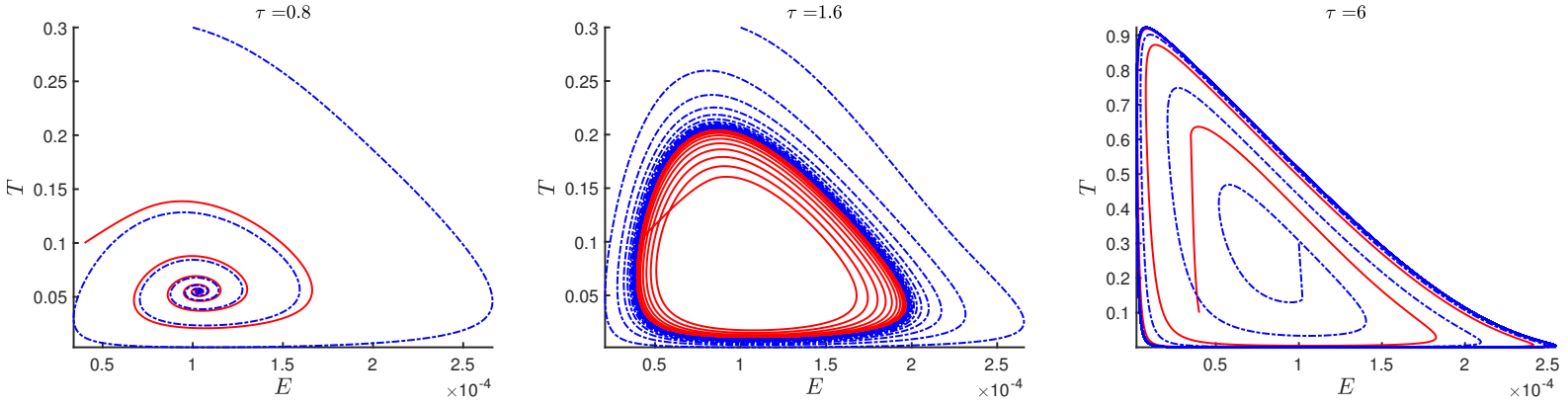

(a) By τ_{01}: $\tau \in [0, \tau_{01})$ (b) By τ_{01}: $\tau \in (\tau_{01}, \tau_{02})$ (c) $\tau \in (\tau_{01}, \tau_{02})$

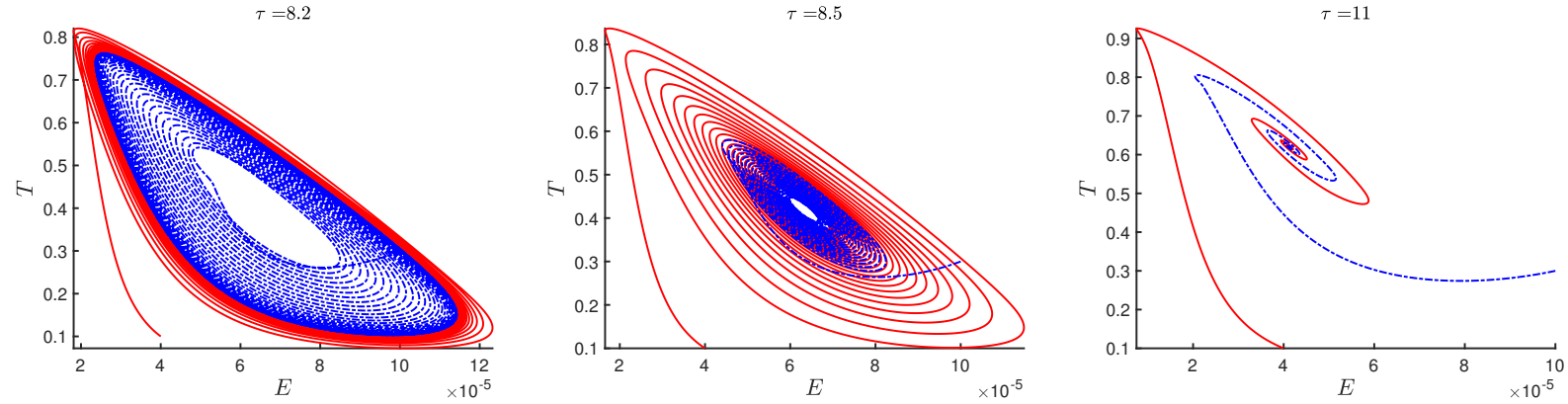

(d) By τ_{02}: $\tau \in (\tau_{01}, \tau_{02})$ (e) By τ_{02}: $\tau \in ((\tau_{02}, \infty) \cap I)$ (f) $\tau \notin I$

Figure 3.9: Phase Portraits of System 3.4.5, Confirming Regions of Stability and Instability Suggested by Figure 3.7. Parameters Are Given As in Figure 3.7.

Figure 3.7 illustrates the case of the low activation/proliferation rate of the CTLs (ρ small). The function $S_0(\tau)$ is shown to have roots at τ_{01} and τ_{02}, with $\tau_{01} < \tau_{02}$. For the choice of parameters, no real roots exist for $S_n(\tau)$ when $n > 0$. The behavior of S_0 indicates E_1 is asymptotically stable, loses its stability for $\tau \in (\tau_{01}, \tau_{02})$, then regains its stability as the delay increases. The switches in stability suggested by Figure 3.7 are confirmed through bifurcation diagrams in Figure 3.8 and phase portraits depicted in Figure 3.9. A Hopf bifurcation occurs when S_0 initially crosses the τ axis and the characteristic equation about E_1 admits two roots with positive real part.

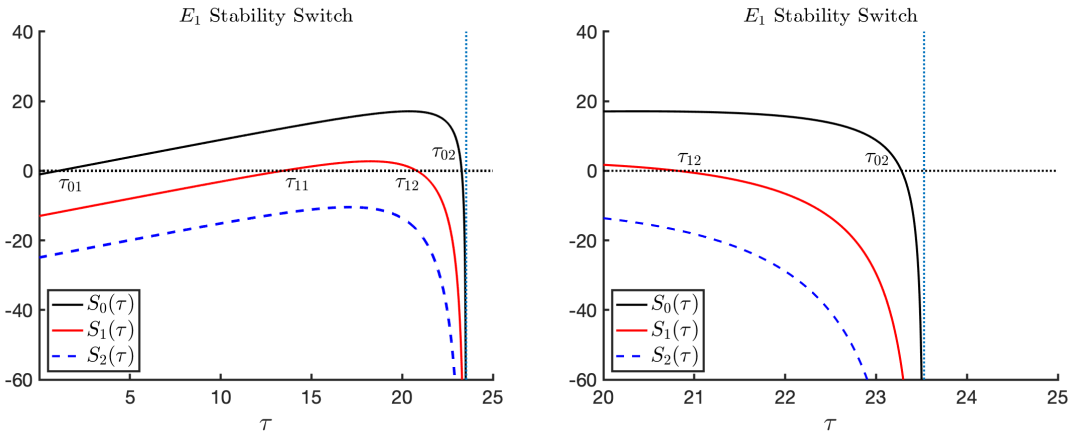

Figure 3.10: Plots of $S_0(\tau), S_1(\tau)$, and $S_2(\tau)$ When $\rho = 8 \times 10^{-2}$ and All Other Parameters Are Given as in Table 3.2. The Vertical Line Provides the Endpoint for the Existence Interval for $S_0(\tau)$. E_1 Is Asymptotically Stable for $\tau \in [0, \tau_{01}) \cup (\tau_{02}, \infty)$ and Unstable for $\tau \in (\tau_{01}, \tau_{02})$, with Added Instability for $\tau \in (\tau_{11}, \tau_{12})$.

Figure 3.10 depicts the case of a intermediate activation/proliferation rate of CTLs (ρ intermediate). Similar to Figure 3.7, E_1 loses stability and regains it as τ increases. However, there additionally exists a region in Figure 3.10 such that an additional pair of unstable eigenvalues appears. We define aperiodic behavior to be when there exist two pairs of eigenvalues with positive real parts. Thus, when $\tau \in (\tau_{11}, \tau_{12})$, there are two pairs of characteristic roots of the characteristic equation about E_1 with positive real parts, giving a region of increased instability and aperiodic behavior

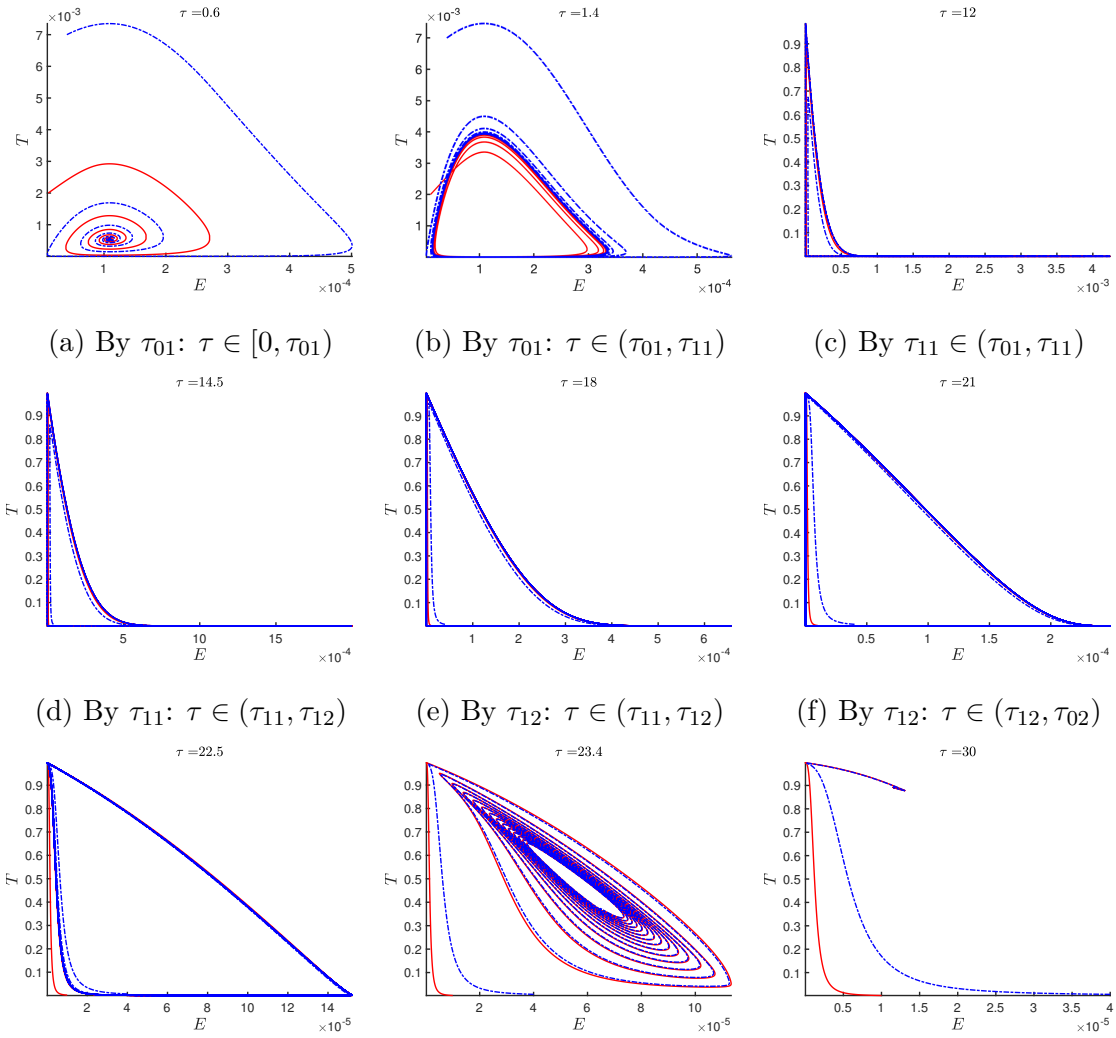

(a) By τ_{01}: $\tau \in [0, \tau_{01})$ (b) By τ_{01}: $\tau \in (\tau_{01}, \tau_{11})$ (c) By $\tau_{11} \in (\tau_{01}, \tau_{11})$

(d) By τ_{11}: $\tau \in (\tau_{11}, \tau_{12})$ (e) By τ_{12}: $\tau \in (\tau_{11}, \tau_{12})$ (f) By τ_{12}: $\tau \in (\tau_{12}, \tau_{02})$

(g) By τ_{02}: $\tau \in (\tau_{12}, \tau_{02})$ (h) By τ_{02}: $\tau \in ((\tau_{02}, \infty) \cap I)$ (i) $\tau \notin I$

Figure 3.11: Phase Portraits of System 3.4.5, Confirming Regions of Stability, Instability, and Added Complexity Suggested by Figure 3.10. Parameters Are Given As in Figure 3.10.

prior to E_1 eventually regaining its stability. The number of eigenvalues with positive real parts jumps by two as the S_n curves increase across the τ axis, making E_1 more unstable, and decreases by two as the S_n curves decrease across the τ axis, lessening the complexity. Similar to computational results outlined in Gourley and Kuang (2004), when τ increases such that $\tau \notin I$ and real ω is no longer feasible, the eigenvalues of the characteristic equation become real and negative. Thus, the

interior equilibrium E_1 continues to exist and be asymptotically stable when real ω is no longer feasible. E_1 is then asymptotically stable for $\tau \in [0, \tau_{01}) \cup (\tau_{02}, \infty)$ and unstable for $\tau \in (\tau_{01}, \tau_{02})$, with added instability for $\tau \in (\tau_{11}, \tau_{12})$, as confirmed by the phase plots in Figure 3.11.

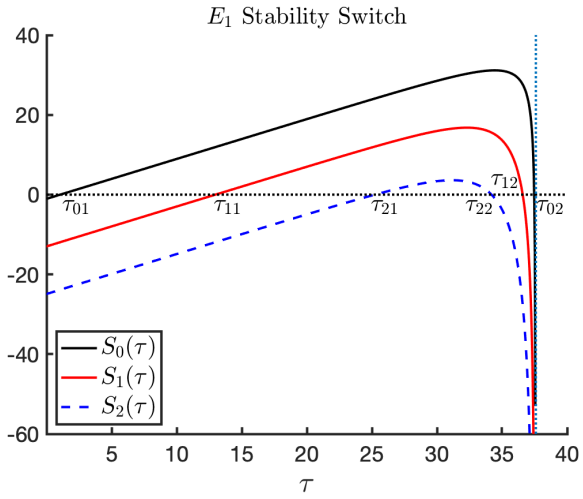

Figure 3.12: Plots of $S_0(\tau), S_1(\tau)$, and $S_2(\tau)$ when $\rho = 8$ and All Other Parameters Are Given As in Table 3.2. The Vertical Line Provides the Endpoint for the Existence Interval for $S_0(\tau)$. E_1 Is Asymptotically Stable for $\tau \in [0, \tau_{01}) \cup (\tau_{02}, \infty)$ and Unstable for $\tau \in (\tau_{01}, \tau_{02})$, with Added Instability for $\tau \in (\tau_{11}, \tau_{12})$ and Chaotic Behavior for $\tau \in (\tau_{21}, \tau_{22})$.

Figure 3.12 considers the case of a high activation/proliferation rate of CTLs (ρ large). For (τ_{21}, τ_{22}), the characteristic equation about E_1 admits three pairs of eigenvalues with positive real parts, which we define as chaotic behavior. The regions of chaos and oscillatory behavior reflect how different initial tumor burdens can have drastically distinct outcomes, as seen in practice.

Eliminating the assumption $\mathcal{C} + \mathcal{D} \neq 0$, there remains one critical case to consider.

Critical Case: $\mathcal{C} + \mathcal{D} = 0$

In the critical case of $\mathcal{C} + \mathcal{D} = 0$, Theorem 5 is no longer valid, and we must analyze the stability in a different way. When $\mathcal{C} + \mathcal{D} = 0$, it follows that

$$\mathcal{A}_2 = \frac{-\rho^2(1 - e^{-\delta\tau})^2 + \mathcal{A}_1^2}{4\mathcal{A}_0},$$

and E_2 is only feasible when $\tau = 0$ and E_2 and E_1 coalesce into a single equilibrium. The characteristic equation (3.5.14) reduces to $\lambda^2 + \mathcal{A}(\tau)\lambda + \mathcal{C}(\tau) + \mathcal{D}(\tau) = 0$ when $\tau = 0$. With the roots given by $\lambda = -\mathcal{A}(\tau) < 0$ and $\lambda = 0$, the interior equilibrium $E_1 = E_2$ is stable. When $\tau > 0$, application of results from Kuang (1993, p. 79-80) prove E_1 loses its stability for $\tau > \frac{\mathcal{A}(\tau)}{\mathcal{D}(\tau)}$.

3.6 Stability of Boundary Equilibrium

In the subsequent analysis, we seek to understand the necessary conditions for tumor elimination, and thus we examine the local and global stability of the boundary equilibrium.

Proposition 3.6.1 *The boundary equilibrium E_0 is locally asymptotically stable when $\mathcal{R}_0 < 1$ and unstable when $\mathcal{R}_0 > 1$.*

Proof. The Jacobian evaluated at the boundary equilibrium $E_0 = (\gamma_\beta/\delta, 0)$ given by

$$\mathbf{J}|_{E_0} = \begin{pmatrix} -\delta & \rho - \eta_e E_0 \\ 0 & 1 - \nu - (\eta_t + 1)E_0 \end{pmatrix} \tag{3.6.29}$$

admits the eigenvalues

$$\lambda_1 = -\delta; \lambda_2 = 1 - \frac{1}{\mathcal{R}_0}.$$

E_0 is then unstable when $\mathcal{R}_0 > 1$ and locally asymptotically stable when $\mathcal{R}_0 < 1$. □

The next result establishes the thresholds for the global stability of the tumor-free equilibrium. We only consider the case when the immunosuppressive environment of the tumor is neutralized, corresponding to $\eta_e = 0$.

Theorem 6 *Let $\eta_e = 0$. If $\mathcal{R}_0 < 1$, then $\lim_{t\to\infty}(E(t), T(t)) = ((\beta + \gamma e^{-\delta\tau})/\delta, 0)$.*

Proof. By (3.4.5), we have

$$\dot{E} = \beta + e^{-\delta\tau}(\gamma + \rho T(t-\tau)) - \delta E,$$
$$\dot{T} = T(1 - (T + E + \nu + \mu T)) - \eta_t E T$$

when $\eta_e = 0$. Since $\mathcal{R}_0 < 1$, $1 - \nu < (1 + \eta_t)E_0$, where $E_0 = (\beta + \gamma e^{-\delta\tau})/\delta$.

We first consider the case when there exists a $t_1 > 0$ such that $E(t_1) \geq E_0$. We claim if $E(t_1) \geq E_0$, then $E(t) \geq E_0$ for $t > t_1$. Otherwise there exists a $t_2 \geq t_1$ such that $E(t_2) = E_0$ and $\dot{E}(t_2) \leq 0$. At $t = t_2$,

$$\begin{aligned}\dot{E}(t_2) &= \beta + e^{-\delta\tau}(\gamma + \rho T(t_2 - \tau)) - \delta E_0 \\ &= \rho e^{-\delta\tau} T(t_2 - \tau) > 0,\end{aligned}$$

a contradiction. Thus, it follows that $E(t) \geq E_0$ for $t > t_1$. We then have for all $t > t_1$,

$$\begin{aligned}\dot{T} &\leq T(1 - \nu - (1 + \mu)T - (1 + \eta_t)E_0) \\ &\leq T(1 - \nu - (1 + \eta_t)E_0).\end{aligned}$$

Thus $T(t) \leq T(0)\exp\{(1 - \nu - (1 + \eta_t)E_0)t\}$ for $t > t_1$, and $\lim_{t\to\infty} T(t) = 0$. By definition, for any $\epsilon > 0$, there is a $t_\epsilon > t_1$ such that for $t > t_\epsilon$, $T(t) < \epsilon$. Hence for $t > t_\epsilon$,

$$\dot{E} < \beta + \gamma e^{-\delta\tau} + \rho e^{-\delta\tau}\epsilon - \delta E,$$

implying $\limsup_{t\to\infty} E \leq (\beta + \gamma e^{-\delta\tau} + \rho e^{-\delta\tau}\epsilon)/\delta$. Additionally,

$$\dot{E} \geq \beta + \gamma e^{-\delta\tau} - \delta E.$$

Then we have $\liminf_{t\to\infty} E \geq (\beta + \gamma e^{-\delta\tau})/\delta$. Thus, it follows that $\lim_{t\to\infty} E(t) = (\beta + \gamma e^{-\delta\tau})/\delta$.

We next consider the case when there exists a $t_3 > 0$ such that $E(t) < E_0$ for $t > t_3$. Note that E is monotonically increasing when $E(t) < E_0$, as

$$\begin{aligned}\dot{E} &= \beta + e^{-\delta\tau}(\gamma + \rho T(t-\tau)) - \delta E \\ &= \rho e^{-\delta\tau} T(t-\tau) - \delta(E - E_0).\end{aligned}$$

We must have a positive constant $E_1 \leq E_0$ such that $\lim_{t\to\infty} E(t) = E_1$. Indeed, we must have $E_1 = E_0$. Otherwise

$$\dot{E} = \rho e^{-\delta\tau} T(t-\tau) - \delta(E - E_0) > \delta(E_0 - E_1)$$

which implies that for $t > t_3$. $E(t) > E(t_3) + \delta(E_0 - E_1)(t - t_3)$ and $\lim_{t\to\infty} E(t) = \infty$, a contradiction to the assumption that $E(t) < E_0$ for $t > t_3$. Recall that $1 - \nu < (1 + \eta_t)E_0$. Hence there is an $\epsilon_1 > 0$ such that $1 - \nu < (1 + \eta_t)(E_0 - \epsilon_1)$. Since $\lim_{t\to\infty} E(t) = E_0$, there is a $t_4 > 0$ such that for $t > t_4$, $E(t) > E_0 - \epsilon_1$. It is easy to see that $\dot{T(t)} \leq T(1 - \nu(1 + \eta_t)E(t)) < T(1 - \nu - (1 + \eta_t)(E_0 - \epsilon_1))$. Let $c_1 = 1 - \nu - (1 + \eta_t)(E_0 - \epsilon_1) < 0$. Then $\dot{T(t)} < c_1 T(t)$. Thus, we have $\lim_{t\to\infty} T(t) = 0$. The proof of the theorem is complete. □

The immunosuppressive nature of the tumor microenvironment has been attributed to unmet expectations in DC vaccine behavior (Ahmed and Bae, 2014). Inhibiting the immunosuppressive factors through a combination treatment allows for less DC vaccines to be necessary for tumor elimination.

3.7 Special Case: $\delta = 0$

In highly aggressive tumors, the death of the effector cells is dominated by the interaction with the tumor cells. We analyze the equivalent scenario in the following

two sections, where $\delta = 0$. The system (3.4.5) becomes

$$\dot{E} = \gamma_\beta + \rho T(t-\tau) - \eta_e ET, \tag{3.7.30a}$$

$$\dot{T} = T(1 - (T + E + \nu + \mu T)) - \eta_t ET, \tag{3.7.30b}$$

where $\gamma_\beta = \gamma + \beta$.

We first establish stability when $\tau = 0$, as it is necessary for understanding the effects of incorporating delay. In the second section, we extend these results to consider when $\tau > 0$.

3.7.1 No Delay

With $\delta = \tau = 0$, system (3.7.30) reduces to

$$\dot{E} = \gamma_\beta + \rho T - \eta_e ET, \tag{3.7.31a}$$

$$\dot{T} = T(1 - (T + E + \nu + \mu T)) - \eta_t ET. \tag{3.7.31b}$$

A boundary equilibrium is no longer feasible. Hence the interior equilibria, E_1 and E_2, are the only possible equilibria, where E_2 corresponds to the intermediate tumor given when $T^* = \frac{-\mathcal{A}_1 - \sqrt{\mathcal{A}_1^2 - 4\mathcal{A}_0\mathcal{A}_2}}{2\mathcal{A}_0}$. Here, $\mathcal{A}_0, \mathcal{A}_1$, and $\mathcal{A}_2$ are given by (3.4.8) with $\delta = \tau = 0$.

The characteristic equation $\lambda^2 + a_1\lambda + b_1 = 0$ with

$$a_1 = (\mu + \eta_e + 1)T^*, \tag{3.7.32a}$$

$$\begin{aligned} b_1 &= (\eta_e(\mu+1)T^* - \eta_e(\eta_t+1)E^* + \rho(\eta_t+1))T^* \\ &= (1+\eta_t)(2\mathcal{A}_0 T^* + \mathcal{A}_1)T^* \end{aligned} \tag{3.7.32b}$$

admits the eigenvalues

$$\lambda_{1,2} = \frac{1}{2}\left(-a_1 \pm \sqrt{a_1^2 - 4b_1}\right). \tag{3.7.33}$$

Hence the stability of the equilibria depends on $\Delta = a_1^2 - 4b_1$. The stability and existence of the equilibria are examined in the following five cases.

Case 1: $b_1 = 0$

We first must examine whether $b_1 = 0$ is feasible for both real, positive equilibria. By (3.7.32b),

$$T^* = \frac{-\mathcal{A}_1 \pm \sqrt{\mathcal{A}_1^2 - 4\mathcal{A}_0\mathcal{A}_2}}{2\mathcal{A}_0} = -\frac{\mathcal{A}_1}{2\mathcal{A}_0}$$

when $b_1 = 0$. Hence $b_1 = 0$ iff $\mathcal{A}_1^2 = 4\mathcal{A}_0\mathcal{A}_2$, and E_1 and E_2 coalesce into a single equilibrium. Since $\lambda_1 = 0$ and $\lambda_2 < 0$ when $b_1 = 0$, the equilibrium $E_1 = E_2$ is stable.

Case 2: $b_1 < 0$

Note that $b_1 < 0$ when

$$T^* = \frac{-\mathcal{A}_1 \pm \sqrt{\mathcal{A}_1^2 - 4\mathcal{A}_0\mathcal{A}_2}}{2\mathcal{A}_0} < -\frac{\mathcal{A}_1}{2\mathcal{A}_0}.$$

Thus $b_1 < 0$ is only feasible for E_2. By (3.7.33), $\lambda_1 > 0$ and $\lambda_2 < 0$, and E_2 is unstable. Therefore, positive E_1 is not feasible, and E_2 is unstable when $b_1 < 0$.

Case 3: $0 < b_1 < \frac{a_1^2}{4}$

From $b_1 = (1 + \eta_t)(2\mathcal{A}_0 T^* + \mathcal{A}_1)T^* > 0$, we have

$$T^* = \frac{-\mathcal{A}_1 \pm \sqrt{\mathcal{A}_1^2 - 4\mathcal{A}_0\mathcal{A}_2}}{2\mathcal{A}_0} > -\frac{\mathcal{A}_1}{2\mathcal{A}_0},$$

a contradiction for E_2. Thus, positive E_2 is not feasible when $b_1 > 0$. To examine the existence of E_1, we see the inequality

$$\begin{aligned} b_1 &= (1 + \eta_t)(2\mathcal{A}_0 T^* + \mathcal{A}_1)T^* \\ &< \left(\left(\frac{1 + \eta_t}{2} + \frac{\mu(1 + \eta_t)}{4\eta_e}\right)\mathcal{A}_0 + \frac{\eta_e^2 + \mu + 1}{4}\right)T^{*2} = \frac{a_1^2}{4} \end{aligned}$$

holds if and only if

$$\mathcal{A}_1 < \frac{c_2}{c_1}\sqrt{\mathcal{A}_1^2 - 4\mathcal{A}_0\mathcal{A}_2},$$

where

$$\begin{aligned} c_1 &= \frac{1}{4} + c_{11}, \\ c_2 &= -\frac{3}{4} + c_{11}, \\ c_{11} &= \frac{\mu}{8\eta_e} + \frac{\eta_e^2 + \mu + 1}{8(1+\eta_t)\mathcal{A}_0}. \end{aligned} \tag{3.7.34}$$

Now it must be that

$$c_{11} = \frac{\mu}{8\eta_e} + \frac{\eta_e^2 + \mu + 1}{8(1+\eta_t)\mathcal{A}_0} = \frac{\eta_e^2 + (1+\mu)^2}{8\eta_e(1+\mu)} \geq \frac{1}{4},$$

else $(\eta_e - (1+\mu))^2 < 0$, a contradiction. Since $\mathcal{A}_1 < 0$ and $\mathcal{A}_0, \mathcal{A}_2 > 0$, then the inequality

$$\begin{aligned} \frac{c_2}{c_1}\sqrt{\mathcal{A}_1^2 - 4\mathcal{A}_0\mathcal{A}_2} &\geq -\sqrt{\mathcal{A}_1^2 - 4\mathcal{A}_0\mathcal{A}_2} \\ &> -\sqrt{\mathcal{A}_1^2} = -|\mathcal{A}_1| = \mathcal{A}_1 \end{aligned} \tag{3.7.35}$$

holds, and the existence of E_1 is satisfied when $0 < b_1 < \frac{a_1^2}{4}$. Then E_1 is asymptotically stable, as $\lambda_1, \lambda_2 < 0$. Thus, positive E_2 is not feasible, and E_1 is asymptotically stable when $0 < b_1 < \frac{a_1^2}{4}$.

Case 4: $b_1 = \frac{a_1^2}{4}$

As shown in the previous case, positive E_2 is not feasible since $b_1 > 0$. Now $b_1 = \frac{a_1^2}{4}$ when

$$\mathcal{A}_1^2\left(1 - \frac{c_1^2}{c_2^2}\right) = 4\mathcal{A}_0\mathcal{A}_2,$$

with constants c_1, c_2, c_{11} given by (3.7.34). Then

$$T^* = -\frac{\mathcal{A}_1 + \sqrt{\mathcal{A}_1^2 - 4\mathcal{A}_0\mathcal{A}_2}}{2\mathcal{A}_0} = -\frac{\mathcal{A}_1}{2\mathcal{A}_0}\left(1 - \frac{|c_1|}{|c_2|}\right),$$

and $T^* > 0$ only when $|c_2| > |c_1|$, since $\mathcal{A}_0 > 0$ and $\mathcal{A}_1 < 0$. By definition, $c_1 > 0$. Suppose $c_2 > 0$. Then $|c_2| > |c_1|$ yields $-\frac{3}{4} + c_{11} > \frac{1}{4} + c_{11}$, a contradiction. Now

suppose $c_2 < 0$. Then $|c_2| > |c_1|$ gives $\frac{1}{4} > c_{11}$, a contradiction, as shown in Case 3. Thus, neither positive E_1 nor positive E_2 are feasible when $b_1 = \frac{a_1^2}{4}$.

Case 5: $b_1 > \frac{a_1^2}{4}$

By Case 3, positive E_2 is not feasible since $b_1 > 0$. Now $b_1 > \frac{a_1^2}{4}$ when

$$\mathcal{A}_1 > \frac{c_2}{c_1}\sqrt{\mathcal{A}_1^2 - 4\mathcal{A}_0\mathcal{A}_2},$$

with constants c_1, c_2, c_{11} given by (3.7.34). As shown in Case 3, we must have $c_{11} \geq \frac{1}{4}$. Thus, we have

$$\begin{aligned}\mathcal{A}_1 &> \frac{c_2}{c_1}\sqrt{\mathcal{A}_1^2 - 4\mathcal{A}_0\mathcal{A}_2} \\ &\geq -\sqrt{\mathcal{A}_1^2 - 4\mathcal{A}_0\mathcal{A}_2} \\ &> -\sqrt{\mathcal{A}_1^2} = -|\mathcal{A}_1| = \mathcal{A}_1,\end{aligned}$$

a contradiction. Thus, neither E_1 nor E_2 are feasible when $b_1 > \frac{a_1^2}{4}$.

We can summarize the preceding results in the following theorem.

Theorem 7 *For the system* (3.7.31)*, the following statements are true, with* a_1, b_1 *given by* (3.7.32)*.*

(1) E_1 *is only feasible when* $0 \leq b_1 < \frac{a_1^2}{4}$*.* E_2 *is only feasible when* $b_1 \leq 0$*.*

(2) If $b_1 = 0$*, then* E_1 *and* E_2 *coalesce into a single stable equilibrium.*

(3) If $b_1 < 0$*, then* E_2 *is unstable.*

(4) If $0 < b_1 < \frac{a_1^2}{4}$*, then* E_1 *is asymptotically stable.*

3.7.2 With Delay

The previous results lend themselves to an extension to determine the impact on the stability when $\tau > 0$. We first linearize (3.7.30) at the interior equilibrium (E^*, T^*). Setting $x = E - E^*, y = T - T^*$, where x, y are small, gives

$$x' = \rho y(t-\tau) - \eta_e T^* x - \eta_e E^* y, \tag{3.7.36}$$

$$y' = -(1+\eta_t)T^* x - (1+\mu)T^* y. \tag{3.7.37}$$

Thus a non-trivial solution of the form $(x, y) = (c_1, c_2)e^{\lambda\tau}$ exists if and only if $G(\lambda, \tau) = 0$, with

$$\begin{aligned} G(\lambda,\tau) = \lambda^2 + (\mu+\eta_e+1)T^*\lambda + \eta_e((\mu+1)T^* \\ - (\eta_t+1)E^*)T^* + \rho(\eta_t+1)T^* e^{-\lambda\tau}. \end{aligned} \tag{3.7.38}$$

The characteristic equation (3.7.38) can be written in the simpler form

$$\lambda^2 + \alpha\lambda^2 e^{-\lambda\tau} + a\lambda + b\lambda e^{-\lambda\tau} + c + de^{-\lambda\tau} = 0, \tag{3.7.39}$$

with

$$\begin{aligned} &\alpha = 0; \quad a = (\mu+\eta_e+1)T^*; \quad b = 0; \\ &c = \eta_e((\mu+1)T^* - (\eta_t+1)E^*)T^*; \quad d = \rho(\eta_t+1)T^*. \end{aligned} \tag{3.7.40}$$

Recall, purely imaginary roots $\lambda = i\omega$ of the characteristic equation indicate possibilities of stability switches. Suppose $\lambda = i\omega$ is a root of the characteristic equation (3.7.39). This assumption yields

$$-\omega^2 + ai\omega + c + de^{-i\omega\tau} = 0,$$

where the real and imaginary parts are respectively given by

$$\begin{cases} -\omega^2 + c + d\cos\omega\tau = 0, \\ \qquad a\omega - d\sin\omega\tau = 0. \end{cases} \tag{3.7.41}$$

Thus,

$$\omega^4 + (a^2 - 2c)\omega^2 + c^2 - d^2 = 0.$$

Its roots are

$$\omega_{\pm}^2 = \frac{1}{2}\Big((2c - a^2) \pm \sqrt{(a^2 - 2c)^2 - 4(c^2 - d^2)}\Big). \tag{3.7.42}$$

By (3.7.40),

$$\begin{aligned} a^2 &= 2\eta_e(\mu + 1)T^{*2} + (\mu + 1)^2 T^{*2} + \eta_e^2 T^{*2} \\ &> 2\eta_e(\mu + 1)T^{*2} - \eta_e E^* T^*(\eta_t + 1) = 2c. \end{aligned}$$

Since $a^2 > 2c$, ω_-^2 will always be negative. Additionally, it always holds that $a, d > 0$, but $\text{sgn}(c)$ is unknown and dependent on parameter choice. We examine several cases via application of Theorem 3.1 in Kuang (1993, p. 77), which is reproduced below for convenience.

Theorem 8 (Kuang (1993)) *Consider the following second order real scalar linear neutral delay equation:*

$$\frac{d^2x(t)}{dt^2} + \alpha\frac{d^2x(t-\tau)}{dt^2} + a\frac{dx(t)}{dt} + b\frac{dx(t-\tau)}{dt} + cx(t) + dx(t-\tau) = 0, \tag{3.7.43}$$

where τ, α, a, b, c, d are real constants, and the corresponding characteristic equation is given by

$$\lambda^2 + \alpha\lambda^2 e^{-\lambda\tau} + a\lambda + b\lambda e^{-\lambda\tau} + c + de^{-\lambda\tau} = 0. \tag{3.7.44}$$

In (3.7.43)*, assume $|\alpha| < 1, c + d \neq 0$, and $a^2 + b^2 + (d - \alpha c)^2 \neq 0$. The number of different imaginary roots with positive (negative) imaginary parts of* (3.7.44) *can be zero, one, or two only.*

(1) If there are no such roots, then the stability of the zero solution does not change for any $\tau \geq 0$.

(2) *If there is one imaginary root with positive imaginary part, $i\omega_+$, an unstable zero solution never becomes stable for any $\tau \geq 0$. If the zero solution is asymptotically stable for $\tau = 0$, then it is uniformly asymptotically stable for $\tau < \tau_{0,1}$, and it becomes unstable for $\tau > \tau_{0,1}$. Define $\tau_{0,1} = \frac{\theta_1}{\omega_+}$, with $0 \leq \theta_1 < 2\pi$, and*

$$\cos\theta_1 = -\frac{ab\omega_+^2 + (c-\omega_+^2)(d-\alpha\omega_+^2)}{b^2\omega_+^2 + (d-\alpha\omega_+^2)^2},$$
$$\sin\theta_1 = -\frac{(d-\alpha\omega_+^2)a\omega_+ - b\omega_+(c-\omega_+^2)}{b^2\omega_+^2 + (d-\alpha\omega_+^2)^2}.$$

(3) *If there are two imaginary roots with positive imaginary part, $i\omega_+$ and $i\omega_-$, such that $\omega_+ > \omega_- > 0$, then the stability of the zero solution can change a finite number of times at most as τ is increased, and eventually it becomes unstable.*

Case 1: $|c| > d$

Suppose $|c| > d$. Then the right-hand side of (3.7.42) is always negative. By Theorem 8, the stability of (E^*, T^*) does not change for any $\tau \geq 0$. As the stability is unchanging, we determine the stability of (E^*, T^*) when $\tau = 0$.

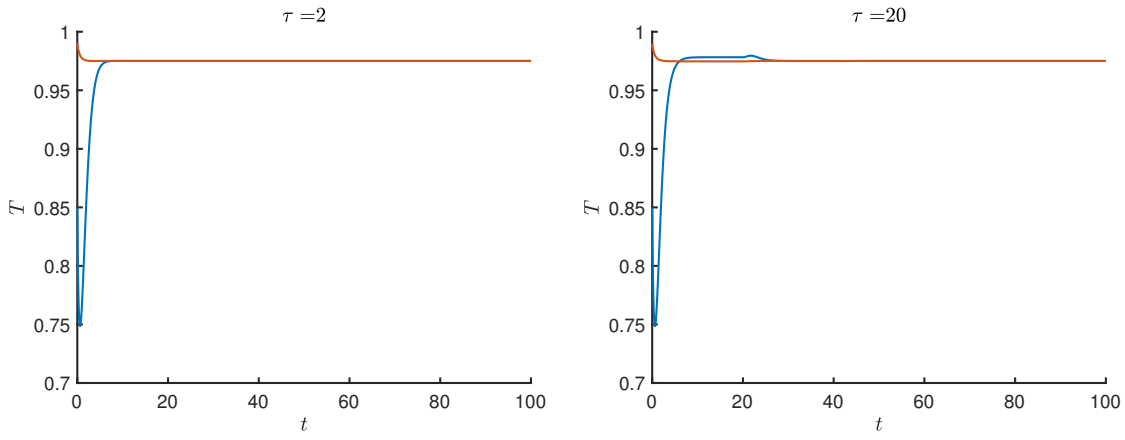

Figure 3.13: The Positive Equilibrium E_1 Is Asymptotically Stable for All $\tau \geq 0$. Parameters Are Chosen Such That $|c| > d$ and $c > 0$.

If $c < 0$, then $c + d < 0$. By Theorem 7, E_2 is unstable and the only positive equilibrium for the system (3.7.30) when $\tau = 0$. If $c > 0$, then $c + d > 0$. It follows from application of Theorem 7 that E_2 is not feasible, and E_1 is asymptotically stable for all $\tau \geq 0$, as depicted by Figure 3.13.

Case 2: $|c| < d$

Suppose $|c| < d$. Evaluating (3.7.42) yields

$$\omega_{\pm}^2 = \frac{1}{2}\Big(-\underbrace{(a^2 - 2c)}_{>0} \pm \Big(\underbrace{(2c - a^2)^2}_{>0} + 4\underbrace{(d^2 - c^2)}_{>0} \Big)^{1/2} \Big).$$

Hence, there exists one imaginary root $\lambda = i\omega$ with a positive imaginary part for the characteristic equation (3.7.39). Since ω_- is always negative, we never have two imaginary roots with positive imaginary part. When $\tau = 0$, by Theorem 7, E_1 is asymptotically stable and E_2 is not feasible since $c + d > 0$.

Define

$$\tau_{0,1} = \frac{\theta_1}{\omega_+},$$

where $0 \leq \theta_1 \leq 2\pi$. Theorem 8 gives that E_1 is uniformly asymptotically stable for $\tau < \tau_{0,1}$ and unstable for $\tau > \tau_{0,1}$. By (3.7.41),

$$\cos\theta_1 = -\left(\frac{c - \omega_+^2}{d}\right); \quad \sin\theta_1 = \frac{a\omega_+}{d}.$$

Thus, the bifurcation point occurs when

$$\tau_{0,1} = \frac{\theta_1}{\omega_+} = -\frac{\operatorname{arccot}\left(\frac{c-\omega_+^2}{a\omega_+}\right)}{\omega_+}. \tag{3.7.45}$$

Figure 3.14 illustrates the loss of stability as τ increases.

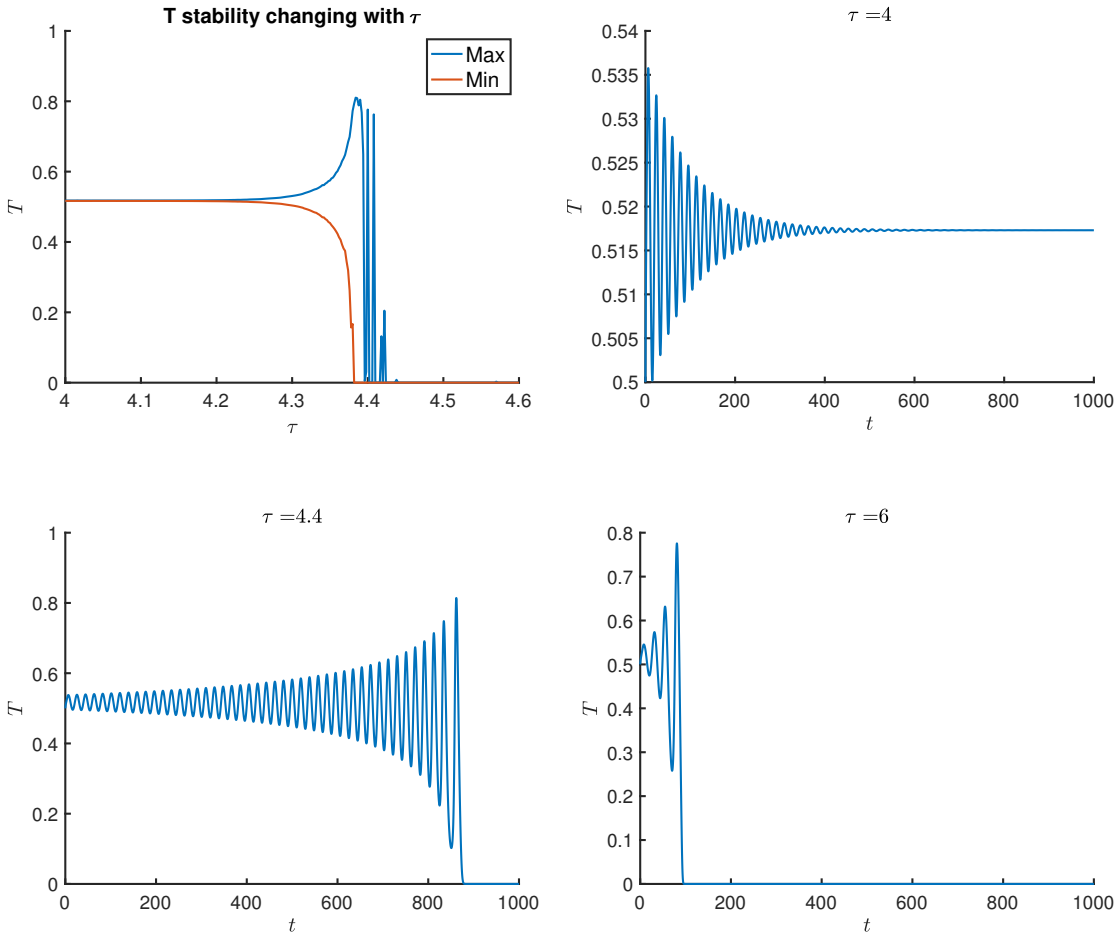

Figure 3.14: The Positive Equilibrium E_1 Is Uniformly Asymptotically Stable for $\tau < \tau_{0,1} = 4.32$ and Unstable for $\tau > \tau_{0,1} = 4.32$. The Parameters Are Chosen Such That $|c| < d$.

Case 3: $|c| = d$

Suppose $|c| = d$. Evaluating (3.7.42) gives

$$\omega_{\pm}^2 = \frac{1}{2}\Big((2c - a^2) \pm (a^2 - 2c)\Big).$$

Thus $\omega_-^2 < 0$ and $\omega_+^2 = 0$. Suppose $c > 0$. Then $c + d > 0$, and Theorem 7 gives that E_1 is the only positive equilibrium and is asymptotically stable when $\tau = 0$. Now if the stability of E_1 changes at some $\tau > 0$, the characteristic equation (3.7.39) admits

a root $\lambda = u + iv$ with $u > 0$ for some $\tau > 0$. Suppose (3.7.39) admits a complex root λ with positive real part. Substituting $\lambda = u + iv$ in the characteristic equation (3.7.39) yields

$$u^2 - v^2 + 2iuv + au + iav + c + de^{-u\tau}(\cos v\tau - i\sin v\tau) = 0.$$

The real and imaginary parts are respectively given by:

$$\begin{cases} u^2 - v^2 + au + c + de^{-u\tau}\cos v\tau = 0, \\ \qquad 2uv + av - de^{-u\tau}\sin v\tau = 0. \end{cases} \tag{3.7.46}$$

Squaring and adding (3.7.46) yields

$$(u^2 - v^2 + au + c)^2 + (2uv + av)^2 = d^2e^{-2u\tau}. \tag{3.7.47}$$

Since $u > 0$ and $\tau \geq 0$ by assumption, it follows that $d^2e^{-2u\tau} \leq d^2$. Therefore

$$(u^2 - v^2 + au + c)^2 + (2uv + av)^2 - d^2 \leq 0. \tag{3.7.48}$$

With $c, u > 0, a^2 > 2c$, and $|c| = d$, expanding (3.7.48) gives

$$\begin{aligned} &\underbrace{(u^2 - v^2)^2}_{>0} + \underbrace{4u^2v^2}_{>0} + \underbrace{2au^3}_{>0} + \underbrace{2auv^2}_{>0} + \underbrace{(a^2 + 2c)u^2}_{>0} \\ &\quad + \underbrace{(a^2 - 2c)v^2}_{>0} + \underbrace{2acu}_{>0} + \underbrace{c^2 - d^2}_{=0} \leq 0, \end{aligned}$$

a contradiction. Thus, it follows that all roots of (3.7.38) have nonpositive real parts. As $\lambda(\tau) = 0$ is clearly never a root of (3.7.39) when $c > 0$ and $|c| = d$, then E_1 is asymptotically stable for all $\tau \geq 0$, as shown in Figure 3.15.

We now suppose $c < 0$. Then $|c| = d$ implies $c + d = 0$. By Theorem 7, $E_1 = E_2$, and the equilibrium is stable. To determine if the stability remains the same for all $\tau \geq 0$, follow the assumption in Kuang (1993, p. 79-80) and let $\tau > \frac{a}{d} > 0$. Consider the following function:

$$F(\lambda, \tau) = \lambda^2 + a\lambda + c + de^{-\lambda\tau}. \tag{3.7.49}$$

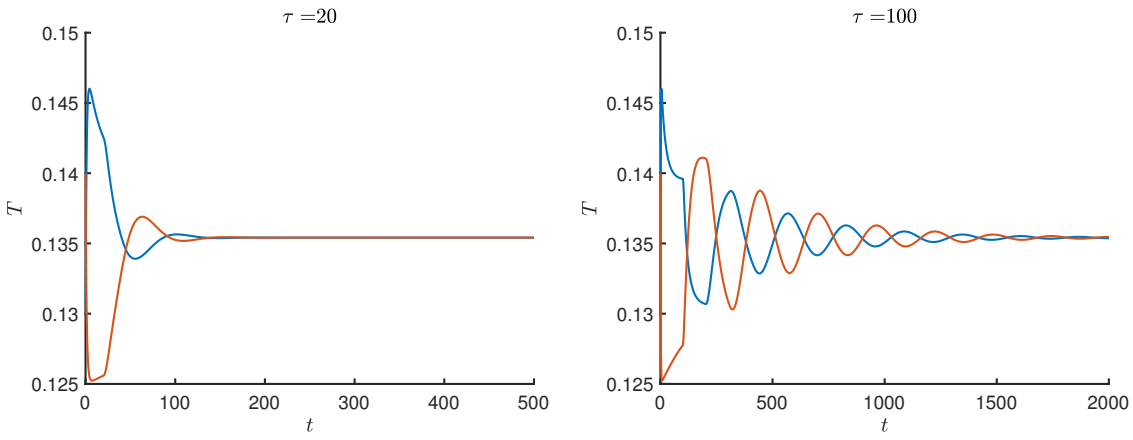

Figure 3.15: The Positive Equilibrium E_1 Is Asymptotically Stable for All $\tau > 0$. Parameters Are Chosen Such That $|c| = d$ and $c > 0$.

Clearly, $F(0,\tau) = 0$ and $\lim_{\lambda\to\infty} F(\lambda,\tau) = \infty$. Additionally, there exists a $N > 0$ such that if $\lambda \geq N, F(\lambda,\tau) \geq 0$. We also have

$$\frac{\partial F(\lambda,\tau)}{\partial \lambda} = 2\lambda + a - d\tau e^{-\lambda\tau}. \tag{3.7.50}$$

Then $\frac{\partial F(0,\tau)}{\partial \lambda} = a - d\tau < 0$, since $\tau > \frac{a}{d}$ by assumption. Then when $\tau > \frac{a}{d}$, there exists a $\delta(\tau) > 0$ such that when $0 < \lambda \leq \delta(\tau), F(\lambda,\tau) < 0$. Thus, there must exist a λ_* with $\delta(\tau) < \lambda_* \leq N$ such that $F(\lambda_*,\tau) = 0$, making (3.7.38) have a positive root. Hence, when $c < 0$ and $|c| = d$, the equilibrium $E_1 = E_2$ is stable for $\tau < \frac{a}{d}$ and unstable for $\tau > \frac{a}{d}$, as displayed in Figure 3.16.

The preceding results are summarized in the following theorem.

Theorem 9 *For the system* (3.7.31)*, the following statements are true, with* a, b, c, d *given by* (3.7.40)*.*

(1) If $|c| > d$*,* E_2 *is unstable and the only feasible equilibrium for* $\tau \geq 0$ *when* $c < 0$*. For* $c > 0$*,* E_1 *is asymptotically stable and the only feasible equilibrium for* $\tau \geq 0$*.*

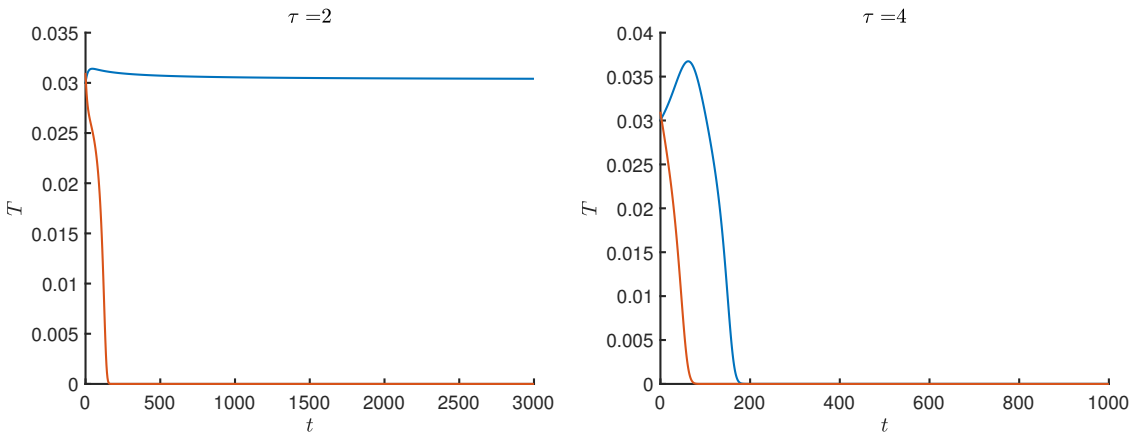

Figure 3.16: Parameters Are Chosen Such That $|c| = d$ and $c < 0$. The Positive Equilibrium $E_1 = E_2$ Is Stable for $\tau < \frac{a}{d}$ and Unstable for All $\tau > \frac{a}{d} \approx 3.6$.

(2) If $|c| < d$, E_1 is the only feasible equilibrium and is uniformly asymptotically stable for $\tau < \tau_{0,1}$ and unstable for $\tau > \tau_{0,1}$, where $\tau_{0,1}$ is calculated by (3.7.45).

(3) If $|c| = d$, E_1 is asymptotically stable and the only feasible equilibrium for $\tau \geq 0$ when $c > 0$. For $c < 0$, $E_1 = E_2$, and the equilibrium is stable when $\tau < \frac{a}{d}$ and unstable when $\tau > \frac{a}{d}$.

When the tumor is highly aggressive, a less rapid immune response (represented by delay) can lead to a loss of stability for a tumorous equilibrium, indicating a loss of tumor control by the immune system. The instability initially reflects a period of tumor growth, followed by uncertainty in tumorous outcomes.

3.8 Health Care Implications

The reduction to a system of two equations yields a model simple enough to allow for clinical use, yet complex enough to produce rich dynamics. Three values, the activation and proliferation rate of CTLs, the time for activated CTLs to kill tumor cells, and the inactivation rate of CTLs by the tumor, are key in driving the

complexity, and the importance of taking their measurements should therefore be emphasized to health care professionals. In evaluating these parameters, as many of the other parameters are commonly known from past experiments, health care workers would then be able to determine which parameter space the tumor falls in and what would accordingly be the best course of treatment. Additionally, the model results suggest to clinicians which combination treatments would be best-suited to pair with DC vaccines. For any patient, treatment to increase the speed at which activated CTLs leave the spleen to kill tumor cells would be a wise combination, as a quick response time results in tumor control, where the tumor is maintained at a low level. When CTLs are activated at a lower rate, the immune response has more flexibility in response time as opposed to when CTLs are activated at a rapid rate, where only a small window of response time results in tumor control. Additionally, treatment to lessen the immunosuppressive environment of the tumor allows for the use of less DC therapy to eliminate the tumor, with the model providing a threshold to guarantee tumor elimination.

3.9 Discussion

The underwhelming results of DC-based clinical trials have led to greater testing of DC vaccines in combination treatments to enhance efficacy. In order to understand when the vaccine will perform most effectively, it is necessary to understand the interactions of tumor and immune cells under different conditions. Mathematical models allow for exploration of these interactions and can aid clinicians in designing better suited monotherapy and combination treatments.

We propose a simple mathematical model which is capable of exhibiting complex dynamics. We incorporate a constant time delay to represent the time for the immune system to respond to the tumor. We have analytically and numerically proven the

conditions necessary for the existence of a Hopf bifurcation and provided a threshold to ensure tumor existence ($\mathcal{R}_0 > 1$). Our reduced model is capable of exhibiting bistability in the region $\mathcal{R}_{crit} < \mathcal{R}_0 < 1$. Numerical experiments suggest the threshold for tumor elimination is $\mathcal{R}_0 < \mathcal{R}_{crit} < 1$. In the special case when the immunosuppressive tumor microenvironment is neutralized ($\eta_e = 0$), less DC treatment is necessary, with the model (3.4.5) guaranteeing tumor elimination for $\mathcal{R}_0 < 1$. Combination treatments pairing DC vaccines with agents to block or neutralize immunosuppressive factors, such as anti-IL-10 and anti-TGF-β, would improve the efficacy of the DC vaccine response, lessening the amount of treatment needed for tumor elimination.

The model outcomes are shown to be sensitive to the time delay. While larger delays are commonly known to destabilize a system through a Hopf bifurcation, our model exhibits richer dynamics than what is commonly observed. Instead of remaining unstable following the Hopf bifurcation, our model regains its stability for a sufficiently large delay. Additionally, our model may produce regions of increased complexity, where the equilibrium becomes increasingly unstable and can even lead to chaotic outcomes (three pairs of complex conjugate eigenvalues with positive real part).

Analytical work and numerical experiments additionally reveal the activation/proliferation rate of CTLs (captured by ρ) to be critical in the dynamics of the system (3.4.5). When the activation/proliferation of CTLs is low (ρ small), the immune system can control the tumor cells for small τ, allowing for coexistence of both populations at a low level. As the delay increases, a Hopf bifurcation introduces oscillatory dynamics for a window of τ. Further increase of τ leads to a return to a stable positive steady state, where a high level of tumor coexist with a low level of CTLs. Taking ρ to be larger, the oscillatory dynamics persist for a wider region of delay and gain added complexity before regaining stability. These complex, aperiodic regions

reflect the clinically relevant variability in treatment outcomes dependent on initial tumor burden. Furthermore, the oscillatory behavior represents the phenomenon of tumor dormancy for long periods of time, suddenly followed by tumor reappearance and growth to a lethal size for unknown reasons, which has been demonstrated *in vivo* (Prehn, 1972) as well as in a variety of mathematical models (Grossman and Berke, 1980; Kuznetsov *et al.*, 1994).x In all cases, when the time for the immune system to respond is too long, the effector cells are unable to control the tumor cells at a low level, and the tumor cells increase to a fatally high level for all initial conditions, aligning with biological intuition.

An analysis of the system when effector cell death is dominated by the interaction with the tumor cells ($\delta = 0$) reveals an increased delay is strictly shown to have a destabilizing effect on the high tumor burden steady state, when conditions allow for a change in the stability. The system with $\delta > 0$ exhibits large delays stabilizing and intermediate delays destabilizing the high tumor burden steady state. Biologically this makes sense, as when the immune system takes too long to respond then there is less resistance to tumor growth, and the tumor will persist. The results highlight the importance of incorporating delay in mathematical models to capture these dynamics and clinically measuring the delay to evaluate the best course of treatment.

Chapter 4

FUTURE WORK

While our models provide insights into the biology of DC vaccines, there remains further work to be done. Underlying this work is the question of whether the outlined conditions and results are satisfied in a clinical or laboratory setting, as the various iterations of the model have parameters with unknown ranges, some of which, as a result of non-identifiability issues discussed in Section 2.7.2, cannot be estimated uniquely with the available data. A main challenge in the process of model formulation lies in correctly parameterizing naturally occurring systems. Parameters are often unknown in value and require estimation with data, which poses a challenge when there is inevitable noise in the data, nonlinearity in the model, or the parameters are structurally or practically non-identifiable. Though optimization methods are commonly utilized in parameter estimation, they generally prove unsuited for overcoming problems with non-identifiability. Sampling-based Markov Chain Monte Carlo (MCMC) algorithms act as an effective solution without requiring removal of non-identifiable parameters, though many alternative methods exist for addressing these difficulties as well (Cao *et al.*, 2008; Zhan *et al.*, 2014).

In Bayesian parameter estimation methods, parameters are categorized as random variables and their posterior distributions are estimated through experimental data. MCMC methods are often used in sampling these parameter distributions. Ballnus *et al.* (2017) outlined a comparison of various MCMC algorithms with single- and multi-chain approaches, including Delayed Rejection Adaptive Metropolis (Haario *et al.*, 2006), Adaptive Metropolis (Haario *et al.*, 2001), and Parallel Hierarchical Sampling (Rigat and Mira, 2012), evaluated against systems with features such as

Hopf bifurcations and bistability. Results from Ballnus *et al.* (2017) and an additional comparison performed by Valderrama-Bahamóndez and Fröhlich (2019) suggest a parallel MCMC approach would be a promising approach for establishing credible intervals for model parameters in future work. Parallel MCMC algorithms are used to cover larger portions of the parameter space at a time (Valderrama-Bahamóndez and Fröhlich, 2019). The parameters' credible intervals can then be densely sampled and propagated through the model to construct prediction confidence intervals as well. Though Bayesian credible intervals require specifying prior distributions for the parameters that pulls upon external information, noninformative priors can be used when little information is known, as is the case with several of the parameters in our models, in which the parameters are assigned uniform distributions with large ranges.

Further open questions exist in each chapter that would additionally be worth exploring in the future. In Chapter 2, open analytical work includes investigating the existence of a Hopf bifurcation, the local stability of the tumorous equilibria, and the existence of the Bogdanov-Takens bifurcation. Additionally, we can explore the tumor-free and tumorous basins of attraction in more detail, better visualizing the relationship between the parameter space and the basins of attraction, thereby determining what range of parameter values and doses are necessary to fall within each basin. Finally, the presence of a singular Hopf bifurcation should be studied in greater depth, including establishing a deeper understanding of the transition near the bifurcation point. Current work is being done to examine a generalized version of the model to firmly establish what is necessary for driving the existence of interesting features, such as backward bifurcations and periodic solutions.

We can then extend and simplify our model in various ways. We can first simplify the model and reduce the parameters to account for problems in identifiability. An extension of the model could reflect a combination of treatments, the common course

of action when employing DC therapies. Furthermore, the metastasis of melanoma can be studied through the incorporation of additional tumor compartments. By modeling multiple tumor compartments simultaneously, we can examine the effects on distant tumors when the primary tumor is treated. Finally, we can explore the effects of incorporating an exhausted effector group. As the tumor inactivates the CTL, a conservation occurs wherein, instead of being eliminated from the system, a group of exhausted effectors is formed that can later be activated again to fight the tumor. We can determine whether these biologically relevant inclusions allow for additional insights.

In Chapter 3, there are similarly many open questions that can be explored in the future, including but not limited to providing more clearly biological interpretations of the established conditions. Primarily, we seek to determine whether the global stability of the interior equilibrium E_1 can be found analytically. Additionally, we can investigate the relationship between the roots of the $S_n(\tau)$ functions, the period, and the amplitude, employing an asymptotic analysis similar to that of Campbell *et al.* (2009). While we represented a constant delay in the response of the immune system, other modes of incorporating delay would be worth exploring in future work. With innate delays present in additional cellular dynamics, such as the binding time required for activation, we could examine whether incorporating a second discrete delay would be significant in the system behavior. Though less frequent, mathematical models of tumors with two discrete delays have been studied (Gosh *et al.*, 2017; Lin and Wang, 2012; Piotrowska, 2008). While the Beretta and Kuang (2002) method employed in this article has allowed for evaluating one-delay systems with delay dependent coefficients, an efficient method for evaluating a two-delay system with delay dependent coefficients remains an open problem (Lin and Wang, 2012). Alternatively, we could assume the tumor cell growth rate is dependent on its population size τ units

before. The different representations are worth comparing to foster a more complete understanding of the tumor-immune dynamics under dendritic cell therapy.

Aerts, J. and J. P. Hegmans, "Tumor-specific cytotoxic t cells are crucial for efficacy of immunomodulatory antibodies in patients with lung cancer", Cancer Research **73**, 8, 2381–2388 (2013).

Agarwal, M. and A. S. Bhadauria, "A generalised prey-predator type model of immunogenic cancer with the effect of immunotherapy", International Journal of Engineering, Science and Technology **5**, 1, 66–84 (2013).

Ahmed, M. S. and Y. S. Bae, "Dendritic cell-based therapeutic cancer vaccines: past, present and future", Clinical and Experimental Vaccine Research **3**, 2, 113–116 (2014).

Allison, J. P., B. W. McIntyre and D. Bloch, "Tumor-specific antigen of murine t-lymphoma defined with monoclonal antibody", The Journal of Immunology **129**, 5, 2293–2300 (1982).

Arabameri, A., D. Asemani and J. Hajati, "Mathematical modeling of in-vivo tumor-immune interactions for the cancer immunotherapy using matured dendritic cells", Journal of Biological Systems **26**, 1, 167–188 (2018).

Ballnus, B., S. Hug, K. Hatz, L. Görlitz, J. Hasenauer and F. J. Theis, "Comprehensive benchmarking of markov chain monte carlo methods for dynamical systems", BMC Systems Biology **11**, 63 (2017).

Bansal, A., M. P. Singh and B. Rai, "Human papillomavirus-associated cancers: A growing global problem", International Journal of Applied & Basic Medical Research **6**, 2, 84–89 (2016).

Berard, M. and D. F. Tough, "Qualitative differences between naive and memory t cells", Immunology **106**, 2, 127–138 (2002).

Beretta, E. and Y. Kuang, "Geometric stability switch criteria in delay differential systems with delay dependent parameters", SIAM J. Math. Anal. **33**, 5, 1144–1165 (2002).

Berryman, A. A., "On the principles of population dynamics and theoretical models", American Entomologist (1997).

Bol, K. F., E. H. Aarntzen, F. E. Hout, G. Schreibelt, J. H. Creemers, W. J. Lesterhuis, W. R. Gerritsen, D. J. Grunhagen, C. Verhoef, C. J. Punt, J. J. Bonenkamp, J. H. de Wilt, C. G. Figdor and I. J. de Vries, "Favorable overall survival in stage iii melanoma patients after adjuvant dendritic cell vaccination", Oncoimmunology **5**, 1, e1057673 (2016a).

Bol, K. F., G. Schreibelt, W. R. Gerritsen, J. M. de Vries and C. G. Figdor, "Dendritic cell-based immunotherapy: State of the art and beyond", Clinical Cancer Research **22**, 8, 1897–1906 (2016b).

Brun, R., P. Reichert and H. R. Künsch, "Practical identifiability analysis of large environmental simulation models", Water Resources Research **37**, 4, 1015–1030 (2001).

Burden, T., J. Ernstberger and K. R. Fister, "Optimal control applied to immunotherapy", Discrete and Continuous Dynamical Systems- Series B **4**, 1, 135–146 (2004).

Busch, W., "Aus der sitzung der medicinischen section vom 13 november 1867", Berlin Klin Wochenschr **5**, 137 (1868).

Campbell, S. A., E. Stone and T. Erneux, "Delay induced canards in high speed machining", Dynamical Systems **00**, 00, 1–15 (2009).

Cann, S. A. H., J. P. van Netten, C. van Netten and D. W. Glover, "Spontaneous regression: a hidden treasure buried in time", Medical Hypotheses **58**, 2, 115–119 (2002).

Cao, J., G. F. Fussmann and J. O. Ramsay, "Estimating a predator-prey dynamical model with the parameter cascades method", Biometrics **64**, 3, 959–967 (2008).

Cappuccio, A., F. Castiglione and B. Piccoli, "Determination of the optimal therapeutic protocols in cancer immunotherapy", Mathematical Biosciences **209**, 1–13 (2007).

Castiglione, F. and B. Piccoli, "Optimal control in a model of dendritic cell transfection cancer immunotherapy", Bulletin of Mathematical Biology **68**, 2, 255–274 (2006).

Castillo-Chavez, C. and B. Song, "Dynamical models of tuberculosis and their applications", Mathematical Biosciences and Engineering **1**, 2, 361–404 (2004).

Castillo-Montiel, E., J. C. Chimal-Eguía, J. I. Tello, G. Piñon-Zaráte, M. Herrera-Enríquez and A. E. Castell-Rodríguez, "Enhancing dendritic cell immunotherapy for melanoma using a simple mathematical model", Theoretical Biology and Medical Modelling **12**, 1, 11 (2015).

Cheever, M. A. and C. S. Higano, "Provenge (sipuleucel-t) in prostate cancer: The first fda-approved therapeutic cancer vaccine", Clinical Cancer Research **17**, 11, 3520–3526 (2011).

Coley, W. B., "The treatment of malignant tumors by repeated inoculations of erisypelas, with a report of ten original cases", The American Journal of the Medical Sciences **105**, 487–511 (1893).

de Pillis, L., A. Gallegos and A. Radunskaya, "A model of dendritic cell therapy for melanoma", Frontiers in Oncology **3** (2013).

de Pillis, L., W. Gu, K. R. Fister, T. Head, K. Maples, A. Murugan, T. Neal and K. Yoshida, "Chemotherapy for tumors: An analysis of the dynamics and a study of quadratic and linear optimal controls", Mathematical Biosciences **209**, 1, 292–315 (2007).

de Pillis, L. G. and A. E. Radunskaya, *Mathematical Models of Tumor-Immune System Dynamics*, chap. Modeling tumor-immune dynamics, pp. 59–108 (Springer, New York, NY, 2014).

Dethlefsen, L. A., J. M. S. Prewitt and M. L. Mendelsohn, "Analysis of tumor growth curves", JNCI: Journal of the National Cancer Institute **40**, 2, 389–405 (1968).

Dickman, L. R., E. Milliken and Y. Kuang, "Tumor control, elimination, and escape through a compartmental model of dendritic cell therapy for melanoma", SIAM Journal on Applied Mathematics **80**, 2, 906–928 (2020).

Diekmann, O., J. A. P. Heesterbeek and J. A. J. Metz, "On the definition and computation of the basic reproduction ratio r_0 in models for infectious diseases in heterogeneous populations", Journal of Mathematical Biology **28**, 365–382 (1990).

Domingues, B., J. M. Lopes, P. Soares and H. Pópulo, "Melanoma treatment in review", ImmunoTargets and Therapy **7**, 35–49 (2018).

d'Onofrio, A., "A general framework for modeling tumor-immune system competition and immunotherapy: mathematical analysis and biomedical inferences", Physica D: Nonlinear Phenomena **208**, 3-4, 220–235 (2005).

Ebbell, B., *The Papyrus Ebers: the greatest Egyptian medical document* (Levin & Munksgaard, Copenhagen, 1937).

Eikenberry, S., C. Thalhauser and Y. Kuang, "Tumor-immune interaction, surgical treatment, and cancer recurrence in a mathematical model of melanoma", PLoS Computational Biology **5**, 4, e1000362 (2009).

Ermentrout, B., *Simulating, Analyzing, and Animating Dynamical Systems: A Guide to XPPAUT for Researchers and Students*, Software, Environments and Tools (SIAM, 2002).

Fagnoni, F. F., R. Vescovini, G. Passeri, G. Bologna, M. Pedrazzoni, G. Lavagetto, A. Casti, C. Franceschi, M. Passeri and P. Sansoni, "Shortage of circulating naive cd8+ t cells provides new insights on immunodeficiency in aging", Blood **95**, 2860–2868 (2000).

Fehleisen, F., "Ueber die züchtung der erysipelkokken auf künstlichem nährboden und ihre übertragbarkeit auf den menschen", Dtsch Med Wochenschr **8**, 553–554 (1882).

Ferrara, A., M. Nonn, P. Sehr, C. Schreckenberger, M. Pawlita, M. Dürst, A. Schneider and A. M. Kaufmann, "Dendritic cell-based tumor vaccine for cervical cancer ii: Results of a clinical pilot study in 15 individual patients", Journal of Cancer Research and Clinical Oncology **129**, 9, 521–530 (2003).

Fong, L., Y. Hou, A. Rivas, C. Benike, A. Yuen, G. A. Fisher, M. M. Davis and E. G. Engleman, "Altered peptide ligand vaccination with flt3 ligand expanded dendritic cells for tumor immunotherapy", Proceedings of the National Academy of Sciences of the United States of America **98**, 15, 8809–8814 (2001).

Fortin, P. and M. C. Mackey, "Periodic chronic myelogenous leukaemia: spectral analysis of blood cell counts and aetiological implications", British Journal of Haematology **104**, 2, 336–345 (1999).

Galach, M., "Dynamics of the tumor–immune system competition–the effect of time delay", International Journal of Applied Mathematics and Computer Science **13**, 3, 395–406 (2003).

Gameiro, S. R., M. L. Jammeh and J. W. Hodge, "Cancer vaccines targeting carcinoembryonic antigen: state-of-the-art and future promise", Expert Review of Vaccines **12**, 6, 617–629 (2013).

Gevertz, J. L. and J. R. Wares, "Developing a minimally structured mathematical model of cancer treatment with oncolytic viruses and dendritic cell injections", Computational and Mathematical Methods in Medicine (2018).

Ghaffari, A. and N. Naserifar, "Optimal therapeutic protocols in cancer immunotherapy", Computers in Biology and Medicine **40**, 261–270 (2010).

Gosh, D., S. Khajanchi, S. Mangiarotti, F. Denis, S. K. Dana and C. Letellier, "How tumor growth can be influenced by delayed interactions between cancer cells and the microenvironment?", Biosystems **158**, 17–30 (2017).

Gossel, G., T. Hogan, D. Cownden, B. Seddon and A. J. Yates, "Memory cd4 t cell subsets are kinetically heterogeneous and replenished from naive t cells at high levels", eLife **6**, e23013 (2017).

Gourley, S. A. and Y. Kuang, "A stage structured predator-prey model and its dependence on maturation delay and death rate", Journal of Mathematical Biology **49**, 188–200 (2004).

Granucci, F. and I. Zanoni, "The dendritic cell life cycle", Cell Cycle **8**, 23, 3816–3821 (2009).

Grossman, Z. and G. Berke, "Tumor escape from immune elimination", Journal of Theoretical Biology **83**, 267–296 (1980).

Gumel, A. B., "Causes of backward bifurcations in some epidemiological models", Journal of Mathematical Analysis and Applications **395**, 355–365 (2012).

Haario, H., M. Laine, A. Mira and E. Saksman, "Dram: Efficient adaptive mcmc", Statistics and Computing **16**, 339–354 (2006).

Haario, H., E. Saksman and J. Tamminen, "An adaptive metropolis algorithm", Bernoulli **7**, 2, 223–242 (2001).

Holling, C. S., "The components of predation as revealed by a study of small-mammal predation of the european sawfly", The Canadian Entomologist **91**, 293–320 (1959a).

Holling, C. S., "Some characteristics of simple types of predation and parasitism", The Canadian Entomologist **91**, 293–320 (1959b).

Hsu, F. J., C. Benike, F. Fagnoni, T. M. Liles, D. Czerwinski, B. Taidi, E. G. Engleman and R. Levy, "Vaccination of patients with b-cell lymphoma using autologous antigen-pulsed dendritic cells", Nature Medicine **2**, 52–58 (1996).

Hsu, S. B., "On global stability of a predator-prey system", Mathematical Biosciences **39**, 1–10 (1978).

Jackson, R., "Saint peregrine, o.s.m.–the patron saint of cancer patients", Canadian Medical Association Journal **111**, 8, 824–827 (1974).

Kantoff, P. W., C. S. Higano, N. D. Shore, E. R. Berger, E. J. Small, D. F. Penson, C. H. Redfern, A. C. Ferrari, R. Dreicer, R. B. Sims, Y. Xu, M. W. Frohlich and P. F. Schellhammer, "Sipuleucel-t immunotherapy for castration-resistant prostate cancer", The New England Journal of Medicine **363**, 411–422 (2010).

Kaur, G. and N. Ahmad, "On study of immune response to tumor cells in prey-predator system", International Scholarly Research Notices (2014).

Kirschner, D. and J. C. Panetta, "Modeling immunotherapy of the tumor-immune interaction", Journal of Mathematical Biology **37**, 3, 235–252 (1998).

Korobeinikov, A., "Lyapunov functions and global stability for sir and sirs epidemiological models with non-linear transmission", Bulletin of Mathematical Biology **3**, 615–626 (2006).

Kronik, N., Y. Kogan, M. Elishmereni, K. Halevi-Tobias, S. Vuk-Pavlović and Z. Agur, "Predicting outcomes of prostate cancer immunotherapy by personalized mathematical models", PLoS ONE **5**, 12, e15482 (2010).

Kuang, Y., *Delay Differential Equations with Applications in Population Dynamics*, vol. 191 of *Mathematics in Science and Engineering* (Academic Press, 1993).

Kuang, Y. and E. Beretta, "Global qualitative analysis of a ratio-dependent predator-prey system", Journal of Mathematical Biology **36**, 389–406 (1998).

Kumar, C., S. Kohli, S. Chiliveru, P. P. Bapsy, M. Jain, V. S. S. Attili, J. Mohan, A. K. Vaid and B. Sharan, "A retrospective analysis comparing apceden(r) dendritic cell immunotherapy with best supportive care in refractory cancer", Immunotherapy **9**, 11, 889–897 (2017).

Kuznetsov, V. A., I. A. Makalkin, M. A. Taylor and A. S. Perelson, "Nonlinear dynamics of immunogenic tumors: Parameter estimation and global bifurcation analysis", Bulletin of Mathematical Biology **56**, 2, 295–321 (1994).

Kuznetsov, Y. A., *Elements of Applied Bifurcation Theory, Second Edition* (Springer, 1998).

Lagarias, J. C., J. A. Reeds, M. H. Wright and P. E. Wright, "Convergence properties of the nelder–mead simplex method in low dimensions", SIAM Journal on Optimization **9**, 1, 112–147 (1998).

Lai, X. and A. Friedman, "Combination therapy of cancer with cancer vaccine and immune checkpoint inhibitors: A mathematical model", PLoS ONE **12**, 5, e0178479 (2017).

Lee, T. H., Y. H. Cho and M. G. Lee, "Larger numbers of immature dendritic cells augment an anti-tumor effect against established murine melanoma cells", Biotechnology Letters **29**, 351–357 (2007).

Li, M. Y., H. L. Smith and L. Wang, "Global dynamics of an seir epidemic model with vertical transmission", SIAM J. Appl. Math. **62**, 1, 58–69 (2001).

Liau, L. M., K. L. Black, N. A. Martin, S. N. Sykes, J. M. Bronstein, L. Jouben-Steele, P. S. Mischel, A. Belldegrun and T. F. Cloughesy, "Treatment of a patient by vaccination with autologous dendritic cells pulsed with allogenic major histocompatibility complex class i-matched tumor peptides. case report", Neurosurgical Focus **15**, 9, e8 (2000).

Lin, X. and H. Wang, "Stability analysis of delay differential equations with two discrete delays", Canadian Applied Mathematics Quarterly **20**, 4, 519–533 (2012).

Lotka, A. J., "Analytical note on certain rhythmic relations in organic systems", Proceedings of the National Academy of Sciences of the United States of America **6**, 7, 410–415 (1920).

Lotka, A. J., *Elements of Physical Biology* (Williams and Wilkins Co., 1925).

Ludewig, B. *et al.*, "Determining control parameters for dendritic cell-cytotoxic t lymphocyte interactions", European Journal of Immunology **34**, 2407–2418 (2004).

Malthus, T., *An Essay on the Principle of Population* (1798).

Markov, O., N. Mironova, S. Sennikov, V. Vlassov and M. Zenkova, "Prophylactic dendritic cell-based vaccines efficiently inhibit metastases in murine metastatic melanoma", PLoS ONE **10**, 9, e0136911 (2015).

McCarthy, E. F., "The toxins of william b. coley and the treatment of bone and soft-tissue sarcomas", The Iowa Orthopaedic Journal **26**, 154–158 (2006).

McCune, J. M., M. B. Hanley, D. Cesar, R. Halvorsen, R. Hoh, D. Schmidt, E. Wieder, S. Deeks, S. Siler, R. Neese and M. Hellerstein, "Factors influencing t-cell turnover in hiv-1-seropositive patients", The Journal of Clinical Investigation **105**, 5, R1–R8 (2000).

Michie, C. A., A. McLean, C. Alcock and P. C. L. Beverley, "Lifespan of human lymphocyte subsets defined by cd45 isoforms", Nature **360**, 264–265 (1992).

Nestle, F. O., S. Alijagic, M. Gilliet, Y. Sun, S. Grabbe, R. Dummer, G. Burg and D. Schadendorf, "Vaccination of melanoma patients with peptide- or tumorlysate-pulsed dendritic cells", Nature Medicine **4**, 3, 328–332 (1998).

Nikolopoulou, E., L. R. Johnson, D. Harris, J. D. Nagy, E. C. Stites and Y. Kuang, "Tumour-immune dynamics with an immune checkpoint inhibitor", Letters in Biomathematics **5**, S137–S159 (2018).

Norton, L., "A gompertzian model of human breast cancer growth", Cancer Research **48**, 7067–7071 (1988).

Oiseth, S. J. and M. S. Aziz, "Cancer immunotherapy: a brief review of the history, possibilities, and challenges ahead", Journal of Cancer Metastasis and Treatment **3**, 250–261 (2017).

Omlin, M., R. Brun and P. Reichert, "Biogeochemical model of lake zürich: sensitivity, identifiability and uncertainty analysis", Ecological Modelling **141**, 1-3, 105–123 (2001).

Pearl, R. and L. J. Reed, "On the rate of growth of the population of the united states since 1790 and its mathematical representation", Proceedings of the National Academy of Sciences of the United States of America **6**, 6, 275–288 (1920).

Piotrowska, M. J., "Hopf bifurcation in a solid avascular tumour growth model with two discrete delays", Mathematical and Computer Modelling **47**, 597–603 (2008).

Pisano, L., *Liber Abaci* (1202).

Polo-Parada, L., G. Gutiérrez-Juárez, D. Cywiak, R. Pérez-Solano and G. A. Baker, "Spectrophotometric analysis at the single-cell level: elucidating dispersity within melanic immortalized cell populations", Analyst **142**, 9, 1482–1491 (2017).

Portz, T. and Y. Kuang, "A mathematical model for the immunotherapy of advanced prostate cancer", in "BIOMAT 2012", edited by R. P. Mondaini, pp. 70–85 (World Scientific, 2013).

Prehn, R. T., "The immune reaction as a stimulator of tumor growth", Science **176**, 4031, 170–171 (1972).

Raue, A., C. Kreutz, T. Maiwald, J. Bachmann, M. Schilling, U. Klingmüller and J. Timmer, "Structural and practical identifiability analysis of partially observed dynamical models by exploiting the profile likelihood", Bioinformatics **25**, 15, 1923–1929 (2009).

Rebecca, V. W., V. K. Sondak and K. S. M. Smalley, "A brief history of melanoma: From mummies to mutations", Melanoma Research **22**, 2, 114–122 (2012).

Ridgway, D., "The first 1000 dendritic cell vaccinees", Cancer Investigation **21**, 6, 873–886 (2003).

Rigat, F. and A. Mira, "Parallel hierarchical sampling: A general-purpose interacting markov chains monte carlo algorithm", Computational Statistics & Data Analysis **56**, 6, 1450–1467 (2012).

Rodriguez-Fernandez, M., J. A. Egea and J. R. Banga, "Novel metaheuristic for parameter estimation in nonlinear dynamic biological systems", BMC Bioinformatics **7**, 483 (2006).

Rohatgi, A., "Webplotdigitizer", URL `https://automeris.io/WebPlotDigitizer` (2019).

Ronchese, F. and I. F. Hermans, "Killing of dendritic cells: a life cut short or a purposeful death?", Journal of Experimental Medicine **194**, 5, F23–F26 (2001).

Rutter, E. M. and Y. Kuang, "Global dynamics of a model of joint hormone treatment with dendritic cell vaccine for prostate cancer", Discrete and Continuous Dynamical Systems- Series B **22**, 3, 1001–1021 (2017).

Siegel, R. L., K. D. Miller and A. Jemal, "Cancer statistics, 2019", CA: A Cancer Journal for Clinicians **69**, 7–34 (2019).

Smith, H. L., *Monotone dynamical systems: An introduction to the theory of competitive and cooperative systems*, vol. 41 of *Mathematical Surveys and Monographs* (American Mathematical Society, 1995).

Soetaert, K. and T. Petzoldt, "Inverse modelling, sensitivity and monte carlo analysis in r using package fme", Journal of Statistical Software **33**, 3, 1–28 (2010).

Solomon, M. E., "The natural control of animal populations", Journal of Animal Ecology **18**, 1–35 (1949).

Sotolongo-Costa, O., L. M. Molina, D. R. Perez, J. C. Antoranz and M. C. Reyes, "Behavior of tumors under nonstationary therapy", Physica D: Nonlinear Phenomena **178**, 242–253 (2003).

Steinman, R. M. and Z. A. Cohn, "Identification of a novel cell type in peripheral lymphoid organs of mice. i. morphology, quantitation, tissue distribution", The Journal of Experimental Medicine **137**, 5, 1142–1162 (1973).

Tjoa, B. A., A.-A. A. Elgamal and G. P. Murphy, "Vaccine therapy for prostate cancer", Urologic Clinics of North America **26**, 2, 365–374 (1999).

Tough, D. F. and J. Sprent, "Turnover of naive- and memory-phenotype t cells", The Journal of Experimental Medicine **179**, 4, 1127–1135 (1994).

U.S. National Library of Medicine, "Clinicaltrials.gov", URL `https://clinicaltrials.gov/` (2018).

Valderrama-Bahamóndez, G. I. and H. Fröhlich, "Mcmc techniques for parameter estimation of ode based models in systems biology", Frontiers in Applied Mathematics and Statistics **5**, 55, 1–10 (2019).

van den Driessche, P. and J. Watmough, "Reproduction numbers and sub-threshold endemic equilibria for compartmental models of disease transmission", Mathematical Biosciences **180**, 29–48 (2002).

van Gulijk, M., F. Dammeijer, J. G. J. V. Aerts and H. Vroman, "Combination strategies to optimize efficacy of dendritic cell-based immunotherapy", Frontiers in Immunology **9**, 2759 (2018).

Verhulst, P. F., "Notice sur la loi que la population suit dans son accroissement", Correspondance mathématique et physique **10**, 113–121 (1838).

Versteven, M., J. M. J. V. den Bergh, E. Marcq, E. L. J. Smits, V. F. I. V. Tendeloo, W. Hobo and E. Lion, "Dendritic cells and programmed death-1 blockade: A joint venture to combat cancer", Frontiers in Immunology **9**, 394 (2018).

Volterra, V., "Variazioni e fluttuazioni del numero d'individui in specie animali conviventi", Memoria della Reale Accademia Nazionale dei Lincei **6**, 2, 31–113 (1926).

Westera, L., J. Drylewicz, I. den Braber, T. Mugwagwa, I. van der Maas, L. Kwast, T. Volman, E. H. van de Weg-Schrijver, I. Bartha, G. Spierenburg, K. Gaiser, M. T. Ackermans, B. Asquith, R. J. de Boer, K. Tesselaar and J. A. Borghans, "Closing the gap between t-cell life span estimates from stable isotope-labeling studies in mice and humans", Blood **122**, 2205–2212 (2013).

Wierecky, J., M. R. Müller, S. Wirths, E. Halder-Oehler, D. Dörfel, S. M. Schmidt, M. Häntschel, W. Brugger, S. Schröder, M. S. Horger, L. Kanz and P. Brossart, "Immunologic and clinical responses after vaccinations with peptide-pulsed dendritic cells in metastatic renal cancer patients", Cancer Research **66**, 11, 5910–5918 (2006).

Wilkie, K. P. and P. Hahnfeldt, "Tumor-immune dynamics regulated in the microenvironment inform the transient nature of immune-induced tumor dormancy", Cancer Research **73**, 12, 3534–3544 (2013).

Wilson, M. A. and L. M. Schuchter, "Chemotherapy for melanoma", in "Melanoma", edited by H. L. Kaufman and J. M. Mehnert, vol. 167 of *Cancer Treatment and Research*, chap. Melanoma (Springer, 2016).

Zhan, C., W. Situ, L. F. Yeung, P. W. Tsang and G. Yang, "A parameter estimation method for biological systems modelled by ode/dde models using spline approximation and differential evolution algorithm", IEEE/ACM Transactions on Computational Biology and Bioinformatics **11**, 6, 1066–1076 (2014).

APPENDIX A

CO-AUTHOR PERMISSIONS

I certify that my co-authors, Dr. Evan Milliken and Dr. Yang Kuang, have given me permission to include all material in my Ph.D. thesis for Chapter 2.

APPENDIX B

JOURNAL PERMISSION

Some of the material in Chapter 2 has been published, under the title "Tumor Control, Elimination, and Escape through a Compartmental Model of Dendritic Cell Therapy for Melanoma" (Dickman *et al.*, 2020). I certify that I have received copyright permission from the journal that published this work, *SIAM Journal on Applied Mathematics*.

APPENDIX C

PARAMETER TABLES FOR CHAPTER 2

Tables C.1 and C.2 provide the parameters for the intermediate model (2.3.5) and simplified model (2.3.6) respectively from Chapter 2. Reasonable values were decided upon through a literature review. Uncertain parameters were estimated through a fitting to the murine data in Lee *et al.* (2007).

Table C.1: Parameters of the Intermediate Model (2.3.5)

Para.	Description	Value	Reference
$v_b(t)$	Intravenous DC dose amount	Range: $[0 - 10^{10}]$ cells	de Pillis *et al.* (2013); Lee *et al.* (2007)
μ_{TB}	Maximum transfer rate of DCs from tumor to blood	0.0011/day	de Pillis *et al.* (2013)
$v_t(t)$	Intratumoral DC dose amount	Range: $[0 - 10^{10}]$ cells	de Pillis *et al.* (2013); Lee *et al.* (2007)
μ_{BT}	Maximum transfer rate of DCs from blood to tumor	1.0016×10^{-5}/day	Fit to Lee *et al.* (2007)
K_T	Value of tumor cells for half-max DC recruitment	10^5 cells	Kirschner and Panetta (1998)
δ_D	Natural death rate of DCs	0.341/day Range: [.116,.5]	de Pillis *et al.* (2013); Granucci and Zanoni (2009); Ludewig *et al.* (2004)
D_i	Number of immature DCs being activated by tumor per day	1001.6 cells/day	Fit to Lee *et al.* (2007)
s_{E^a}	Source of activated CTLs	1.0076×10^{-4} cells/day	Fit to Lee *et al.* (2007)
δ_{E^a}	Natural death rate of activated CTLs	0.1155/day Range: $[0.00970 - 0.1199]$	de Pillis *et al.* (2013); Ludewig *et al.* (2004)
τ	Time accounting for history of dendritic cells (travel from spleen)	0.3038 days	Fit to Lee *et al.* (2007)
$\tilde{E}_n$	Number of naive CTLs contributing to primary clonal expansion	8×10^4 cells	Fagnoni *et al.* (2000)
b_n	Maximum activation/proliferation rate of naive CTLs by DCs	1.00118×10^{-2}/day	Fit to Lee *et al.* (2007)
$E_n = \tilde{E}_n b_n$	Maximum number of naive CTLs being activated and proliferating per day	800.944 cells/day	Calculated
θ_n	Threshold in DC density for half-maximal proliferation/activation of naive CTLs	1001.26 cells	Fit to Lee *et al.* (2007)
b_m	Maximum activation/proliferation rate of memory CTLs by DCs	0.01/day	Ludewig *et al.* (2004)
θ_m	Threshold in DC density for half-maximal proliferation/activation of memory CTLs	102.015 cells	Fit to Lee *et al.* (2007)

r_{am}	Inactivation rate of activated CTLs	0.01/day	Ludewig *et al.* (2004)
μ_{BTE}	Maximum rate of CTL recruitment to tumor from blood	5.7/day	de Pillis *et al.* (2013)
c_e	Maximum rate activated CTLs are inactivated by tumor cells	9.42×10^{-12}/day Range: $[9.42 \times 10^{-12} - 10^{-3}]$	Kronik *et al.* (2010); Kuznetsov *et al.* (1994); Wilkie and Hahnfeldt (2013)
$K_{E_t^a}$	Value for half-max activated CTL toxicity	5007.11 cells	Fit to Lee *et al.* (2007)
s_{E^m}	Source of memory CTLs	1.0013×10^{-3} cells/day	Fit to Lee *et al.* (2007)
δ_{E^m}	Natural death rate of memory CTLs in blood	0.0903/day Range: $[0.065 - .0903]$	Gossel *et al.* (2017); Ludewig *et al.* (2004); Westera *et al.* (2013)
r	Tumor cell growth rate	0.3954/day Range: $[0.17 - 0.69]$	de Pillis *et al.* (2013); Eikenberry *et al.* (2009); Kuznetsov *et al.* (1994); Lai and Friedman (2017)
k	Tumor cell carrying capacity	1.0×10^9 cells	de Pillis *et al.* (2013)
c_t	Maximum rate activated CTLs kill tumor cells	0.35/day Range: [0-1]	de Pillis *et al.* (2013); Kirschner and Panetta (1998)

Table C.2: Parameters of the Simplified Model (2.3.6)

Para.	Description	Value	Reference
$v_b(t)$	Intravenous DC dose amount	Range: $[0 - 10^{10}]$ cells	de Pillis *et al.* (2013); Lee *et al.* (2007)
μ_{BT}	Transfer rate of DCs from blood to tumor	5.9096×10^{-4}/day	Fit to (Lee *et al.*, 2007)
$v_t(t)$	Intratumoral DC dose amount	Range: $[0 - 10^{10}]$ cells	de Pillis *et al.* (2013); Lee *et al.* (2007)
μ_{TB}	Transfer rate of DCs from tumor to blood	0.0011/day	de Pillis *et al.* (2013)
δ_D	Natural death rate of DCs	0.34/day Range: [.116,.5]	de Pillis *et al.* (2013); Granucci and Zanoni (2009); Ludewig *et al.* (2004)
D_i	Rate of immature DCs being activated by tumor per day	6.2292×10^{-4}/day	Fit to Lee *et al.* (2007)
s_E	Source of activated CTLs	4.9348×10^{-4} cells/day	Fit to Lee *et al.* (2007)
c	Activation/proliferation rate of CTLs	6.4253×10^{-3}/day	Fit to Lee *et al.* (2007)
c_e	Maximum rate activated CTLs are inactivated by tumor cells	5.539×10^{-14}/(cells×day) Range:$[9.42 \times 10^{-14} - 10^{-3}]$	Kronik *et al.* (2010); Kuznetsov *et al.* (1994); Wilkie and Hahnfeldt (2013)
r_{am}	Inactivation rate of activated CTLs	0.002/day Range: $[4 \times 10^{-4} - 1.2]$	Ludewig *et al.* (2004)
δ_E	Natural death rate of activated CTLs	0.1155/day Range: $[0.00970 - 0.1199]$	de Pillis *et al.* (2013); Ludewig *et al.* (2004)
r	Tumor cell growth rate	0.39155/day Range: $[0.17 - 0.69]$	de Pillis *et al.* (2013); Eikenberry *et al.* (2009); Kuznetsov *et al.* (1994); Lai and Friedman (2017)
k	Tumor cell carrying capacity	10^9 cells	de Pillis *et al.* (2013)
c_t	Maximum rate activated CTLs kill tumor cells	0.001/(cells×day) Range: [0-1]	de Pillis *et al.* (2013); Kirschner and Panetta (1998)